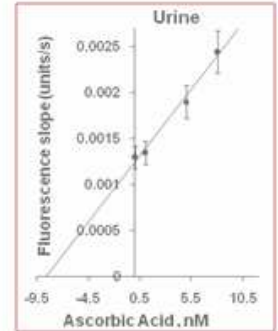
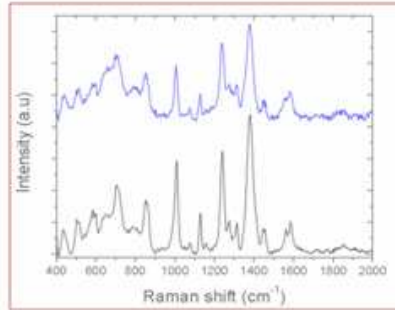
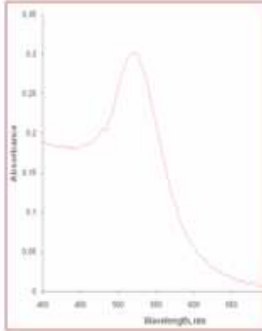
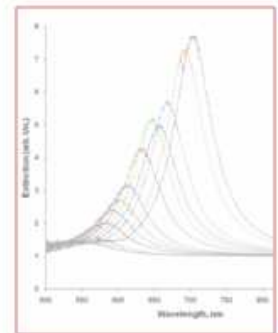
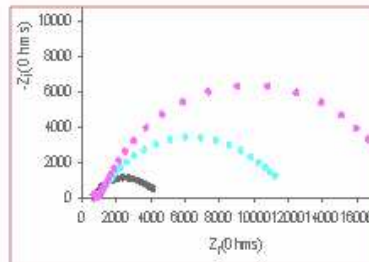
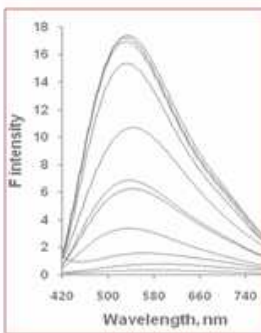


Universidad del País Vasco Euskal Herriko Unibertsitatea



# DEVELOPMENT OF NEW METHODS FOR SIGNAL AMPLIFICATION IN BIOANALYTICAL ASSAYS



Natalia Malashikhina

2013

eman ta zabal zazu



Universidad  
del País Vasco

Euskal Herriko  
Unibertsitatea

# **Development of new methods for signal amplification in bioanalytical assays**

Dissertation submitted to the Department of  
Biochemistry and Molecular Biology  
University of the Basque Country (UPV/EHU)  
for the degree of Doctor of Philosophy

***presented by***

**NATALIA MALASHIKHINA**

Thesis supervisor: Dr. Valery Pavlov

University tutor: Dr. Félix María Goñi Urcelay

2013



**This PhD thesis has been performed at,**

Biofunctional Nanomaterials Unit  
CICbiomaGUNE  
San Sebastián



Laboratoire CSPBAT - UFR SMBH  
Université Paris 13  
Paris



Grup de Sensors i Biosensors  
Departament de Química  
Universitat Autònoma de Barcelona





# Acknowledgements

I would like to take this opportunity to thank all those who have contributed in any way, shape or form to the completion of my PhD thesis.

A special thanks must go to the members of my evaluation committee, for their kind agreement to read this thesis, for their advice and criticism.

I would like to thank my scientific supervisor Dr. Valery Pavlov for keeping me motivated during these four years and for the invaluable help and guidance he has given me. I especially feel thankful to Valery for his calmness. I greatly appreciate his extraordinary knowledge in the field of Biosensing, as well as his professional organization. Valery's open-minded and kindhearted character converted our research group into a small family.

I would also like to give special thanks to the groupmembers of Laboratory 3 of the Biofunctional Nanomaterials Unit at CICbiomaGUNE (Spain): to Dr. Laura Saa Peña for her professional help in all manner of experimental work and personal problems, to Dr. Gaizka Garai-Ibabe for providing me with ideas and for the profound comments on the resulting publications, to Ruta Grinyté for her interesting and fruitful scientific discussions.

I would like to thank Prof. Marc Lamy de la Chapelle for offering me the opportunity to carry out exciting research in his laboratory at the Université Paris 13 (France), where the nanoplatform for MnSOD-2 detection was developed.

I would also like to thank Prof. Manel del Valle for hosting me at his laboratory in Universitat Autònoma de Barcelona (Spain), where the impedimetric sensor for copper (II) ions detection was developed in conjunction with Cristina Ocaña.

Finally, I wish to express my gratitude to my family and my friends for their love, understanding, support and inspiration.

To conclude, I wish to add that I would never have been able to finish this work without my PhD fellowship from CIC biomaGUNE, and the financial support of the Spanish Ministry of Science and Innovation (project BIO2008-04856), NANOANTENNA project (FR/-HEALTH-F5-2009-241818), which covered my travel expenses to Universitat Autònoma de Barcelona and also to Université Paris 13, France.

# Contents

Abstract.....	1
Resumen.....	4
List of figures.....	8
List of abbreviations .....	13
Chapter 1. General introduction .....	16
1.1 Background.....	16
1.1.1 Bio-amplification methods .....	17
1.1.2 Nano-amplification methods.....	18
1.2 Objectives and scopes of this study .....	21
Chapter 2. Experimental methods .....	23
2.1 UV-Vis spectroscopy.....	23
2.2 Fluorescence spectroscopy.....	23
2.3 Enzyme-linked immune sorbent assay (ELISA).....	25
2.4 Localized surface plasmon resonance (LSPR).....	28
2.5 Surface enhanced Raman spectroscopy (SERS).....	29
2.6 Solid-phase oligonucleotide synthesis.....	31
2.7 Plate reader .....	33



2.8	Matrix-assisted laser desorption/ionization mass spectrometry (MALDI-MS)	
	33	
2.9	Electrochemical impedance spectroscopy (EIS) .....	35
	Chapter 3. DNA-decorated nanoparticles as nanosensors for rapid detection of ascorbic acid.....	36
3.1	Introduction.....	36
3.2	Experimental part.....	38
3.2.1	Materials and methods.....	38
3.2.2	Preparation and characterization of oligonucleotides .....	38
3.2.3	Gold NPs synthesis and characterization.....	40
3.2.4	Preparation of oligonucleotide modified gold NPs.....	41
3.2.5	Quantification of AA by <i>catalyst DNA</i> and <i>substrate DNA</i> .....	43
3.2.6	Quantification of AA by <i>catalyst DNA</i> and Au NPs decorated with <i>thiolated substrate DNA</i> .....	43
3.2.7	Determination of AA in real samples.....	44
3.3	Results and discussion .....	45
3.4	Conclusions .....	57
	Chapter 4. Label-Free selective impedimetric detection of Cu <sup>2+</sup> ions using catalytic DNA .....	58
4.1	Introduction.....	58
4.2	Experimental part.....	60
4.2.1	Materials and methods.....	60
4.2.2	Preparation and characterization of oligonucleotide.....	60
4.2.3	Impedimetric sensor preparation.....	62
4.2.4	Copper ions detection.....	63

4.3	Results and discussion .....	65
4.3.1	Optimization of electrode surface .....	65
4.3.2	Detection of $\text{Cu}^{2+}$ .....	66
4.3.3	Sensitivity of <i>DNAzyme</i> -based sensor .....	68
4.3.4	Selectivity of <i>DNAzyme</i> based sensor .....	69
4.4	Conclusions .....	70
	Chapter 5. Unconventional application of conventional enzymatic substrate: First fluorogenic immunoassay based on enzymatic formation of QDs .....	71
5.1	Introduction .....	71
5.2	Experimental part .....	75
5.2.1	Materials and methods .....	75
5.2.2	Detection of ALP by standard method .....	75
5.2.3	Detection of ALP activity by QD based method .....	76
5.2.4	Detection of Anti-BSA antibody by standard immunoassay .....	76
5.2.5	Detection of Anti-BSA Antibody by QD based method .....	76
5.3	Results and discussion .....	78
5.4	Conclusions .....	87
	Chapter 6. Development of SERS sensor for MnSOD-2 protein detection based on specific DNA probe and gold nanostructure substrate .....	88
6.1	Introduction .....	88
6.2	Experimental part .....	91
6.2.1	Materials and methods .....	91
6.2.2	Preparation and characterization of oligonucleotides .....	91
6.2.3	Functionalization protocol .....	93

6.2.4	LSPR and SERS detection .....	94
6.3	Results and discussion .....	95
6.3.1	Sensor work.....	95
6.3.2	Extinction measurements: nanocylinders.....	99
6.3.3	SERS measurements: nanocylinders.....	102
6.3.4	SERS measurements: nanoantennas .....	104
6.4	Conclusions .....	108
	General conclusions .....	109
	Appendix.....	111
	References .....	120
	Curriculum Vitae .....	143

---

## ***Abstract***

Bioanalytical assays are routinely used to detect analytes of interest in biological samples for applications such as pharmacokinetics, toxicokinetics, forensic investigations and environmental concerns. These assays frequently require highly sensitive detection systems for successful quantification of the target of interest in biological matrices. The necessary sensitivity can be achieved by employment of biosensors based on new biological and nano-sized materials.

This PhD thesis was focused on the development of various approaches for signal amplification in bioanalytical assays and application of these methods for the sensitive quantification of biomolecules in real samples. This work employed biochemical reactions combined with the surface chemistry of metal and semiconductor nanoparticles (NPs).

First, we designed a system for the detection of ascorbic acid (AA) based on gold NPs modified with a fluorophore labeled substrate deoxyribonucleic acid (DNA) which is cleaved by *catalyst DNA* (DNAzyme) in the presence of AA and copper (II) ions. After the oxidative breakage of *substrate DNA*, fluorescein is separated from the gold NPs surface which leads to an increase in fluorescence intensity. To perform this assay *substrate DNA* was modified with thiol groups to provide strong covalent binding with the gold surface of the NPs. The reaction conditions were optimized to maximize signal enhancement and, consequently, to provide high sensitivity. Finally, we applied the method to detect AA in real samples, such as urine, orange juice and vitamin C tablets.

We developed a further bioanalytical assay based on the self-cleaving *DNAzyme*; by combining the interesting catalytic properties of *DNAzyme* with Electrochemical Impedance Spectroscopy (EIS) we were able to sensitively detect and quantify copper ions. The assay involved immobilizing of *DNAzyme* on the surface of the electrode which then undergoes self-cleavage in the presence of copper ions and AA. These minute changes in the interfacial space of the electrode are easily converted to the detectable electrochemical signal proportional to the concentration of the analyte in the sample. To undertake this assay, *DNAzyme* was immobilized onto the surface of the electrode using avidin-biotin chemistry and the conditions of this reaction were optimized to provide maximum surface coverage. Finally, the developed assay was applied for quantification of  $\text{Cu}^{2+}$  ions.

The third approach developed for signal enhancement in conventional immunoassay is based on the generation of fluorescence CdS quantum dots (QDs) in the presence of the products of an enzymatic reaction. The conventionally used enzyme alkaline phosphatase (ALP) is able to convert enzymatically the substrate, p-nitrophenylphosphate (pNPP), into p-nitrophenol (pNP) and orthophosphate. The later is capable of stabilizing QDs generated *in situ* when in the presence of cadmium (II) and sulphide ions. In this work, the concentrations of all components of the immunoassay were optimized to maximize the generation of fluorescent CdS QDs and, therefore a high sensitivity of the desired analyte detection. The developed approach was compared with classical enzyme-linked immune sorbent assay (ELISA) which are based on colorimetric detection of the analyte rather than fluorescence.

In the last of the developed assays we fabricated nanobiosensors capable of detection human manganese superoxide dismutase 2 (MnSOD-2). This was achieved by using the optical properties of specially designed nanostructures (nanocylinders and nanorods) and a *DNA probe* binding which binds specifically with analyzed protein. Oligonucleotide was labeled with the thiol groups to provide strong chemical binding with the surface of the gold nanoarray. To avoid non-

specific adsorption of the protein to the gold nanostructure, the surface was blocked using 6-mercapto-1-hexanol (6-MHO). The presence of the protein was detected by Raman spectroscopy. This nanobiosensor allowed us to detect enhanced vibrational signal from MnSOD-2 and significantly increased the response of the system in comparison with optical methods which do not take advantage of nanoplatfoms.

## ***Resumen***

El objetivo de la química bioanalítica es realizar una medida cuantitativa de los analitos activos y/o metabolito(s) para distintas aplicaciones tales como farmacocinética, toxicocinética, ciencia forense y medioambiente. La utilización de biosensores con nuevas características permite amplificar la señal en los ensayos bioanalíticos y como consecuencia detectar las concentraciones de los analitos no detectables con técnicas analíticas habituales. Los biosensores en general transforman información de una reacción química a una señal medida por los métodos analíticos y proporcional a la concentración de un componente específico de una muestra. Ultimamente la aplicación de bio y nanoplataformas ha sido muy prometedora en el diseño de biosensores aplicables en los ensayos bioanalíticos ultrasensibles.

El objetivo principal de esta tesis es el desarrollo de nuevos biosensores y técnicas bioanalíticas basadas en las propiedades específicas de nanoestructuras metálicas y semiconductoras en combinación con biomoléculas tales como enzimas y ADN. Los métodos propuestos han demostrado el aumento de sensibilidad en la detección de varias biomoléculas y su aplicación para cuantificación de los analitos en concentraciones bajas en muestras reales.

En esta tesis, se han aplicado distintas reacciones bioquímicas y química superficial de nanomateriales, dando lugar a varios métodos bioanalíticos.

El primer ensayo descrito en el capítulo 3 está basado en la utilización de nanopartículas (NPs) de oro modificadas con ADN y está diseñado para cuantificar ácido ascórbico (AA). El ADN sustrato está marcado con un fluoróforo cuya

fluorescencia está atenuada por estar próximo a la superficie de NPs de Au. Otra cadena de ADN con propiedades catalíticas (ADNzima) en presencia de AA y  $\text{Cu}^{2+}$  es capaz de cortar el *ADN sustrato* separando partes fluorogénicas desde la superficie del oro y así provocando un aumento de fluorescencia. Para realizar este ensayo, el *ADN sustrato* estaba modificado con un grupo de tiol con el objetivo de incrementar su afinidad al oro y así cubrir el máximo la superficie de las NPs. A continuación se optimizaron las condiciones de reacción para lograr la máxima señal y rapidez de la detección de AA. Finalmente, se aplicó el método para detectar AA en las muestras reales tales como orina, pastillas de vitamina C, zumos de naranja. Los resultados obtenidos muestran que el aumento de la señal se produce debido a las propiedades únicas de las NPs del oro. Gracias a las características ópticas, las NPs de Au pueden servir como un silenciador de fluorescencia efectivo, pero la mayor contribución al aumento de la señal es debido a las propiedades catalítica de las NPs de Au.

El segundo ensayo propuesto se describe en el capítulo 4 y está desarrollado para detectar iones del cobre (II) por impedancia electroquímica. El sensor consiste de un electrodo modificado con el *ADNzima* que se somete a autoescisión en presencia de  $\text{Cu}^{2+}$  y AA. El resultado de esa reacción son pequeñas alteraciones en la interfase que producen cambios impedimétricos. En este ensayo la superficie del electrodo estaba modificada con el oligonucleótido a través de enlaces químicos entre la avidina y biotina. Las condiciones de esa reacción estaban optimizados para alcanzar la saturación de la superficie del electrodo con las moléculas de ADN y así producir la mayor señal impedimétrica. Finalmente, se aplicó el biosensor para detectar  $\text{Cu}^{2+}$  y también se investigó la influencia de los metales interferentes. Los resultados obtenidos demostraron que la *ADNzima* reconstituido con cobre cataliza la oxidación del AA llevando a cabo la acumulación de los productos de la oxidación en la superficie del electrodo produciendo un incremento de la señal impedimétrica.



El capítulo 5 está enfocado al desarrollo de un inmunoensayo fluorogénico basado en el crecimiento *in situ* de “quantum dots” (QDs) de CdS. El método aplica el protocolo de ensayos por inmunoabsorción ligado a enzimas (ELISA). La fosfatasa alcalina (ALP) unida a un anticuerpo es capaz de hidrolizar el sustrato, p-nitrofenilfosfato (pNPP), con la liberación del ión fosfato, cuya presencia estabiliza la generación de los QDs de CdS formados *in situ* a través de la reacción entre los iones  $\text{Cd}^{2+}$  y  $\text{S}^{2-}$ . La interacción entre el analito y anticuerpo se detecta por un aumento de la señal de fluorescencia debida a la formación de QDs. En este ensayo las concentraciones del sustrato y todos los componentes de la reacción estaban optimizadas para generar el máximo de crecimiento de QDs de CdS. El ensayo propuesto se comparó con ensayos clásicos de ELISA basados en la detección colorimétrica de la señal. Los resultados obtenidos demostraron que la aparición de la señal fluorogénica es debida a la formación de las NPs semiconductoras, cuya presencia se confirmó por microscopía electrónica de transmisión (TEM). La presencia del ión fosfato era necesaria para formación de los QDs, lo que se confirmó por los experimentos de control.

El último ensayo que se describe en el capítulo 6 está dirigido a la fabricación de una plataforma basada en estructuras metálicas (“nanocylinders y nanorods”) modificadas con un ADN con afinidad específica para la proteína MnSOD-2. La presencia del analito se detecta por espectroscopía Raman. Para realizar este ensayo el oligonucleótido estaba marcado con grupo tiol para conferir una mayor afinidad a la superficie de las nanoestructuras. Para evitar la adsorción inespecífica de la proteína en las nanoestructuras, las superficies se bloquearon con 6-mercaptop-1-hexanol (6-MHO). Para detección de la interacción entre el ADN y MnSOD-2, se coleccionaron los espectros de Raman en las posiciones diferentes de nanoestructura. Los resultados obtenidos demostraron la presencia de MnSOD-2 unida al ADN por la aparición de bandas vibracionales nuevas, respecto al espectro de de Raman de MnSOD-2 realizado en disolución. Finalmente, se compararon los resultados obtenidos en “nanocylinders y nanorods”.



## List of figures

Figure 2.1. Direct ELISA .....	25
Figure 2.2. Indirect ELISA .....	26
Figure 2.3. Sandwich ELISA .....	27
Figure 2.4. Schematic illustration of localized surface plasmon, reproduced with consent from [41]. .....	28
Figure 2.5. A schematic representation of a SERS experiment with molecules absorbed on a metal rough surface, showing the incident laser and Raman scattered light, the intensities of which are both influenced by the enhanced field at the metal surface resulting from surface plasmon excitation. ....	30
Figure 2.6. Solid-phase oligonucleotide synthesis cycle .....	31
Figure 3.1. Fluorometric assay for detection of AA using catalyst DNA and substrate DNA modified with fluorescein/dabcyl FRET pair across the cleavage site. ....	47
Figure 3.2. (A) Emission spectra of buffer solutions on DNAzyme based sensor that include different concentrations of AA a) 0, b) 2.5, c) 5, d) 10, e) 15, f) 40, g) 80, h) 100, i) 150 $\mu$ M, $\lambda=522$ nm. (B) The effect of AA concentration on the initial rate of substrate DNA cleavage during first 3 minutes of the assay. Inset: linear part of the calibration plot. (RSD=12.1 % , n=3). .....	48

Figure 3.3. Quantification of AA in human urine (RSD=2.9%, n=3), orange juice (RSD=5.5%, n=3), and vitamin C tablets (RSD=11.3%, n=3) with the method of standard addition.....	49
Figure 3.4. Fluorometric assay for detection of AA using catalyst DNA and gold NPs modified with DNA substrate carrying fluorescein moiety. ....	52
Figure 3.5. (A) Emission spectra of buffer solutions that include different concentrations of AA a) 0, b) 10, c) 25, d) 50, e) 75, f) 100, g) 150, h) 200, i) 250 nm, $\lambda=522$ nm. (B) The effect of AA concentration on the initial rate of substrate DNA cleavage from Au NPs during first 2 minutes of the assay. Inset: linear part of the calibration plot (RSD=16.1 %, n=3). ....	53
Figure 3.6. Quantification of AA in human urine (RSD=9.5%, n=3), orange juice (RSD=26.3%, n=3), and vitamin C tablets (RSD=25.7%, n=3) with the method of standard addition using catalyst DNA and gold NPs modified with DNA.....	54
Figure 4.1. Schematic illustration of impedimetric DNAzyme sensor for $\text{Cu}^{2+}$ .....	65
Figure 4.2. Optimization of the concentration of DNAzyme placed onto the electrode. Uncertainty values corresponding to replicated experiments (n=5).....	66
Figure 4.3. Nyquist Diagram of: (a) Electrode-buffer ●, (b) DNAzyme, and (c) AA and $\text{Cu}^{2+}$ 30 $\mu\text{M}$ .....	67
Figure 4.4. Calibration curve versus $\text{Cu}^{2+}$ concentration. Uncertainty values corresponding to replicated experiments (n = 5).....	68
Figure 4.5. Impedimetric response obtained with different metals assayed at the same concentration (30 $\mu\text{M}$ ). Uncertainty values corresponding to replicated experiments (n = 5). ....	69

Figure 5.1. Emission spectra of the CdS QDs formed in the presence of Na <sub>2</sub> S (0.3 mM), Na <sub>3</sub> PO <sub>4</sub> (0.3 mM), Cd(NO <sub>3</sub> ) <sub>2</sub> (1.25 mM) (a) and in the absence of Na <sub>3</sub> PO <sub>4</sub> (b) .....	79
Figure 5.2. Detection of ALP activity by enzymatic growth of CdS QDs. ....	80
Figure 5.3. (A) Emission spectra of CdS QDs in the system containing Cd(NO <sub>3</sub> ) <sub>2</sub> (1.25 mM), Na <sub>2</sub> S (0.9 mM), pNPP (0.5 mM), MgCl <sub>2</sub> (0.5 mM) and various concentrations of ALP: (a) 0 mU mL <sup>-1</sup> ; (b) 0.5 mU mL <sup>-1</sup> ; (c) 5 mU mL <sup>-1</sup> ; (d) 8 mU mL <sup>-1</sup> (e) 10 mU mL <sup>-1</sup> (f) 25 mU mL <sup>-1</sup> ; (g) 50 mU mL <sup>-1</sup> ; (h) 200 mU mL <sup>-1</sup> ; (i) 400 mU mL <sup>-1</sup> ; (j) 800 mU mL <sup>-1</sup> . (B) Calibration curve of ALP at λ=520 nm (RSD=3.9 %, n=3). ....	81
Figure 5.4. Emission spectra of the CdS QDs formed in the presence of Na <sub>2</sub> S (0.3 mM), Cd(NO <sub>3</sub> ) <sub>2</sub> , ALP 800 mU/mL, pNPP 0.5 mM (a) and in the absence of pNPP (b). (B) TEM image of the CdS QDs formed in the presence of Na <sub>2</sub> S (0.6 mM), ALP (250 mU mL <sup>-1</sup> ) and Cd(NO <sub>3</sub> ) <sub>2</sub> (12.5 mM), pNPP 0.5 mM.....	82
Figure 5.5. Calibration curve of ALP measured by the QD-based method (●) and the standard pNPP-based method (○). ....	83
Figure 5.6. Detection of Anti-BSA antibody based on enzymatic growth of CdS QDs. ....	84
Figure 5.7. (A) Emission spectra of CdS QDs in the system containing Cd(NO <sub>3</sub> ) <sub>2</sub> (1.25 mM), Na <sub>2</sub> S (0.9 mM), pNPP (0.5 mM), MgCl <sub>2</sub> (0.5 mM) and various concentrations of anti-BSA antibody: (a) 0 mU mL <sup>-1</sup> ; (b) 0.4 ng mL <sup>-1</sup> ; (c) 1 ng mL <sup>-1</sup> ; (d) 2.5 ng mL <sup>-1</sup> ; (e) 5 ng mL <sup>-1</sup> ; (f) 8 ng mL <sup>-1</sup> ; (g) 25 ng mL <sup>-1</sup> ; (h) 50 ng mL <sup>-1</sup> ; (i) 100 ng mL <sup>-1</sup> ; (j) 250 ng mL <sup>-1</sup> ; (k) 500 ng mL <sup>-1</sup> . (B) Calibration curve of anti-BSA antibody at λ=520 nm (RSD=9.9%, n=3).....	85
Figure 5.8. Calibration curve of anti-BSA antibody measured by the QD-based method (●) and the standard pNPP-based method (○).....	86

Figure 6.1. Schematics of illustration of labelless SERS sensor for MnSOD-2 detection. ....	96
Figure 6.2. Schematic representation of nanocylinders (A) and nanoantenna (B) based SERS substrate. ....	97
Figure 6.3. Scanning electron microscopy images of the nanocylinder (A) and nanoantenna (B) array obtained by EBL.....	98
Figure 6.4. Extinction spectra of clean gold nanocylinders. ....	99
Figure 6.5. Position of the LSPR Vs nanocylinder diameter after each deposition step.....	100
Figure 6.6. SERS spectra at excitation wavelength of 785 nm (A) and 660 nm (B) acquired on nanocylinders after each deposition step: DNA probe functionalization (black curve), 6-MHO blocking (red curve), different concentrations and incubation time with MnSOD-2 10 nM, 1h (green curve), 100 nM, 1h (blue curve), 1 $\mu$ M 1h (purple curve) and 1 $\mu$ M 18h (brown curve).....	102
Figure 6.7. SERS spectra at excitation wavelength of 785 nm acquired on nanoantennas after each deposition step: DNA probe functionalization (black curve), 6-MHO blocking (red curve), different concentrations of MnSOD-2 10 nM, 1h (green curve), 100 nM, 1h (blue curve) and 1 $\mu$ M 1h (purple curve).....	104
Figure 6.8. SERS spectra of MnSOD-2 protein after the incubation of the antennas sample in a proteins solution at concentration of 10 $\mu$ M (black curve) and 100 nM (red curve). These spectra are compared with the one acquired after the DNA probe immobilization. The arrows highlight the difference between the spectra before (blue line) and after the capture of the MnSOD-2 protein by the DNA probe. (The appeared bands are assigned to the respective vibrations of MnSOD-2, following to that what found in the Raman measurements in solution at concentration higher than 10 mM (limit of detection for our Raman setup)).....	105

Figure 6.9. Nanocylinder functionalization with the DNA probe (black curve), blocking with 6-MHO (red curve) and incubation with human serum (blue line)... 107

## ***List of abbreviations***

- 3-HPA - Hydroxypicolinic acid, 34  
6-MHO - 6-Mercapto-1-hexanol, 3  
AA – Ascorbic acid, 1  
AC - Alternating current, 35  
ACN - Acetonitrile, 38  
ALP - Alkaline phosphatase, 2  
Av–GEC - Avidin–graphite epoxy composite, 62  
BSA - Albumin from bovine serum, 76  
CBNs - Carbon based nanomaterials, 19  
CE - Capillary electrophoresis, 16  
CHCA -  $\alpha$ -Cyano-4-hydroxycinnamic acid, 34  
CNTs - Carbon nanotubes, 19  
DEA - Diethanolamine, 76  
DHB - 2, 5-Dihydrobenzoic acid, 34  
Dmc - Duanomycin, 20  
DMT - Dimethoxytrityl, 31  
DNA - Deoxyribonucleic acid, 1  
DNAzyme - catalytic DNA, 1  
DNTB - 5, 5'- Dithiobis(2-nitrobenzoic acid), 38  
dNTP - deoxynucleotide triphosphate, 17  
DTT - DL-dithiothreitol, 38  
E - electric field, 29  
EBL - Electron beam lithography, 97  
EIS - Electrochemical Impedance Spectroscopy, 2  
ELISA - Enzyme-linked immune sorbent assay, 2  
EPA - U.S. Environmental Protection Agency, 58  
FFT - Fast Fourier transformation, 35  
FP - Fluorescence polarization, 33



FRET - Förster resonant energy transfer, 50	NADH - Betanicotinamide adenine dinucleotide, 36
GEC - Graphite epoxy composite, 21	NIR - Near-infrared, 23
GO - Glucose oxidase, 17	NMI - N-Methylimidazole, 32
GO - Graphene oxide, 20	NMR - Nuclear magnetic resonance, 16
HEPES - 4-(2-Hydroxyethyl)piperazine-1-ethanesulfonic acid, 38	NPs - Nanoparticles, 1
HIV - Human immunodeficiency virus, 17	OD - Optical density, 42
HPLC - High-performance liquid chromatography, 16	OPC - Oligonucleotide purification cartridges, 32
HPR - Horseradish peroxidase, 17	PBS - phosphate buffered saline, 38
ICP-MS - inductively coupled plasma mass spectroscopy, 58	PCR - Polimerase chain reaction, 17
IgG - Immunoglobulin G, 74	pNP - p-Nitrophenol, 74
LSPR - Localized surface plasmon resonance, 28	pNPP - p-Nitrophenylphosphate, 2
MALDI - Matrix-assisted laser desorption/ionization, 33	PSA - Prostate specific antigen, 19
miRNA - MicroRNA, 19	PVC - Polyvinyl chloride, 62
MnSOD-2 - manganese superoxide dismutase-2, 2	QDs - QDs, 2
MQ - Milli-Q, 38	RCA - Rolling circle amplification, 18
MS - Mass spectrometry, 33	ROS - reactive oxygen species, 45
MS - Mass-spectrometry, 16	SDS - Sodium dodecyl sulphate, 38
	SERS - Surface enhanced Raman spectroscopy, 19

SPR - Surface plasmon  
resonance, 19

ssDNA - Single-stranded DNA, 18

TCA - Trichloroacetic acid, 32

TEAA - Triethylamine acetate  
buffer, 38

TEM - transmission electron  
microscopy, 41

TFA - Trifluoroacetic acid, 38

TOF - Time-of-flight, 34

TRF - time resolved fluorescence,  
33

UV-Vis - Ultraviolet-visible, 23

WB - Working buffer, 94

WHO - The World Health  
Organization, 58

$\lambda$  - Wavelength, 41

## ***Chapter 1. General introduction***

### **1.1 Background**

Bioanalytical assays play an important role in a variety of areas such as diagnostic medicine, pharmacokinetics, toxicokinetics, forensics, sports doping testing, bioequivalence and environmental concerns. Bioanalytical methods are used for quantitative measurements of small and large molecules: drugs and their metabolites, macromolecules, proteins and DNA. These assays often require highly sensitive detection methods for successful determination of analyte of interest in the sample.

Traditional bioanalytical tools include high-performance liquid chromatography (HPLC), mass-spectrometry (MS), capillary electrophoresis (CE), (ELISA), nuclear magnetic resonance (NMR), Infrared/Raman spectroscopy, spectrophotometry, fluorimetry and other optical methods. However, some biomolecules are undetectable by former methods. An amplification of the signal in current assays enables to detect low concentrations of the analytes.

All previously developed strategies of signal amplification in bioanalysis can be divided into molecular biological (bio-) and nano-approaches.

### 1.1.1 Bio-amplification methods

Various approaches for bio-signal amplification are based on different biomolecules, such as enzymes and DNA. Traditional ELISA method is among them. In this assay the analyte of interest (antigen or antibody) interacts with an antibody. In order to produce a measurable signal in response to a binding event, antibody (or antigen) is linked to enzyme which acts on a substrate leading products detectable by measuring characteristic properties such as absorption, fluorescence or luminescence. Enzymes are the most widely used labels in immunoassays and are especially useful in analysis of low concentrations of the target in the sample, as a single enzyme molecule can transform catalytically many molecules of substrate into a product. This amplification event provides the basis for an ultrasensitive detection of analytes through affinity interactions. Horseradish peroxidase (HPR), ALP, and glucose oxidase (GO) are the most commonly used labeling enzymes for immunoassay applications. Large quantities of ELISA tests are used in clinical laboratories for the detection of tumor markers [1-3], human immunodeficiency virus HIV [4, 5] and potential food allergens [6-8].

Polymerase chain reaction (PCR) is also one of the earliest applied techniques for signal amplification in this category and is often used in clinical assays for the detection of pathogens [9, 10] and genetic variations [11, 12]. It is capable of producing from thousands to millions of identical copies of a short DNA sequence from a single molecule of starter DNA. The method is based on amplifying of target DNA by the addition of thermostable DNA polymerase, two oligonucleotide primers, deoxynucleotide triphosphates (dNTPs) in appropriate buffer and setting the temperature cycle which consists of the repeating heating and cooling steps of the reaction mixture. Typically, PCR contains 20-40 cycles and achieves better sensitivity and high level of amplification of specific sequence in less time compare to conventional methods based on DNA sequence cloning into a vector and replicating it in a living cell.

Rolling circle amplification (RCA) is one of the modern tools that have been applied to amplify the electrochemical, optical and visual signals. In this method long single-stranded DNA (ssDNA) molecules are enzymatically synthesized on a short circular ssDNA template, such as plasmid. The process is driven by DNA polymerase and generates amplification around  $10^9$ -fold. RCA amplifies signals from proteins as well as from DNA and RNA and becomes highly versatile method with wide-ranging application in proteomics [13], biosensing [14] and nanotechnology [15].

DNAzyme-based signal amplification strategy recently became very popular in the field of bioanalysis. DNAzymes possessing several interesting catalytic functions, such as DNA phosphorylation, DNA adenylation, porphyrin metalation and DNA cleavage often find their application in biosensing as amplifying labels [16-18]. They have been widely used as signal amplifiers for highly sensitive detection of DNA and other biomolecules. Catalytic enhancement in these reactions was found to be two orders of magnitude higher compared to the uncatalysed process. The majority of these sensing approaches include inactive DNAzyme sequences with no catalytic activity which is activated upon interaction with target molecule.

### 1.1.2 Nano-amplification methods

Recently, with the development of nanotechnology and nanoscience nanomaterial-based signal amplification methods opened new horizons for bioanalysis. These novel approaches become promising for improvement of sensitivity and, therefore, miniaturization of the whole procedure. Nano-signal amplification methods are based on using nanomaterials such as metal, magnetic and semiconductor NPs, carbon nanotubes and graphene.

Au and Ag NPs exhibit several interesting properties, such as high-fluorescence quantum yields, photostability, size-dependent tunable absorbance

and fluorescence, which make them attractive fluorescence labels for biorecognition events [19-21]. The enhancement of the signal produced by Au and Ag NPs has been widely used in DNA and antibody-antigen analysis by surface enhanced Raman spectroscopy (SERS) [22-24]. Metal NPs also can be used as carriers of signaling molecules. Biorecognition elements are immobilized on the surface of NPs, providing more binding sites and therefore amplification of the signal [25, 26]. Au NPs are often employed for sensitive detection of DNA and protein targets. A nicking endonuclease assisted Au NPs amplification assay was used for recognizing of long single-stranded DNAs with single-base mismatch selectivity.

Extensive application of magnetic NPs in biosensing allowed to achieve low detection limits of the desired analyte, even reaching a femtomolar concentrations. Krishnan and co-workers have reported application of supermagnetic particles as signal amplifiers for ultrasensitive detection (10 fg/ml) of serum prostate specific antigen (PSA) by surface plasmon resonance (SPR) based immunoassay. In the other work, magnetic NPs were used for liver-specific microRNA (miRNA) detection at picogram levels.

Semiconductor NPs, also called QDs, due to their high quantum yield and superior photostability are often used as fluorescence labels in biorecognition processes, such as immunoassays for protein or nucleic acids detection [27-31]. QDs have attracted recently substantial research interest in bioanalysis. Willner and co-workers have developed aptamer or DNA sensing platforms based on CdSe/ZnS QDs with 10 nm sensitivity.

Carbon based nanomaterials (CBNs), such as carbon nanotubes (CNTs), graphene and graphene oxide possess interesting mechanical and optical properties as well as electrical and thermal conductivity. A great amount of scientific work has been focused on utilizing these advantageous properties of CNTs in various fields of biomedical assays.

CNTs with their interesting electrochemical properties offer a great advantage for amplified electrochemical detection of various analytes. Chemical functionalization of CNTs allows to attach any desired biomolecule to their surface and, therefore, to employ them as components of biosensors. CNT-based microelectrode for detection of dopamine with  $70 \text{ nmol L}^{-1}$  sensitivity was reported. The assay provides possibilities to detect dopamine at physiological concentrations in microvolume probes [32]. In other work, CNT-based electrode modified with ssDNA in the presence of electroactive intercalator daunomycin (Dmc) was used for enhanced DNA hybridization detection [33].

Graphene is a strictly two dimensional and one-atom-thick sheet, which has been attracting lately growing scientific attention because of its fascinating physicochemical properties. Excellent conductivity properties make graphene a promising material for enhanced electrochemical biosensing. Several graphene-based electrochemical biosensors for glucose detection have been reported and showed to be more sensitive in comparison with widely-investigated CNTs-based assays [34, 35]. However, graphene oxide (GO), produced by oxidation of graphite is more commonly used in biosensing than pure graphene because of the several advantages, such as dispersibility in aqueous media and presence of hydrophilic functional groups essential for chemical functionalization. Several sensitive GO-based FRET biosensors employed for the detection of target DNA and proteins was reported [36].

## 1.2 Objectives and scopes of this study

The aim of this study is to develop different approaches for the signal enhancement in bioanalytical assays and to apply developed platforms for highly sensitive and selective detection of various analytes. The scope of the research includes creating amplification systems relying on complex biochemical reactions and surface chemistry of graphite and nanomaterials.

The first objective of this PhD thesis is the development of new amplification system for AA detection based on DNAzyme served as bioreceptor immobilized on the surface of gold NPs. We shall design novel transduction method coupling extraordinary catalytic properties of gold clusters and specificity of DNA cleavage reaction towards AA. To realize the first task fluorophore-labeled *thiolated substrate DNA* will be synthesized and loaded on the surface of Au NPs. The obtained DNA-NPs conjugates then will be used for the amplified detection of AA. Experimental conditions will be optimized to achieve maximum sensitivity of the proposed method.

The second objective of this PhD thesis is the development of electrochemical biosensor for copper (II) ions detection. In this case, the amplification strategy will be based on employment of copper dependent self-cleavage *DNAzyme* loaded on the surface of graphite epoxy composite (GEC) electrode. To realize this approach oligonucleotide will be modified with biotin moiety to provide strong chemical bonding with the surface of avidin-GEC electrode. Experimental conditions, such as surface coverage will be optimized to receive maximum electrochemical response. The created method will be applied for the sensitive detection of  $\text{Cu}^{2+}$  ions.



The third objective of this PhD thesis is development of amplified immunoassay based on enzymatic growth of semiconductor QDs *in situ* in the presence of the products of biochemical reaction. The signal enhancement in current assay will be based on advantageous properties of CdS QDs, such as higher brightness, better resistance to photobleaching and longer lifetime, which will resolve the problem of high background signal of conventionally used fluorophores. To perform this method the concentrations of all participants of immunoassay will be optimized to provide maximum of QDs generation. Developed method will be applied for the detection of primary antibodies as an analyte of interest.

The fourth objective of this PhD thesis is devoted to development of gold nanoarrays in combination with DNA probe binding specifically to the target protein. The amplification strategy in this assay will be based on local electromagnetic field (EM) enhancement created by coupled and uncoupled nanostructures. To perform this method specially designed DNA probe will be modified by thiol groups on one of the ends to provide strong affinity with the gold surface of the nanostructure. Different types of nanoplatfoms will used to find maximum of EM field enhancement and, therefore protein vibrational signal amplification. The developed biosensor will be applied for the sensitive detection of MnSOD-2 protein.

## ***Chapter 2. Experimental methods***

### **2.1 UV-Vis spectroscopy**

Ultraviolet-visible (UV-Vis) spectroscopy is a routinely used method in analytical chemistry for the quantitative analysis of samples based on their absorbance spectra. Electromagnetic radiation used in UV-Vis spectrophotometry covers a range from approximately 400 to 800 nm. It corresponds to a visible and adjacent (near UV and near-infrared (NIR)) diapason. The absorption of light in this range depends on the molecular structure of each substance. When the sample is irradiated with light a portion of energy is absorbed by the molecules, and the electrons in the analyte are promoted to move from the ground state to a higher energy state orbital. The instrument used for the detection of absorbance is called a UV-Vis spectrophotometer. It records the degree of absorption by a sample at different wavelengths. The intensity of absorption of a sample in solution is directly proportional to its concentration and the path length [37].

### **2.2 Fluorescence spectroscopy**

Fluorescence spectroscopy is a type of electromagnetic spectroscopy which analyses fluorescence emission from certain molecules called *fluorophores*. When a molecule is irradiated, it absorbs the photon of energy. This energy is enough to

push electrons from the low energy state to a one of the various vibrational states in the excited electronic state. During this time (1-10 ns) excited molecules undergo conformational changes and also collide with other molecules. This causes lose of vibrational energy until the lowest vibrational state of the excited electronic state is reached. Finally the photon of lower energy, and therefore of longer wavelength, is emitted, returning the fluorophore to its ground state [38]. The amount and the wavelength of the emitted light depend on the nature of fluorophore and its chemical environment. Emission spectra are measured in a fluorescence spectrometer. Fluorescence spectroscopy is used for detection of organic compounds in biochemical, clinical and chemical fields.

## 2.3 Enzyme-linked immune sorbent assay (ELISA)

Enzyme-linked immune sorbent assay (ELISA) is a sensitive analytical test that uses antibodies as reagents and color change to identify a substance. Antibodies specifically interact with their targets, even in the presence of a huge range of other materials in the sample [39]. ELISAs involve stepwise addition and reaction of reagents with a solid phase-bound substance, through incubation and separation of bound and free reagents using washing steps [40]. ELISA has three basic parameters: one reactant is attached to a solid phase, usually a plastic microtiter plate with in 8 x 12-well format; reagents are added subsequently and the simple washing step is used to remove unbound material; color change during the enzymatic reaction is used for quantification of the analyte. ELISAs can be divided in three major groups: *direct*, *indirect* and *sandwich* ELISA.

In *direct* ELISA analyte (antigen) is adhered to the plastic by passive adsorption (Figure 2.1, Step 1).

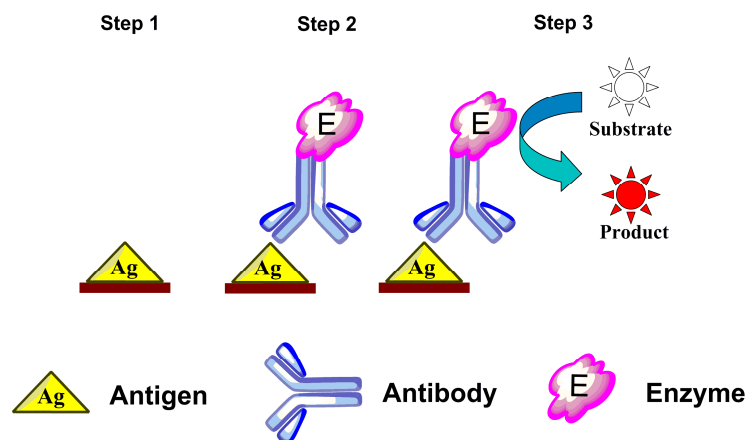
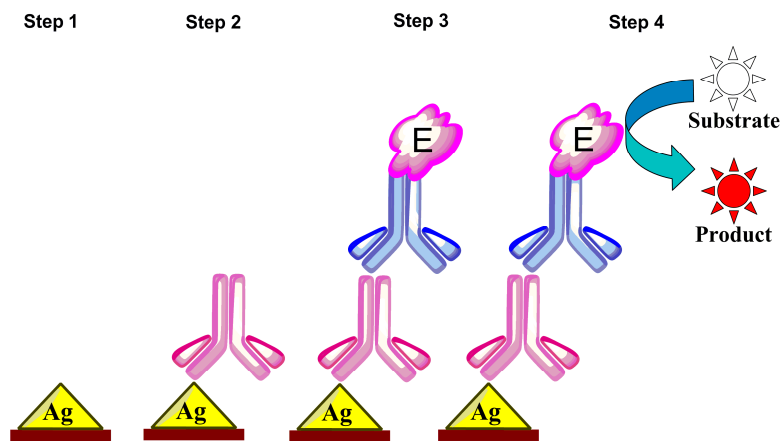


Figure 2.1. Direct ELISA

After incubation, any non-bound antigen is washed away and enzyme-conjugated primary antibodies are added (Figure 2.1, Step 2). After an incubation period and washing, a substrate solution is added (Figure 2.1, Step 3). The change of the color upon the reaction of substrate and enzyme is detected by spectrophotometer.

The first stage of *indirect* ELISA is similar to the direct system in which the antigen is directly attached to the solid phase (Figure 2.2, Step 1). After the washing step, unlabeled primary antibodies are added (Figure 2.2, Step 2). This is followed by incubation and washing away of unbound antibodies to achieve specific binding. Any bound antibodies are detected by the addition of enzyme labeled secondary antibodies (Figure 2.2, Step 3), again followed by incubation and washing. Substrate is added on the next stage (Figure 2.2, Step 4) and color development is monitored by spectrophotometer.



**Figure 2.2.** Indirect ELISA

*Sandwich* ELISA involves the passive attachment of capture antibodies to the solid phase (Figure 2.3, Step 1). These capture antibodies then bind antigen(s) that are added in the next stage (Figure 2.3, Step 2). In the next stage specific for this antigen unlabeled antibodies are introduced (Figure 2.3, Step 3). After incubation and washing, enzyme-linked secondary antibodies are applied (Figure

2.3, Step 4). The plate is washed to remove the unbound species. The bound conjugate is then processed as described in the other system (Figure 2.3, Step 5).

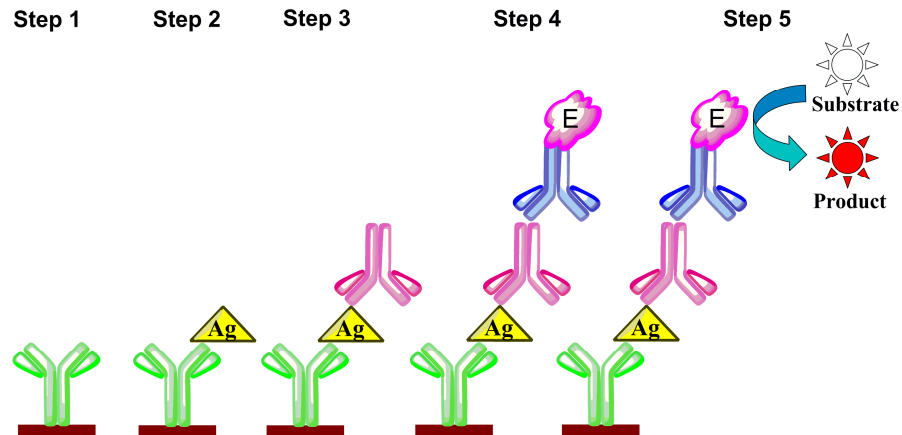


**Figure 2.3.** Sandwich ELISA

ELISA can be performed in a qualitative or quantitative format. Qualitative analysis provides simple negative or positive result for a sample of interest. To distinguish positive sample from negative two or three times the standard deviation (error inherent in a test) is usually used. Quantitative analysis is based on a comparison of optical density (OD) of the sample with unknown concentration of the analyte to a standard curve, which represents a serial dilution of a known-concentration solution of the target molecule.

## 2.4 Localized surface plasmon resonance (LSPR)

Localized surface plasmon resonance (LSPR) is an optical phenomenon generated when light is trapped by conductive NPs that are smaller than the incident wavelength. LSPR is a result of the interactions between the incident light and electron density of each NP [41]. This interaction causes collective oscillations of electrons in metallic NPs (Figure 2.4).

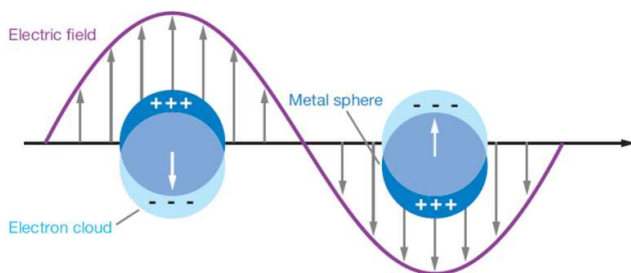


**Figure 2.4.** Schematic illustration of localized surface plasmon, reproduced with consent from [41].

The collective charge oscillation causes a large resonant enhancement of the local field inside and near NP. The maximum of the enhancement is located at the NP surface and decays fast at the nanoparticle-dielectric background interface. LSPR depends on the size, shape, composition, surrounding medium and particle-particle separation distance of NPs. Small alterations in local dielectric environment of the NPs affect the LSPR, which is revealed as changes in the amount of scattered and/or absorbed light at various wavelengths. This difference is exhibited in spectral shift of extinction (absorption plus elastic light-scattering) and scattering spectra. For many organic molecules with a relatively high refractive index

compared to solvent or air, binding to NPs leads to a red shift. Nanostructures that support plasmons find extensive application in fluorescence enhancement [42], biomolecular interaction detection [43] and surface-enhanced Raman scattering [44].

## 2.5 Surface enhanced Raman spectroscopy (SERS)

Surface-enhanced Raman spectroscopy (SERS) is a technique in which Raman Scattering intensity from an analyte absorbed on the rough metal surfaces is greatly enhanced. The enhancement factor can be as much as  $10^8$  to  $10^{14}$  for different systems, which means the method is capable to detect a single molecule [45-49]. Raman spectra arise from the vibrational frequencies of molecules and provide “molecular fingerprint” information that is particularly valuable in chemistry. The inherently low sensitivity of conventional Raman scattering limits its application in bioanalysis, but sensitivity enhancement by SERS has resulted in more widespread function, especially in surface chemistry where the environmental sensitivity of vibrational spectra reveals how molecules interact with surfaces [50]. Two main contributors to the intensity enhancement in SERS are electromagnetic and chemical effects [48]. Electromagnetic mechanism arises from the laser excitation of localized surface plasmon (collective electron oscillation) at rough metal surfaces, which creates an enhanced electric field ( $E$ ). Both the incident and scattered light are influenced by this field enhancement, resulting in a total Raman signal enhancement proportional to  $E^4$ . The experimental situation is shown in Figure 2.5.



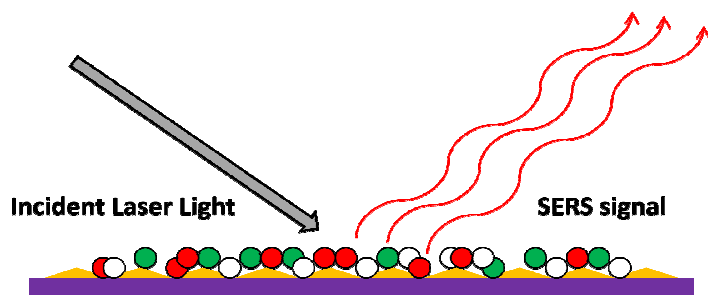


**Figure 2.5.** A schematic representation of a SERS experiment with molecules adsorbed on a metal rough surface, showing the incident laser and Raman scattered light, the intensities of which are both influenced by the enhanced field at the metal surface resulting from surface plasmon excitation.

Chemical enhancement comes from a charge transfer mechanism for adsorbed molecules with appropriate acceptor or donor orbitals that interact with the metal substrate. The metals exhibiting the largest SERS enhancement are silver, gold and copper. SERS occurs when molecules are brought to the surface of metal in a variety of morphologies. Molecules adsorbed in the first layer on the surface show the largest enhancements.

## 2.6 Solid-phase oligonucleotide synthesis

Solid-phase oligonucleotide synthesis is carried out on a glass support by a subsequent addition of phosphoramidites to the 5'-end of the growing chain until the desired sequence is hanged out [51]. The first monomer is linked to a solid support by the 3'-OH while 5'-OH terminus is protected by dimethoxytrityl (DMT) group. Each nucleoside is attached through synthetic cycle illustrated in Figure 2.6.

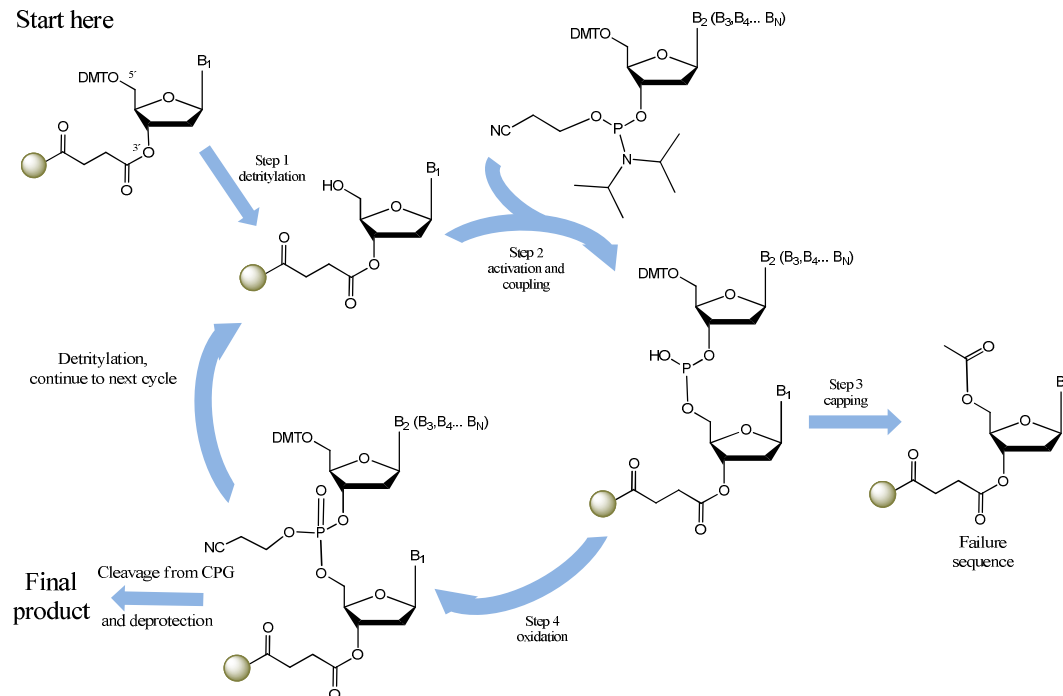


**Figure 2.6.** Solid-phase oligonucleotide synthesis cycle

The cycle consists of four steps: de-blocking (detritylation); coupling; capping and oxidation. In the classic de-blocking step, the DMT protection group is removed with a solution of trichloroacetic acid (TCA) leaving a reactive 5'-hydroxyl group on the first base. In the coupling step, the phosphoramidite monomer is activated by a weak acidic tetrazole. This mixture is delivered to support-bound nucleoside whose 5'-hydroxyl group rapidly reacts with the activated phosphoramidite moiety, creating a phosphate triester linkage. After the completion of coupling reaction, a few unreacted 5'-hydroxyl groups on the resin-bound nucleotide are left. To prevent the formation of the chains with lack of one base the 5'-OH group is further blocked using mixture of acetic anhydride and N-methylimidazole (NMI). The phosphite-triester (P(III)) formed in the previous step is unstable under the conditions of oligonucleotide synthesis, it must be converted to a stable P(V) species. This is achieved by treatment with iodine solution in the presence of water and pyridine. The cycles (Figure 2.6, Steps 1-4) are repeated until desired amount of phosphoramidites have been added to the oligonucleotide. After having synthesized the full length sequence, the oligonucleotide is then cleaved from the support and deprotected incubating the chain in concentrated ammonia at elevated temperature for an extended amount of time. Afterwards, the oligonucleotide is ready for further desalting or purification on oligonucleotide purification cartridges (OPC) or by HPLC.

## 2.7 Plate reader

The plate reader is one of the most basic laboratory instruments used in detection of biological, physical and chemical events. There is a wide variety approaches to detect changes in the sample: photometry, fluorimetry, luminometry, time resolved fluorescence (TRF), fluorescence polarization (FP). The most common microplate format used in academic research laboratories or clinic diagnostic laboratories is 96-well with a typical reaction volume between 100 and 200  $\mu\text{l}$  per well. The principle of working of microplate reader is based on illumination of the sample using a specific wavelength. Then adsorbed or emitted light coming from each well is quantified by a detector. The range of application of fluorescent mode is much broader than the absorbance detection. The main advantage of fluorescence detection is higher sensitivity, as well as application range, given the wide selection of fluorescent labels available today.

## 2.8 Matrix-assisted laser desorption/ionization mass spectrometry (MALDI-MS)

The general objective of mass spectrometry (MS) is generation and subsequent detection of separate gas-phase ions. Matrix-assisted laser desorption/ionization (MALDI) is a soft ionization technique used in MS for analysis of large biomolecules [52]. First, the sample is introduced in the crystalline structure of small organic compound (matrix) and deposited on a MALDI plate (usually a metal plate specially designed for this purpose). The cocrystallized analyte

molecules are irradiated with a UV laser beam with a wavelength of 266 or 337 nm. The laser energy causes ablation of upper layer (~micron) of the matrix material and generates a hot plume (a particle cloud) from which ions are extracted in the electric field (E). Following accelerating through the E, the ions enter in the field-free tube. During the flight through the drift space different molecules are separated according to their mass to charge ratio and reach the detector at different times. The method of MS that exploits this phenomenon is called time-of-flight (TOF) MS. The TOF mass analyzer is mainly used with MALDI to determine ion masses (mass-to-charge ratios [m/z]).

The quality of spectra in terms of resolution, mass accuracy, signal-to-noise ratio, and sensitivity is highly dependent on sample preparation and the choice of matrix compound [53]. The standard method for sample preparation is the so-called dried droplet method [54], when the small volume of highly diluted sample solution is mixed with a near saturated solution of matrix. After, the mixture is allowed to dry before introducing into spectrometer. There are different matrices for various classes of analytes and analytical problems. The commonly used matrices for peptides and proteins are  $\alpha$ -cyano-4-hydroxycinnamic acid (CHCA), sinapinic acid and 2, 5-dihydrobenzoic acid (DHB). 3-Hydroxypicolinic acid (3-HPA) is the best matrix for oligonucleotides analysis [55]. MALDI-TOF MS is applied for detection and characterization of proteins, peptides, oligosaccharides and oligonucleotides, with molecular masses between 400 and 350,000 Da.

## 2.9 Electrochemical impedance spectroscopy (EIS)

Electrochemical impedance spectroscopy (EIS) is a method applied to the characterization of electrode processes and complex interfaces. Electrochemical impedance is usually measured by applying an alternating current (AC) potential to an electrochemical cell and then measuring the current through the cell. Assume that we apply a sinusoidal potential excitation. The response to this potential is an AC current signal. This current signal can be analyzed as a sum of sinusoidal functions (a Fourier series). The fast Fourier transformation (FFT) is used to convert the current signal into the frequency domain. EIS data are commonly analyzed by fitting it to an equivalent electrical circuit model. Most of the circuit elements in the model are common electrical elements such as resistors, capacitors, and inductors. To be useful, the elements in the model should have a basis in the physical electrochemistry of the system. As an example, most models contain a resistor that models the cell's solution resistance. Analysis of the system response contains the information about the interface, its structure and reactions taking place there. In the majority of EIS experiments a fixed sinusoidal voltage is applied by a potentiostat across a 3 electrode cell containing (normally) a solution of electrolyte which is in contact with the molecules of analyte [56]. The amplitude and load (viz. magnitude of the voltage) of the fixed sinusoidal voltage should be dependent upon the type of molecular system under investigation.

## ***Chapter 3. DNA-decorated nanoparticles as nanosensors for rapid detection of ascorbic acid***

### **3.1 Introduction**

Catalytic RNA and DNA oligonucleotides (RNAzymes and DNAzymes) are employed as recognition elements, and as a means for transduction and amplification of the read out signal in analytical chemistry [57]. DNAzymes are capable of cleaving RNA in the presence of  $\text{Pb}^{2+}$  and  $\text{Mg}^{2+}$  [58, 59],  $\text{Ca}^{2+}$  and  $\text{Cd}^{2+}$  [60],  $\text{Tb}^{3+}$ ,  $\text{Tm}^{3+}$ ,  $\text{Lu}^{3+}$  [61]. The  $\text{Pb}^{2+}$ -dependent DNAzyme was frequently utilised to quantify lead ions [62, 63]. The DNA aptamer forming a complex with hemin [64-66] also found numerous applications for detection of DNA. Self-assembly of a supramolecular hemin-nucleic acid with peroxidase-like activity modulated by target oligonucleotides was reported [67-70]. DNAzymes catalyzing redox reactions are frequently damaged during their operation by free radicals originating from reductants [66]. The DNA cleaving activity of many reducing agents such as betanicotinamide adenine dinucleotide (NADH) and AA was reported in the literature long before invention of DNAzymes [71, 72]. AA is a radical scavenger providing protection against free radicals. Nevertheless, in the presence of oxygen this compound yields hydrogen peroxide [73] causing the strand breakage of DNA in chromosomes. The degree of DNA cleavage with participation of AA is significantly

increased in the presence of copper ions [72]. AA or Vitamin C is naturally occurring in fruits and vegetables. It is also used as antioxidant in food and beverages [74]. On the other hand, it behaves as copper dependent prooxidant leading to oxidative DNA breakage in lymphocytes and lymphocyte nuclei [75]. The detection of this controversial vitamin has attracted great attention in clinical, pharmaceutical and food industry. Previously reported methods for its quantification include titration [76, 77], spectrophotometry [78, 79], optosensors based on Prussian blue modified beads [80] liquid chromatography [81, 82], capillary electrophoresis [83-85], electrochemistry using different catalysts of electrochemical AA oxidation such as cobalt tetramethylpyridopyrroazine [86], enlarged gold NPs self-assembled on Au-electrode through 2,5-dimercapto-1,3,4- thiazole [87], gold NPs deposited on poly(dimethylsiloxane) [88], potentiometry with a solvent polymeric membrane electrode [89], electrocatalytic voltammetry with Methylene Blue [90]. Colorimetric detection of AA based on formation of anisotropic silver nanoparticle was reported [91]. AA was detected in the microtiter reader plates modified with polyaniline, which changed its optical absorption upon reduction [92]. The commercially available colorimetric/titration assays suffer from bad detection limit (10–50 mg/l) and relatively high price (AA kits from Hach and Alfa Aesar). Other methods suffer from long analysis times during which AA degrades [81], overestimates due to the presence of other reducing compounds in a sample [76], electrode fouling [93], overlapping UV spectra of other matrix molecules [79, 94]. The recently published fluorescence probe for AA requires the complicated synthesis of phthalocyaninatosilicon covalently linked to one or two tetramethyl-1-piperidinyloxyl radicals. It has demonstrated poor sensitivity [95]. The detection limit of this assay is 0.5 mM. Here we report a new fluorometric assay for quick and more sensitive quantification of AA by following the rate of oxidative breakage of DNA with the oxidative deoxyribozyme dependent on  $\text{Cu}^{2+}$  [96, 97].



## 3.2 Experimental part

### 3.2.1 Materials and methods

L-Ascorbic acid, 4-(2-hydroxyethyl)piperazine-1-ethanesulfonic acid (HEPES), sodium hydroxide, potassium chloride, sodium chloride, copper (II) chloride, gold (III) chloride trihydrate, 5, 5'- dithiobis(2-nitrobenzoic acid) (DNTB), sodium citrate tribasic dihydrate, phosphate buffered saline system (PBS), ammonium hydroxide solution 28%-30%, ammonium citrate dibasic, DL-dithiothreitol (DTT), 3-hydroxypicolinic acid (3-HPA), sodium dodecyl sulfate (SDS) were purchased from Sigma-Aldrich (Spain). Standard DNA phosphoramidites, Fluorescein-dT-CE Phosphoramidite, Dabcyl-dT-CE Phosphoramidite, Spacer-CE Phosphoramidite 18, 5'-Thiol-Modifier C6-CE Phosphoramidite and other reagents required for solid-phase oligonucleotide synthesis were purchased from Link Technologies (UK). Oligonucleotide purification cartridges (OPG), 2.0 M triethylamine acetate buffer (TEAA), trifluoroacetic acid (TFA), acetonitrile (ACN) were ordered in Applied Biosystems (Spain). NAP<sup>TM</sup>-5 columns for oligonucleotides desalting were purchased in GE Healthcare Life Science (UK). Milli-Q (MQ) water (18.2 M $\Omega$ ) was used to prepare all solutions.

### 3.2.2 Preparation and characterization of oligonucleotides

**Synthesis of oligonucleotides.** Following DNA sequences were synthesized: *catalyst DNA* (5'-TAA ATC TGG GCC TCT TTT TTA AGA AC-3'); *substrate DNA*:(5'-TTC TAA T<sub>D</sub>AC GAT<sub>F</sub> TTA-3'), where T<sub>D</sub> and T<sub>F</sub> are dabcyl-dT

and fluorescein-dT respectively; *thiolated substrate DNA* (5'-HS (-O-CH<sub>2</sub>-CH<sub>2</sub>-O)<sub>6</sub> TTC TAA TAC GATF TTA-3'), where (-O-CH<sub>2</sub>-CH<sub>2</sub>-O)<sub>6</sub> corresponds to spacer-CE phosphoramidite 18. Synthetic DNA oligonucleotides were prepared by automated solid-phase chemical synthesis on 3400 DNA synthesizer (Applied Biosystems). The powdered prepackaged phosphoramidites were dissolved in anhydrous ACN at 0.1 M concentration and attached manually to DNA synthesizer ports. The oligonucleotide sequence was created using Web Browser connected to 3400 DNA Synthesizer. The synthesis run was set up by creating a custom cycle script with modified coupling times for fluorescein-dT CE phosphoramidite and dabcyI-dT CE phosphoramidite. The synthesis was realized in 1 μM scale. The DNA was synthesized on the solid-phase column with the first appropriate phosphoramidite attached. After the synthesis was finished the column was removed from the 3400 DNA Synthesizer and the oligonucleotide was collected to a tightly sealed oligonucleotide collection vial. Base deprotection step was performed by ammonolysis reaction. 1.5 ml of concentrated ammonium hydroxide was added to the collection vial with oligonucleotide. After it was placed in the heating block (Eppendorf) and heated for 8-15 hours at +55 °C while shaking. After the oligonucleotide solution in ammonium hydroxide was put in a refrigerator for 10 minutes and the later was removed by vacuum. Final purification of oligonucleotide was performed on the OPC cartridge.

***Purification of oligonucleotides.*** Cleaved and deprotected on the previous stage oligonucleotide was purified using OPC column. The 5-ml Luer slip-tip syringe was connected to the end of the OPC cartridge, a male-to-male Luer tip was connected to other end. The OPC cartridge was flushed with 5 mL of HPLC-grade ACN followed by 5 mL of 2.0 M TEAA. Crude deprotected oligonucleotide was diluted by deionized water to achieve final volume of 1.5 ml. The above solution was loaded to the syringe and gently pushed through the column, collecting the eluted fractions. The eluate was reloaded and pushed through the cartridge again. The column was flushed with 5 ml of 1.5 M ammonium hydroxide and then twice with 5

ml of deionized water. The OPC cartridge-bound oligonucleotide was detritylated by 3% solution of TFA. 1 mL of TFA was gently pushed through the column and incubated for 5 minutes. After incubation step, remaining TFA solution was flushed through the cartridge, followed by washing with 5 ml of deionized water (twice). Purified, detritylated oligonucleotide was slowly eluted with 1 mL of 20 % ACN/H<sub>2</sub>O solution. The concentration of pure oligonucleotide was determined by measuring absorbance at  $\lambda=260$  nm on ND 1000 Spectrophotometer. The oligonucleotide solution was lyophilized and 200  $\mu$ M aliquots were prepared in Milli-Q sterilized water and stored at -80 °C. The purity of the prepared oligonucleotides was further analyzed by MALDI-TOF MS.

**MALDI-TOF spectra measurements.** *Matrix:* 50 mg/ml of 3-HPA in 50:50 H<sub>2</sub>O/ACN; *Ammonium citrate dibasic solution:* 50 mg/ml in water; *DNA samples:* 10<sup>-5</sup>-10<sup>-6</sup> M in 50:50 H<sub>2</sub>O/ACN. The dried droplet method of the sample preparation was used: matrix and ammonium citrate dibasic solution were mixed in proportion 9:1. First, 0.9  $\mu$ l of above prepared solution was spotted on a metal plate and after 0.1  $\mu$ l of DNA sample was spotted onto matrix and allowed to co-crystallize. The spectra were scanned on Voyager-DE PRO workstation in linear, static acceleration mode, with negative polarity and accelerating voltage 20000 V. MALDI-TOF spectra of *catalyst DNA* (Figure A-1, Appendix), *substrate DNA* (Figure A-2, Appendix) and reduced by DTT *thiolated substrate DNA* (Figure A-3, Appendix) were typically acquired by averaging 20-25 laser shots. Each sample was spotted up to three times to a MALDI plate.

### 3.2.3 Gold NPs synthesis and characterization

**Synthesis of gold NPs.** 13 nm Au particles were prepared using citrate for reduction of Au<sup>3+</sup> [98]. Firstly, all glassware was cleaned in aqua regia (HCl/HNO<sub>3</sub> 3:1 v/v), rinsed with nanopure water and then oven dried prior to use. Vigorously vortexed, 250 ml of 1 mM water solution of HAuCl<sub>4</sub> was brought to boiling in an oil

bath (at 125-150 °C). After, 25 ml of 38.8 mM trisodium citrate was added rapidly to the flask while stirring. The resulting solution changed color from pale yellow to dark blue and then red. After the color change, the solution was refluxed for additional 15 minutes and then removed from the heating mantle.

**Characterization of gold NPs.** Au NPs prepared in the previous section were characterized using ND-1000 Spectrophotometer in the wavelength range from 220 to 750 nm (Figure A-4, Appendix). The surface plasmon resonance (SPR) spectrum possessed maximum at 519 nm, from which the size of the NPs was estimated and showed to be 13 nm. This value was further confirmed by transmission electron microscopy (TEM) (Figure A-5, Appendix). Using Beer's law ( $A = \epsilon * b * c$  where  $A$  is the absorbance represented in absorbance units (A),  $\epsilon$  is the molar extinction coefficient expressed with units of  $M^{-1}cm^{-1}$ ,  $b$  is the path length in cm, and  $c$  is the analyte concentration in M), the particle concentration of citrate stabilized Au NP solution was determined to be 11 nM; the extinction coefficient of 13 nm Au NPs at  $\lambda=520$  nm is  $2.7 \times 10^8 M^{-1}cm^{-1}$ .

### 3.2.4 Preparation of oligonucleotide modified gold NPs

**Reduction of thiolated substrate DNA.** Gold NPs received on the previous stage were functionalized with *thiolated substrate DNA*. Prior to use, the disulfide functionality of the oligonucleotide was reduced by the reaction with DTT. Lyophilized oligonucleotide was redispersed in 400  $\mu$ l of 0.1 M DTT, 0.18 M phosphate buffer (PB) (pH 8.0) and incubated at room temperature for 2 h. The cleaved oligonucleotide was then purified using desalting NAP-5 column. The column was equilibrated with 0.01 M PB (pH 8.0) and 400  $\mu$ l of reduced DNA was applied. Purified sample was eluted from the column with 0.01 M PB (pH 8.0) and quantified by measuring absorbance  $\lambda=260$  nm. The presence of a free thiol groups in DNA was detected using DNTB (Ellman's reagent). The product of the reaction

between thiolated oligonucleotide and Ellman's reagent was detected by measuring absorbance at  $\lambda=412$  nm.

**Loading of the DNA on the surface of gold NPs.** Freshly cleaved oligonucleotide was mixed with gold NPs (1 OD of DNA/1 ml of Au NPs, where OD is optical density), and solution was brought to 0.01 M PB (pH 8.0), 0.01 % SDS. After 20 minutes of incubation, the concentration of sodium chloride was increased to 0.05 M using 2 M NaCl in 0.01 M PB, while maintaining an SDS concentration equal to 0.01%. After, the DNA/gold NP solution was sonicated for 10 s and incubated for 20 min at RT. The process was repeated for one more increment of 0.05 M NaCl and after for every 0.1 M increment of NaCl until a concentration of 1 M NaCl was achieved. After overnight incubation, the excess of oligonucleotide was removed by centrifugation (20 min, + 4°C, 14 000 x rpm). After elimination of the supernatant, the red pellet was dissolved in 0.01 M PB solution. This washing process was repeated for a five total supernatant removal. The particles then were resuspended in 0.01 M PB.

**Quantification of the DNA on the surface of gold NPs.** To quantify the amount of oligonucleotide loaded on each particle, the concentration of the fluorescent DNA and the concentration of NPs in each sample were determined. The concentration of Au NPs in each aliquot was determined via Beer's law. The maximum of absorbance at  $\lambda=524$  nm and extinction coefficient of 13 nM GNPs ( $\epsilon=2.7 \cdot 10^8 \text{ M}^{-1}\text{cm}^{-1}$ ) were used for calculations. In order to determine the concentration of fluorescent DNA in each sample, it was chemically displaced from the surface of NPs by overnight incubation with 0.1 M DTT in 0.18 M PB (pH 8.0). To separate released DNA from gold precipitate, the sample was centrifuged. The fluorescence of the supernatant was measured and compared with the standard curve, prepared in the equal conditions (0.1 M DTT, 0.18 M PB (pH 8.0)). The fluorophore was excited at 495 nm and the emission was collected at 522 nm.

### 3.2.5 Quantification of AA by *catalyst DNA* and *substrate DNA*

**Sensor preparation.** In this experiment, 10  $\mu\text{l}$  of 10  $\mu\text{M}$  *substrate DNA*, 10  $\mu\text{l}$  of 20  $\mu\text{M}$  *catalyst DNA*, 10  $\mu\text{l}$  of 300  $\mu\text{M}$   $\text{CuCl}_2$  were subsequently added to 50  $\mu\text{l}$  of HEPES buffer (1 M KCl, 1 M NaCl, 100 mM HEPES (pH 7.0)). After, 10  $\mu\text{l}$  of freshly prepared aqueous solution of various concentration of AA (from 0 to 1.5 mM) was added to the reaction mixture. The final reaction volume was 100  $\mu\text{l}$ .

**Detection.** The above prepared microtiter plate was placed into a Varioscan Flash spectral scanning multimode reader and fluorogenic assay was performed at the kinetics mode by exciting at 495 nm and collecting emission at 522 nm with 3 minute interval.

### 3.2.6 Quantification of AA by *catalyst DNA* and Au NPs decorated with *thiolated substrate DNA*

**Sensor preparation.** In this experiment, 10  $\mu\text{l}$  of 6.6  $\mu\text{M}$  Au NPs decorated with thiolated *substrate DNA*, 10  $\mu\text{l}$  of 20  $\mu\text{M}$  *catalyst DNA*, 10  $\mu\text{l}$  of 300  $\mu\text{M}$   $\text{CuCl}_2$  were subsequently added to 50  $\mu\text{l}$  of HEPES buffer. After, 10  $\mu\text{l}$  of freshly prepared aqueous solution of various concentration of AA (from 0 to 2.5  $\mu\text{M}$ ) was added to the reaction mixture.

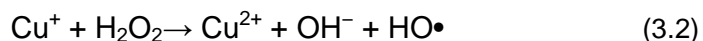
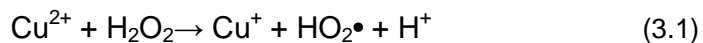
**Detection.** The above prepared microtiter plate was placed into a Varioscan Flash spectral scanning multimode reader and fluorogenic assay was performed at the kinetics mode by exciting at 495 nm and collecting emission at 522 nm with 2 minute interval.

### 3.2.7 Determination of AA in real samples

All measurements were performed following the working procedure described for the standard AA solution. Vitamin C tablets (Cebión 1000, Merck, Spain), orange juice (Pascual) and urine were used as real samples for detection of AA concentration. A portion of vitamin C tablets was dissolved in 100 ml of MQ water, orange juice containing fruit pulp was centrifuged and supernatant was collected, urine was used without any treatment. The standard addition method was performed to determine AA concentration in real samples. The following procedure was performed: to 10  $\mu\text{l}$  of unknown concentration of the sample was added increasing volume (0, 2, 5, 8, 10  $\mu\text{l}$ ) of 50  $\mu\text{M}$  AA. The mixture was introduced to the sensor solution described in 3.2.5 and 3.2.6 and kinetics of the reaction was measured.

### 3.3 Results and discussion

Oxidative breakage of DNA is caused by reactive oxygen species (ROS) among which hydroxyl radicals (HO•) are the most active ones. Usually, they are produced via Fenton-type reactions with participation of transition metal ions such as copper or iron in the presence of H<sub>2</sub>O<sub>2</sub> or AA [99]. Resulting hydroxyl radicals are so reactive that they oxidize any neighboring molecules including proteins and DNA. Degradation of these biopolymers by OH• *in vivo* initiates the process of programmed cell death, apoptosis, or carcinogenesis in multicellular organisms. The mechanism of DNA oxidative breakage *in vitro* was studied in earlier work [72]. The primary agents of DNA cleavage are hydroxyl radicals generated by the interaction between hydrogen peroxide and Cu<sup>2+</sup> ions during which Cu<sup>2+</sup> is reduced to Cu<sup>+</sup> by H<sub>2</sub>O<sub>2</sub>. Then Cu<sup>+</sup> reacts with H<sub>2</sub>O<sub>2</sub> to give OH• radicals according to the following equations:



Hydrogen peroxide can be produced by the oxidation of AA (AA) with oxygen as follows.





Generation of great quantity of hydroxyl radicals via DNA breakage in a  $\text{Cu}^{2+}/\text{AA}$  system at neutral pH was monitored experimentally [100]. Extreme reactivity of  $\text{OH}\cdot$  radicals towards water molecules limits even their short distance migration in aqueous solutions. Therefore, hydroxyl radicals tend to break DNA strands in close vicinity to the site of their formation. It was demonstrated that  $\text{Cu}^{2+}$  ions bind strongly to the guanosine and cytidine bases of calf-thymus DNA at physiological pH perturbing the A-T base pairs and disrupting its double helical structure in the presence of hydrogen peroxide [101]. The AA dependent DNA-cleaving DNAzyme was published by the group of Breaker [102]. According to the original report the DNA substrate should have the following sequence: 5'-YYYYAATACGNNNNN-3', where Y and N represent pyrimidine base and any nucleotide, respectively (corrected from the previously published paper). AATACG is the conserved sequence domain. The authors claim that according to their experimental results the DNA substrate is cleaved between the last G base of the conserved domain and the first of any nucleotide, i.e. between G and N bases. The previously reported DNAzyme had the following sequence: 5'-NNNNNCTGGGCCYYYYTTTTRRRRAC-3', where R represents purine base (corrected from the previously published paper). The DNAzyme binds to its substrate through Watson–Crick and Hoogsteen hydrogen bonding according to Figure 3.1. We used the sequences of the DNAzyme and its DNA substrate as a basis for our fluorogenic assay for AA. In previously published works the extent of DNA breakage caused by AA was evaluated by gel electrophoresis. This method is time consuming and inconvenient to study the kinetics of DNA cleavage in real time and assess the effect of varying concentrations of AA on the reaction rate. To facilitate the real time kinetics study we synthesised substrate DNA modified with quencher, dabcyI-dT, and fluorescent dye, fluorescein-dT (Figure 3.1). The latter recovers its fluorescence upon irreversible oxidative cleavage from quenching moiety according to Figure 3.1.

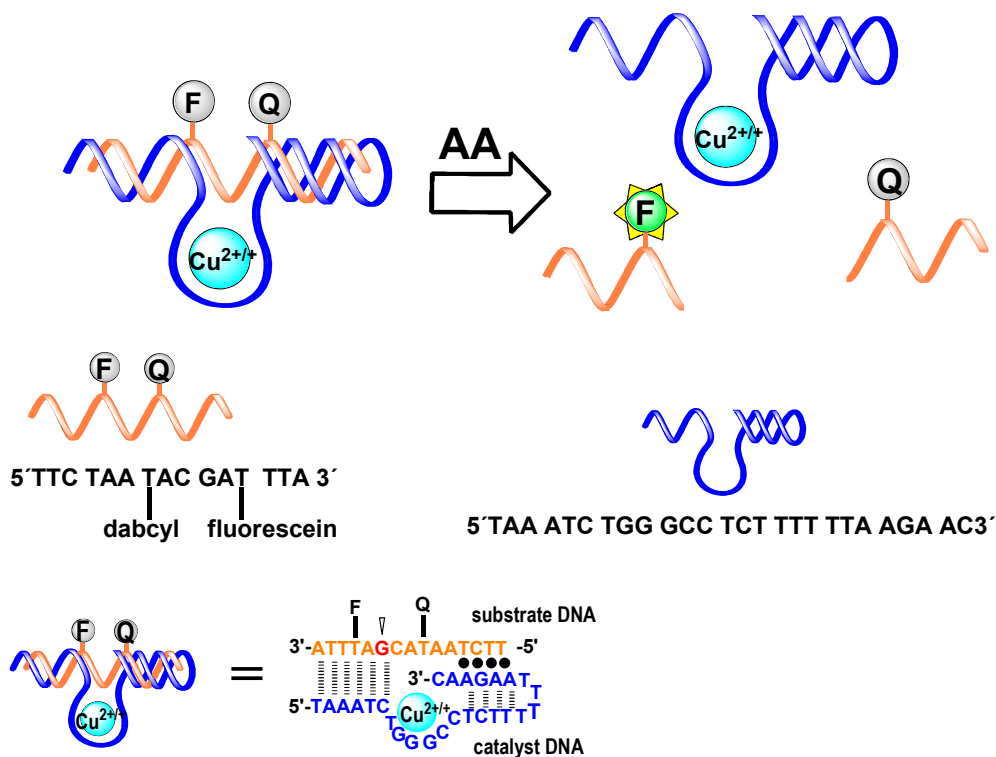


**Figure 3.1.** Fluorometric assay for detection of AA using catalyst DNA and substrate DNA modified with fluorescein/dabcyyl FRET pair across the cleavage site.

This assay for AA requires copper ions in buffer for operation of the DNAzyme. We found out that the modification of thymine nucleotides with fluorescein and dabcyyl did not prevent recognition of substrate DNA by catalyst DNA through Watson–Crick and Hoogsteen hydrogen bonding, depicted as bold dots between catalyst DNA and substrate DNA in Figure 3.1. The sequences for DNAzyme/substrate binding were optimised by us in order to achieve the maximum reaction rate at low AA concentrations. Figure 3.2 (A) shows the emission spectra of DNAzyme/substrate complex in the presence of variable concentrations of AA, using a fixed reaction

time interval of 3 min. The fluorescence of the system rises when the amount of AA increases.

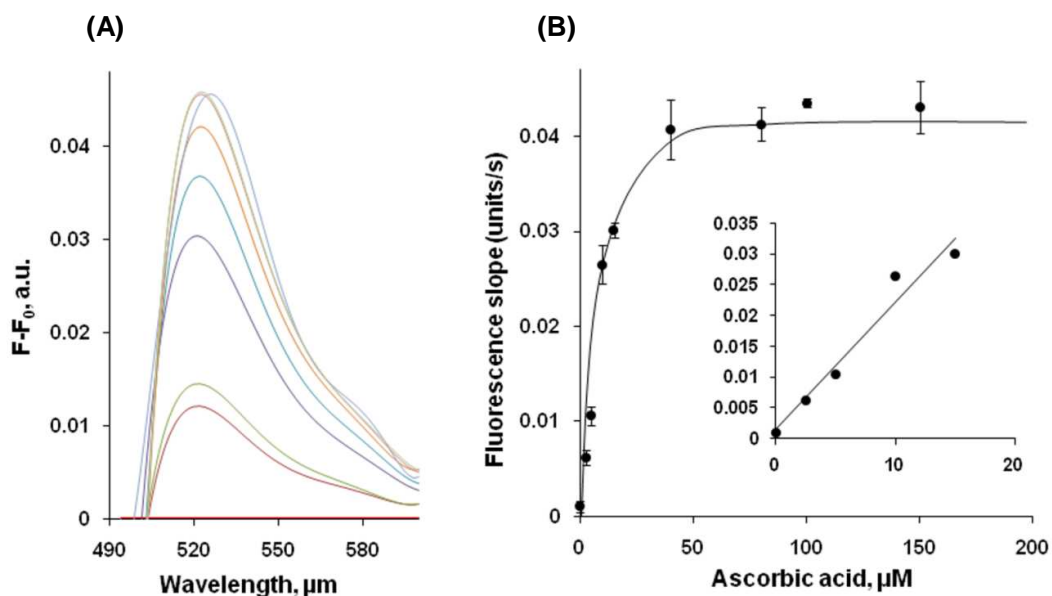


**Figure 3.2.** (A) Emission spectra of buffer solutions on DNAzyme based sensor that include different concentrations of AA a) 0, b) 2.5, c) 5, d) 10, e) 15, f) 40, g) 80, h) 100, i) 150  $\mu\text{M}$ ,  $\lambda=522$  nm. (B) The effect of AA concentration on the initial rate of substrate DNA cleavage during first 3 minutes of the assay. Inset: linear part of the calibration plot. (RSD=12.1 % , n=3).

The effect of AA concentration on the initial rate of DNA cleavage measured during first 3 min of assay is shown in Figure 3.2 (B). The evolution of fluorescence in the reaction mixtures was followed by monitoring the emission signal at 522 nm wavelength and exiting at 494 nm. The assay demonstrated a linear relationship between the cleavage rate and the concentration of AA in the range up to 20  $\mu\text{M}$  and the detection limit of 2.5  $\mu\text{M}$  (S/N = 6, n = 3).

The control experiments demonstrated absence of DNA cleavage in the absence of copper and DNA catalyst. We studied the possible interferences by reducing agents such as fructose, sucrose, glucose, urea, and citric acid. None of

them interfered with our assay even at concentration of 1 mM (Table A-1, Appendix). To evaluate the potential of this assay for practical applications, we measured the concentration of AA in Vitamin C tablets, orange juice and urine. We used standard addition method to determine AA concentration in the samples (Figure 3.3).

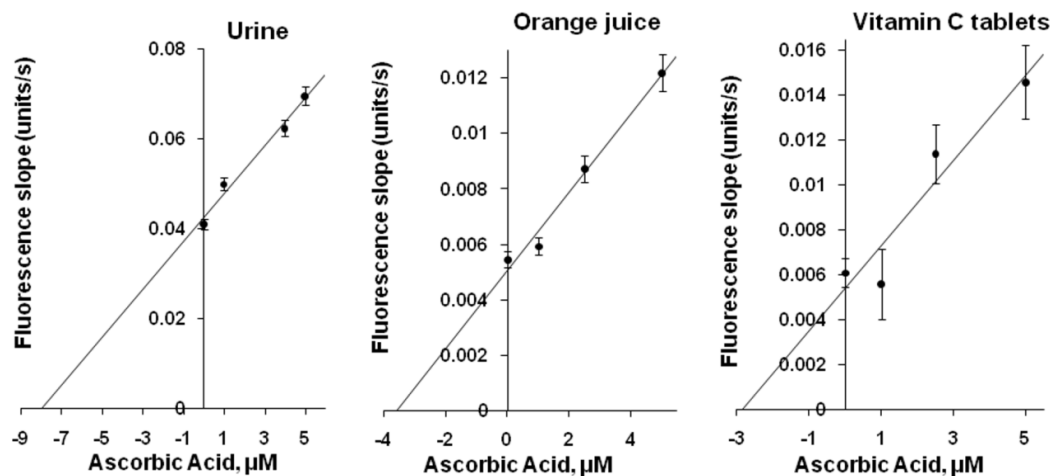


**Figure 3.3.** Quantification of AA in human urine (RSD=2.9%, n=3), orange juice (RSD=5.5%, n=3), and vitamin C tablets (RSD=11.3%, n=3) with the method of standard addition.

The procedure for standard additions is to split the sample into several even aliquots in separate eppendorfs. A standard containing 50 μM AA solution was added in increased volumes of 0 μl, 2 μl, 5 μl, 8 μl, 10 μl to the subsequent eppendorfs and the rate of fluorescence increase was measured with the fluorimeter. The data was plotted with the concentration standard added in the x-axis and the rate of fluorescence increase in the y-axis of the calibration plot. The linear regression was performed, the intercept of the calibration curve with x-axis showed the concentration of AA in the diluted real samples. All dilutions of samples were taken into consideration in order to calculate the initial concentration of AA. The determined amounts of AA are shown in Table 3.1.

Determination of AA in different samples	
Vatamin C tablets (1000 mg/bag)	997±100 mg/bag
Orange juice	16±1 mg/100 ml
Urine	0.42±0.01 mM

**Table 3.1.** Results of AA quantification in real samples by the standard addition method.

*Substrate DNA* and *DNAzyme* proved to be stable in real samples during 3 min, the time required for AA quantification.

The classical donor–acceptor pairs of organic dyes based on Forster resonant energy transfer (FRET) show low quenching efficiency and poor photostability [103, 104]. FRET occurs also when the donor fluorescent organic molecule is situated close to the surface of noble metal macro films and NPs. This energy transfer takes place simultaneously with the change in the radiative lifetime of the organic dye [105]. According to theoretical calculations energy transfer rates and radiative decay rates depend on shape and size of the nanoparticle and the distance between the dye and the surface of NP. The overlap of dye's emission the with NP adsorption spectrum also plays an important role [106]. The experimental investigations demonstrated the drastic quenching of the fluorescence yield in vicinity of gold NPs with radius varied from 1 to 30 nm. This phenomenon is accompanied by the reduction of the dye's radiative rate by an order of magnitude [107].

On another hand, metal NPs have excellent catalytic properties. Gold NPs possess good conductivity, so they can enhance the electron transfer between molecules catalyzing redox reactions. Gold clusters can dissociatively chemisorb  $O_2$  to give O adatoms which trigger the subsequent catalytic chemistry [108]. Electrochemical studies of gold NPs immobilised on the surface of electrodes demonstrated their strong electrocatalytic activity towards the oxidation of AA [109]. So, one can expect the enhancement of redox transformations in vicinity of the gold NPs, including the oxidative cleavage of nucleic acids by DNAzyme.

Our second assay for AA is based on the use of gold NPs as quenchers instead of dabcyI-dT-CE phosphoramidite (Figure 3.4). We synthesised substrate DNA modified with mercapto anchoring group at 5'-end. This nucleic acid also includes the sequence for binding of the DNAzyme with the fluorescein-dT nucleotide separated by the cleavable section from the 5'-end. The citrate stabilized Au-NPs (13 nm) were synthesised by the reduction of  $HAuCl_4$  with citric acid according to the previously published method [98]. They were functionalised with thiolated substrate DNA as reported previously and the excess of non immobilised DNA was washed away.

Loading of Au-NPs with oligonucleotides was evaluated by reducing Au-S bonds with DTT followed by centrifuging to separate Au-NPs from the supernatant containing cleaved DNA. The amount of that was quantified with Oli Green™ fluorescent dye using corresponding calibration plots obtained for known varying concentrations of *thiolated substrate DNA*. The concentration of Au-NPs was found from the absorbance spectra,  $\lambda = 519$  nm and by using the appropriate extinction coefficient. By our estimation the loading was 300 oligonucleotides per gold nanoparticle. Considering gold NPs as spheres of 13 nm in diameter this corresponds to  $6.5 \times 10^{-11}$  mol/cm<sup>2</sup>. Figure 3.4 depicts the method for analyzing AA by Au NPs modified with thiolated substrate nucleic acid.

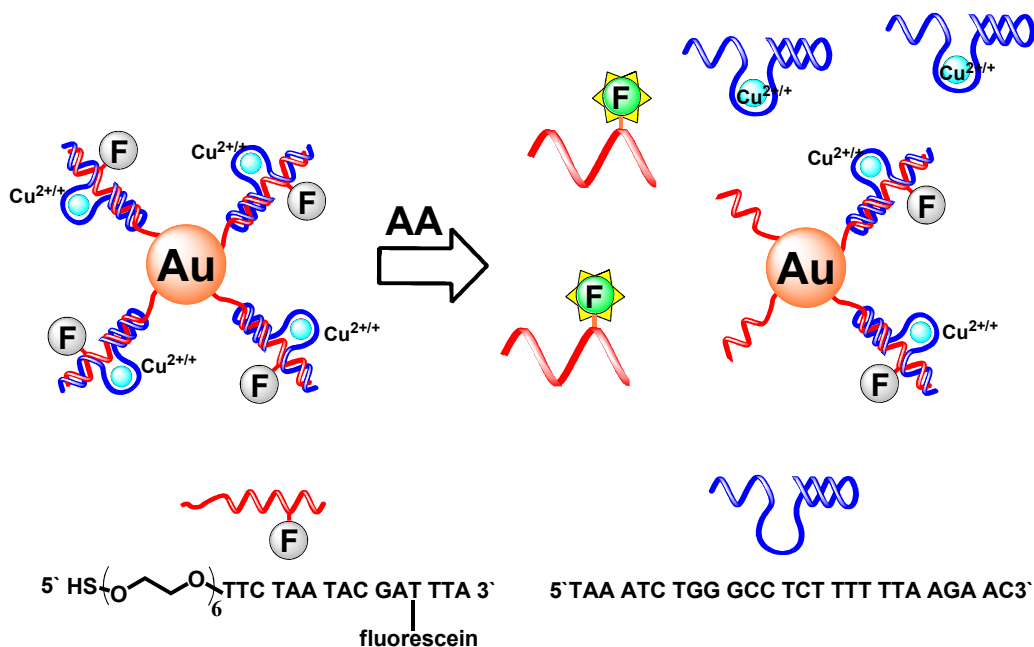


**Figure 3.4.** Fluorometric assay for detection of AA using catalyst DNA and gold NPs modified with DNA substrate carrying fluorescein moiety.

Upon immobilization of substrate DNA on the surface of gold NPs the fluorescence of fluorescein-dT is efficiently quenched. DNAzyme forms a complex with substrate DNA and Cu<sup>2+</sup> ions on the surface of gold NPs. Ascorbate is oxidized by oxygen to give hydrogen peroxide (Equation (3.3)), which interacts with Cu<sup>2+</sup> ions yielding Cu<sup>+</sup> ions (Equation (3.1)). They also react with hydrogen peroxide generating very active and unstable hydroxyl radicals (Equation (3.2)), which break *substrate DNA* in close vicinity to complexed Cu<sup>2+</sup> releasing the oligonucleotide fragment with the fluorescein moiety. The latter recovers its fluorescence after physical separation from the quenching surface of Au-NP. Figure 3.5 (A) shows the emission spectra of this system in the presence of variable concentrations of AA, using a fixed reaction time interval of 2 min.

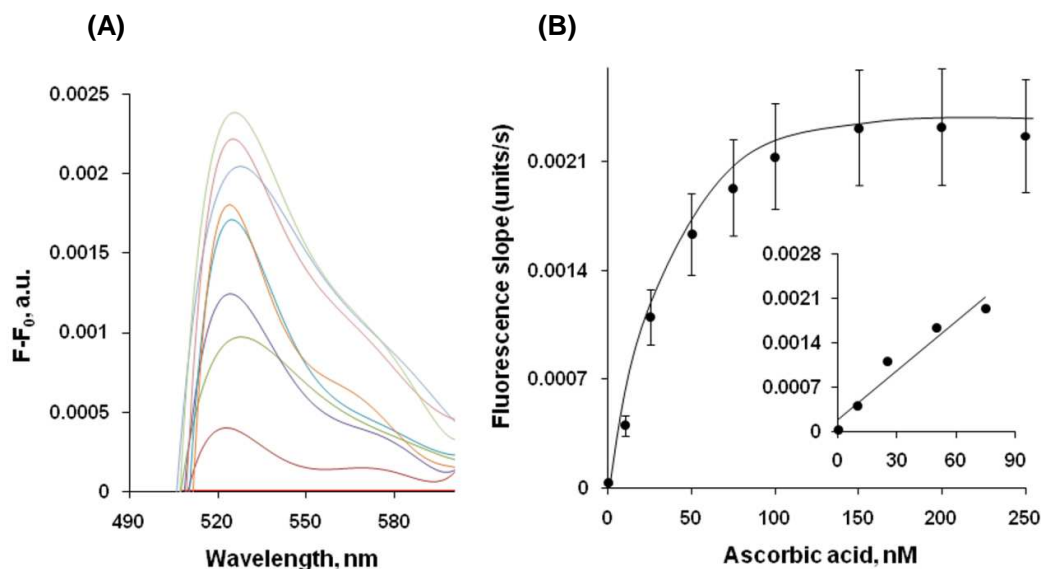


**Figure 3.5.** (A) Emission spectra of buffer solutions that include different concentrations of AA a) 0, b) 10, c) 25, d) 50, e) 75, f) 100, g) 150, h) 200, i) 250 nM,  $\lambda=522$  nm. (B) The effect of AA concentration on the initial rate of substrate DNA cleavage from Au NPs during first 2 minutes of the assay. Inset: linear part of the calibration plot (RSD=16.1 %, n=3).

The fluorescence of the system rises when the amount of AA increases. The effect of varying AA concentrations on the initial rate of fluorescence intensity growth in this system during first 2 min is represented in Figure 3.5 (B).

The emission signal was recorded at 522 nm wavelength using excitation at 494 nm. As the concentration of AA is higher the rate of DNA cleavage increases, as expected. The detection limit corresponds to 10 nM of AA in the analyzed sample ( $S/N = 14$ ,  $n = 3$ ). It is much lower than that of a recently published fluorescence probe for AA (0.5 mM), which is synthesized by a complicated procedure from phthalocyaninatosilicon. The sensitivity of the AA assay based on quenching of fluorescein with Au-NPs was two orders of magnitude better than that of the first assay based on quenching with organic dye, dabcyf. This improvement in sensitivity allowed us to diminish the volume of real samples required for our second AA assay



by 250 times in comparison with that for the fluorescein/dabcyl FRET pair system. We applied Au-NPs decorated with substrate DNA to quantify AA in Vitamin C tablets, orange juice, and urine by the standard addition method (Figure 3.6).

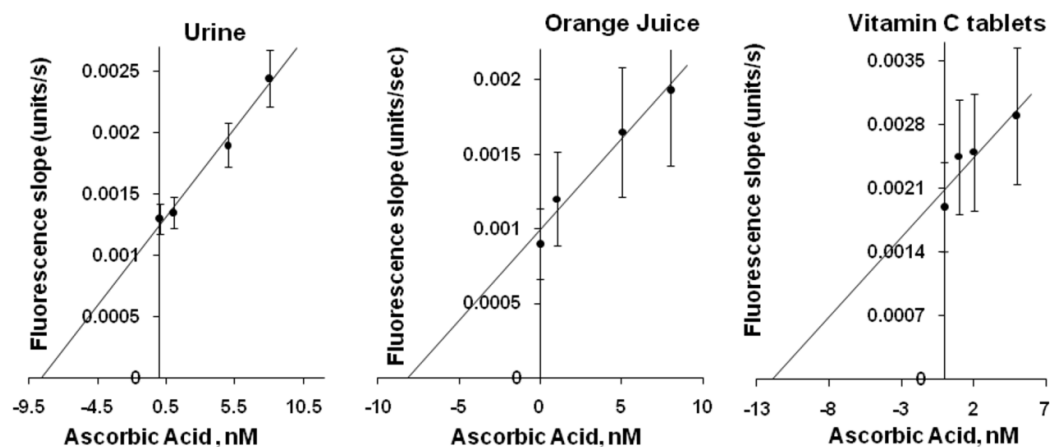


**Figure 3.6.** Quantification of AA in human urine (RSD=9.5%, n=3), orange juice (RSD=26.3%, n=3), and vitamin C tablets (RSD=25.7%, n=3) with the method of standard addition using catalyst DNA and gold NPs modified with DNA.

The results of that assays are summarized in Table 3.2. We found out that 4  $\mu\text{M}$  solution of fructose, glucose, sucrose, urea and citric acid do not interfere with that assay (Table A-2, Appendix). The elevated relative standard deviations can be explained by technical reasons originating from increased number of dilutions used by us to prepare extremely diluted samples of AA in the course of this work.

Determination of AA in different samples	
Vitamin C tablets (1000 mg/bag)	1050±260 mg/bag
Orange juice	14.2±3.7 mg/100 ml
Urine	8.6±0.8 mM

**Table 3.2.** Results of AA quantification in real samples by the standard addition method.

During this assay the total concentration of substrate DNA immobilised on Au NPs was 0.2  $\mu\text{M}$ . In the assay for AA based on the nucleic acid modified with fluorescein/dabcyl FRET pair across the cleavage site the concentration of free substrate DNA was 1  $\mu\text{M}$ . So, despite the 5-fold decrease in the concentration of the substrate DNA in the system based on Au NPs the sensitivity of the latter system was improved by 250 times. This impressive improvement in sensitivity demonstrated by the assay based on nucleic acid decorated Au NPs can be attributed to redox catalytic properties of gold clusters, which simultaneously enhance the oxidation rate of AA [109] and catalyse the reduction of oxygen [110]. Control experiments performed in the absence of DNAzyme or  $\text{Cu}^{2+}$  ions did not show any detectable cleavage of substrate DNA from the surface of Au NPs. Apparently, oxidation of AA catalysed by gold clusters alone does not lead to destructive hydroxyl radicals.

Our assays have some advantages over previously published optical assays for AA acid determination. The spectrophotometric method employing reduction with AA of ferric iron to ferrous iron followed by coupling with  $\alpha,\alpha'$ -dipyridyl requires at least 20 min and demonstrated a detection limit of 60  $\mu\text{M}$  [78]. A Prussian blue

based flow-through surface optosensor for analysis of AA showed a detection limit of 0.45  $\mu\text{M}$ , it requires for operation peristaltic pumps, chromatography columns, a flow cell and a spectrophotometer [80]. Polyaniline-coated microplates, which display the changes in optical absorption resulting from reduction by AA detect as low as 5.7  $\mu\text{M}$  of this analyte [92] but is not selective against other reducing agents in a sample. The colorimetric detection of AA based on formation of anisotropic silver NPs generated by the reduction of silver ions by ascorbate has similar detection limit of 6  $\mu\text{M}$  and also suffers from overestimation due to other reducing agents present in the matrix [91]. The fluorescence probe for AA demonstrated poor sensitivity [95]. The detection limit of this assay is 0.5 mM. Our fluorimetric assay based on DNA decorated Au NPs can detect as low as 10 nM of AA in the analysed sample requiring only 2 min to accomplish the measurement using a commonly available fluorescence microplate reader.

### 3.4 Conclusions

The present study demonstrated that DNAzyme cleaving the substrate DNA in the presence of copper ions can be applied for selective sensitive fluorometric detection of AA in fruit juices and urine. This assay is not interfered by reducing agents such as fructose, sucrose, glucose, urea, citric acid. Use of gold NPs decorated with substrate nucleic acid incorporating the fluorescent dye fluorescein resulted in the improvement of AA detection limit by two orders of magnitude due to catalytic properties of Au clusters. Our assay requires only 2–3 min to complete measurements and does not suffer from interferences. The synthesis of all its components is straightforward. It is performed by the standardized solid phase synthesis on a DNA synthesizer, therefore it can be easily reproduced. Thus, we believe that the present two methods have obvious practical advantages over other previously reported assays for AA.

## ***Chapter 4. Label-Free selective impedimetric detection of Cu<sup>2+</sup> ions using catalytic DNA***

### **4.1 Introduction**

Copper is a redox-active nutrient required in a number of electron transfer processes of many biological reactions [111]. However, at elevated concentrations it has been considered to be toxic for human health. Short-term exposure to excess of copper can cause gastrointestinal disturbance, while long-term exposure causes liver or kidney damage, neurodegenerative diseases, and etc [112]. The World Health Organization (WHO) as well as the U.S. Environmental Protection Agency (EPA) has set the limit of copper in drinking water to be 2 mg/L (32  $\mu$ M) and 1.3 ppm (20  $\mu$ M) respectively.[113] Therefore, the development of the sensitive, selective, comparatively inexpensive and portable sensor for Cu<sup>2+</sup> ions detection is of great importance.

Various analytical methods for the detection of copper ions such as atomic absorption/emission spectroscopy [114, 115], inductively coupled plasma mass spectroscopy (ICP-MS) [116, 117], capillary electrophoresis [118] provide reliable and accurate results, but require expensive and sophisticated instrumentation and complicated sample pretreatment. Many electrochemical sensors such as ion-

selective electrode [119-122], voltammetric [123, 124] and electrochemiluminescence sensors [125, 126] are simple and relatively inexpensive, however, suffer from low reproducibility, have high detection limit and low selectivity. Metal-selective fluorescent chemosensors have attracted intense attention during last decades, however, they need complicated organic synthesis and surface modification; they require as well expensive instruments [127-130].

Recently DNAzyme-based assays have attracted considerable interests for the detection of various analytes, including heavy metal ions. DNAzymes (deoxyribozymes, catalytic DNAs, DNA enzymes) are DNA molecules that exhibit different catalytic activities such as RNA cleavage, ligation, phosphorylation and porphyrin metallation [131]. DNAzymes cleaving RNA in the presence of different divalent ion metals have been reported [58, 59, 132-134]. Considering a DNAzyme promising platform for an application in biosensing various attempts were made for the detection of target DNA [69, 135], or ion metals such as lead [136], uranyl ions [137], mercury [138]. So far, only a few DNAzyme based sensors for copper ions have been reported [139-141]. The design of these DNAzyme probes involves labeling of the oligonucleotide by fluorogenic molecules. In this paper we report a novel label-free electrochemical DNAzyme based biosensor for the detection of copper ions using avidin graphite-epoxy composite electrodes.[142] Electrochemical impedance spectroscopy (EIS) is a powerful and sensitive technique for following of biosensing events that take place at the surface of the electrode. Any tiny disturbance in the interface would lead to impedimetric changes [143]. This method is of general use in laboratories and has been already extensively studied and applied for amperometric, enzymatic, immune and genosensing assays [144, 145]. Combination of benefits of DNAzyme and electrochemical impedance spectroscopy allowed selective detection of copper with the detection limit of 6.5  $\mu\text{M}$ .

## 4.2 Experimental part

### 4.2.1 Materials and methods

Potassium ferricyanide  $K_3[Fe(CN)_6]$ , potassium ferrocyanide  $K_4[Fe(CN)_6]$ , L-ascorbic acid, 4-(2-hydroxyethyl)piperazine-1-ethanesulfonic acid (HEPES), phosphate buffered saline system (PBS), sodium hydroxide, ammonium hydroxide solution 28%-30%, potassium chloride, sodium chloride, avidin from egg white, 5, 5'-dithiobis(2-nitrobenzoic acid) (DNTB), diammonium citrate, 3-hydroxypicolinic acid (3-HPA), and copper (II) chloride were purchased from Sigma-Aldrich (Spain). Standard DNA Phosphoramidites, Biotin-CE Phosphoramidite, Spacer-CE Phosphoramidite 18 and other reagents required for solid phase oligonucleotide synthesis were purchased from Link Technologies (UK). Oligonucleotide purification cartridges (OPG), 2.0 M triethylamine acetate buffer (TEAA), trifluoroacetic acid (TFA), acetonitrile (ACN) were ordered in Applied Biosystems (Spain). NAP<sup>TM</sup>-5 columns for oligonucleotides desalting were purchased in GE Healthcare Life Science (UK). Solid-state electrodes (GECs) were prepared using 50 mm particle size graphite powder (Merck, Darmstadt, Germany) and Epotek H77 resin and its corresponding hardener (both from Epoxy Technology, Billerica, MA, USA). MilliQ water (18.2 M $\Omega$ ) was used to prepare all solutions.

### 4.2.2 Preparation and characterization of oligonucleotide

**Synthesis of oligonucleotide.** Following DNA sequence was synthesized: DNAzyme (5'-biotin-( $-O-CH_2-CH_2-O-$ )<sub>6</sub> TTC TAA TAC GAT TTA GAA TAA ATC TGG GCC TCT TTT TAA GAA C-3'), where ( $-O-CH_2-CH_2-O-$ )<sub>6</sub> corresponds to spacer-CE phosphoramidite 18. Synthetic DNA oligonucleotides were prepared by

automated solid-phase chemical synthesis on 3400 DNA synthesizer (Applied Biosystems). The powdered prepackaged phosphoramidites were dissolved in anhydrous ACN at 0.1 M concentration and attached manually to DNA synthesizer ports. The oligonucleotide sequence was created using Web browser connected to 3400 DNA Synthesizer. The synthesis run was set up by creating a custom cycle script. The synthesis was realized in 1  $\mu$ M scale. The DNA was synthesized on the solid-phase column with the first appropriate phosphoramidite attached. After the synthesis was finished the column was removed from the 3400 DNA Synthesizer and the oligonucleotide was collected to a tightly sealed oligonucleotide collection vial. Base deprotection step was performed by ammonolysis reaction. 1.5 ml of concentrated ammonium hydroxide was added to the collection vial with oligonucleotide. After it was placed in the heating block (Eppendorf) and heated for 8-15 hours at +55 °C while shaking. After the oligonucleotide solution in ammonium hydroxide was put in a refrigerator for 10 minutes and the latter was removed by vacuum. Final purification of oligonucleotide was performed on the OPC cartridge.

***Purification of oligonucleotide.*** Cleaved and deprotected on the previous stage oligonucleotide was purified using OPC column. The 5-ml Luer slip-tip syringe was connected to the end of the OPC cartridge column, a male-to-male Luer tip was connected to other end. The OPC cartridge was flushed with 5 mL of HPLC-grade acetonitrile followed by 5 mL of 2.0 M TEAA. Crude deprotected oligonucleotide was diluted with deionized water to achieve final volume of 1.5 ml. The above solution was loaded to the syringe and gently pushed through the column, collecting the eluted fractions. The eluate was reloaded and pushed through the cartridge again. The column was flushed with 5 ml of 1.5 M ammonium hydroxide and then twice with 5 ml of deionized water. The OPC cartridge-bound oligonucleotide was detritylated by 3% solution of TFA. 1mL of TFA was gently pushed through the column and incubated for 5 minutes. After incubation step, remaining TFA solution was flushed through the cartridge, followed by washing with 5 ml of deionized water (twice). Purified, detritylated oligonucleotide was slowly eluted with 1 mL of 20 %



ACN/H<sub>2</sub>O solution. The concentration of pure oligonucleotide was determined by measuring absorbance at  $\lambda=260$  nm on ND 1000 Spectrophotometer. The oligonucleotide solution was lyophilized and 200  $\mu$ M aliquots were prepared in MQ sterilized water and stored at -80 °C. The purity of the prepared oligonucleotides was further analyzed by MALDI-TOF MS.

**MALDI-TOF spectra measurements.** *Matrix:* 50 mg/ml of 3-HPA in 50:50 H<sub>2</sub>O/ACN; *Ammonium citrate dibasic solution:* 50 mg/ml in water; *DNA samples:* 10<sup>-5</sup>-10<sup>-6</sup> M in 50:50 H<sub>2</sub>O/ACN. The dried droplet method of the sample preparation was used: matrix and ammonium citrate dibasic solution were mixed in proportion 9:1. First, 0.9  $\mu$ l of above prepared solution was spotted on a metal plate and after 0.1  $\mu$ l of DNA sample was spotted onto matrix and allowed to co-crystallize. The spectra were scanned on Voyager-DE PRO workstation in linear, static acceleration mode, with negative polarity and accelerating voltage 20000 V. MALDI-TOF spectra of DNAzyme (Figure A-6, Appendix), were typically acquired by averaging 20-25 laser shots. Each sample was spotted up to three times to a MALDI plate.

### 4.2.3 Impedimetric sensor preparation

**Electrode preparation procedure.** Avidin-graphite epoxy composite (Av-GEC) electrodes, used for easy immobilization of biotinylated DNAzyme, were prepared using a polyvinyl chloride (PVC) tube body (6 mm i.d.) and a small copper disk soldered at the end of an electrical connector. The working surface is an epoxy-graphite conductive composite, formed by a mixture of graphite (18%), avidin (2%) and epoxy resin (80%), deposited on the cavity of the plastic body [146, 147]. The composite material was cured at 40 °C for 7 days. Before each use, the electrode surface was moistened with Milli-Q water and then thoroughly smoothed with abrasive sandpaper and finally with alumina paper (polishing strips 301044-001, Orion) in order to obtain a reproducible electrochemical surface. The electrodes

were then washed twice for 10 minutes in the working buffer at room temperature while stirring.

**Immobilization of DNAzyme probe.** An Av–GEC electrode was immersed in 160 mL of the desired concentration of biotinylated *DNAzyme* in 50 mM HEPES, pH 7.0, 0.5 M KCl, and 0.5 M NaCl. After incubation for 1 h at RT while stirring, the electrodes were washed twice for 10 minutes in the working buffer at room temperature.

#### 4.2.4 Copper ions detection

**Reaction of DNAzyme with copper.** After the immobilization of *DNAzyme* the electrode was immersed for 20 minutes in the solution of the desired concentration of  $\text{CuCl}_2$  and 30 mM concentration of AA in the working buffer at RT while stirring. The electrodes were then washed twice for 10 minutes in the working buffer at room temperature.

**Impedimetric detection.** AC impedance measurements were performed with an IM6e Impedance Measurement Unit (BAS-Zahner, Kronach, Germany) and Autolab PGStat 20 (Metrohm Autolab B.V, Utrecht, The Netherlands). Thales (BAS-Zahner) and Fra (Metrohm Autolab) software, respectively, were used for data acquisition and control of the experiments. A conventional three-electrode system was used to perform impedance measurements: an avidin–graphite epoxy composite (Av–GEC) electrode as a working electrode, an Ag/AgCl electrode as a reference electrode and a platinum-ring auxiliary electrode (Crison 52-67 1, Barcelona, Spain) as a counter electrode. Temperature controlled incubations were done using an Eppendorf Thermomixer 5436. Impedance spectra were recorded between 50 kHz and 0.05 Hz, at a sinusoidal voltage perturbation of 10 mV amplitude and a sampling rate of 10 points per decade above 66 Hz and 5 points per decade at the lower range. The experiments were carried out under open circuit potential conditions in an unstirred solution of 0.1 M PBS buffer solution containing a

0.01 mM  $K_3[Fe(CN)_6]/K_4[Fe(CN)_6]$  (1 : 1) mixture, used as a redox marker. The impedance spectra were plotted in the form of complex plane diagrams (Nyquist plots,  $-Z_{im}$  vs.  $Z_{re}$ , where  $Z_{im}$  is the imaginary impedance change and  $Z_{re}$  is the realized impedance change) and fitted to a theoretical curve corresponding to the equivalent circuit with  $Z_{view}$  software (Scribner Associates Inc., USA). The equivalent circuit was formed by one resistor/capacitor element in series with a resistance. The chi-square goodness of fit was calculated for each fitting by the FRA software employed (Eco Chemie, the Netherlands). In all cases impedance data were recorded in the following order after each of above described steps. In order to compare the results obtained from the different electrodes used, and to obtain independent and reproducible results, relative signals are needed [146]. Thus, the  $\Delta_{ratio}$  value was defined according to the following equations:

$$\Delta_{ratio} = \Delta_s / \Delta_p$$

$$\Delta_s = R_{ct(DNAzyme-AA-Cu)} - R_{ct(electrode-buffer)}$$

$$\Delta_p = R_{ct(DNAzyme)} - R_{ct(electrode-buffer)}$$

where  $R_{ct(DNAzyme-AA-Cu)}$  was the electron transfer resistance value measured after incubation with AA and copper;  $R_{ct(DNAzyme)}$  was the electron transfer resistance value measured after *DNAzyme* immobilization on the electrode, and  $R_{ct(electrode-buffer)}$  was the electron transfer resistance of the blank electrode and buffer.

### 4.3 Results and discussion

The analytical procedure for biosensing consists of the immobilization of the biotinylated *DNAzyme* onto the surface of the avidin modified GEC electrodes, followed by binding of copper ions to -CTGGGCC- section of DNA. The reconstituted *DNAzyme* enhances the rate of AA oxidation by oxygen. The accumulated oxidation products insulate the surface of GEC electrodes changing their interfacial properties followed by EIS in the presence of the reversible redox couple  $[\text{Fe}(\text{CN})_6]^{3-}/[\text{Fe}(\text{CN})_6]^{4-}$  as a marker as depicted in Figure 4.1.

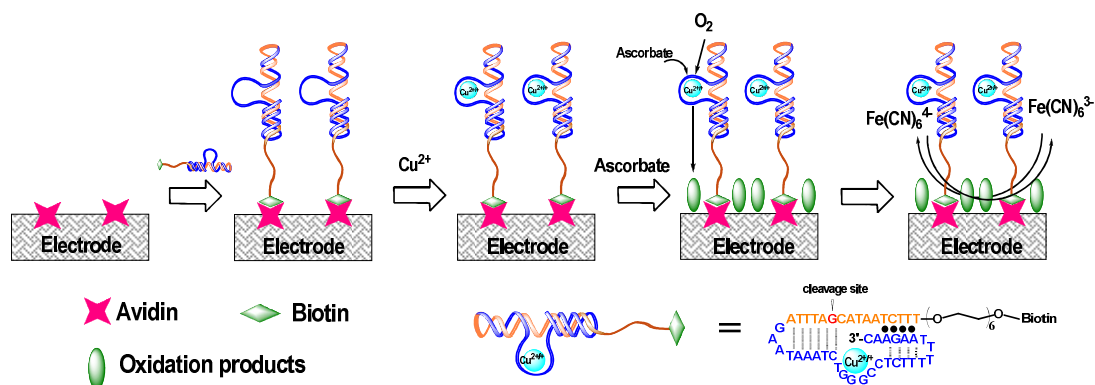


**Figure 4.1.** Schematic illustration of impedimetric *DNAzyme* sensor for  $\text{Cu}^{2+}$

#### 4.3.1 Optimization of electrode surface

First, the concentration of *DNAzyme* immobilized onto the GEC electrode surface was optimized in order to achieve the maximum surface coverage. For this purpose, increasing concentrations of *DNAzyme* were used to carry out the immobilization, evaluating the changes in the  $\Delta_p$  caused by the DNA layer. The

curve of adsorption of *DNAzyme* on the electrode surface is shown on Figure 4.2. It can be observed that the difference in resistance ( $\Delta_p$ ) asymptotically approaches its maximum value starting from 0.2  $\mu\text{M}$  of *DNAzyme* concentration. This is due to the formation of a chemical bond between biotin moiety of *DNAzyme* and avidine on the electrode surface, which followed a Langmuir isotherm. The concentration of *DNAzyme* equal to 0.2  $\mu\text{M}$  was chosen as the optimal concentration.

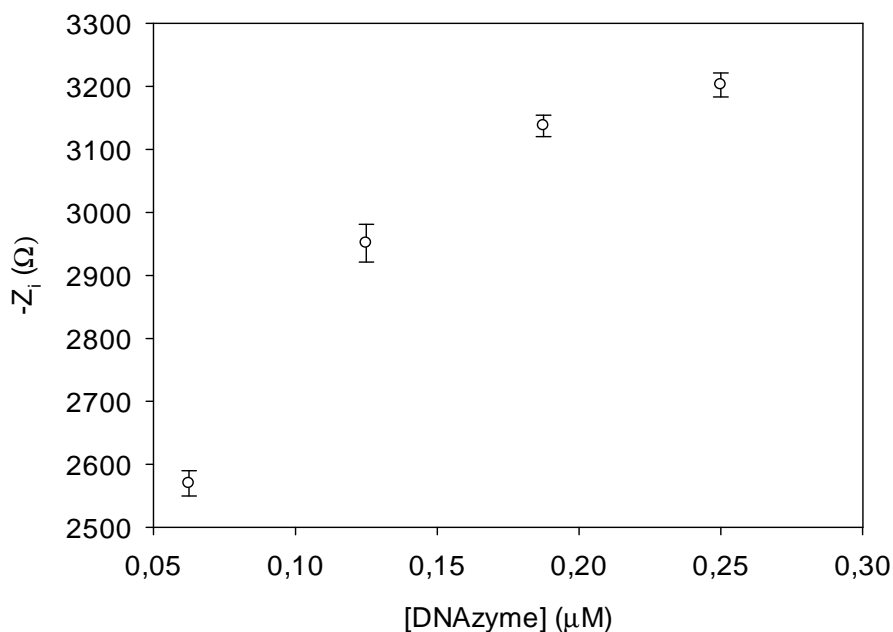


**Figure 4.2.** Optimization of the concentration of *DNAzyme* placed onto the electrode. Uncertainty values corresponding to replicated experiments ( $n=5$ ).

### 4.3.2 Detection of $\text{Cu}^{2+}$

After the optimization of *DNAzyme* concentration, and following the above mentioned experimental protocol for the detection of copper, the biosensor response was initially evaluated.  $\text{Cu}^{2+}$  ions captured by the layer of *DNAzyme* significantly enhance the rate of AA oxidation[96, 97] in vicinity of the electrode, consequently

the electrode surface is partially blocked due to the adsorption of oxidation products on it, resulting in an increase in the interfacial electron-transfer resistance. Representative Nyquist plots of *DNAzyme* in the absence and presence of  $\text{Cu}^{2+}$  are shown in Figure 4.3.

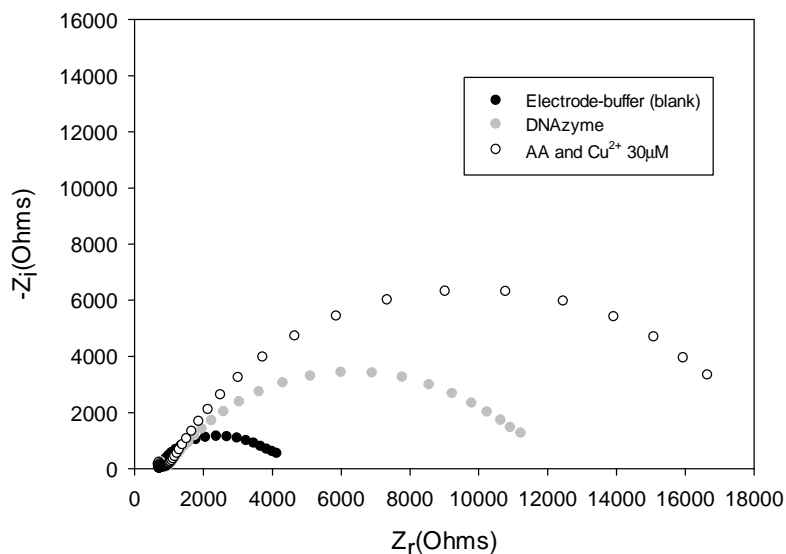


**Figure 4.3.** Nyquist Diagram of: (a) Electrode-buffer ●, (b) *DNAzyme*, and (c) AA and  $\text{Cu}^{2+}$  30  $\mu\text{M}$ .

As can be seen, resistance  $R_{ct}$  between the electrode surface and the solution is increased. This fact is due to the effect of the kinetics of the electron transfer redox marker  $[\text{Fe}(\text{CN})_6]^{3-}/[\text{Fe}(\text{CN})_6]^{4-}$  which is delayed at the interface of the electrode, mainly caused by steric hindrance and electrostatic repulsion presented by the oxidized products formed.

### 4.3.3 Sensitivity of *DNAzyme*-based sensor

To evaluate the sensitivity of the assay, new experiments with solutions containing different amount of copper were performed and the calibration curve was built. Figure 4.4 shows the evolution of the  $\Delta_{\text{ratio}}$  relative signal, as extracted from the Nyquist diagrams, for the calibration of the copper sensor. To evaluate the linear range and detection limit of this *DNAzyme*-based copper sensor, the calibration curve was built, representing the analytical signal expressed as  $\Delta_{\text{ratio}}$  vs. copper concentration (Figure 4.4.).

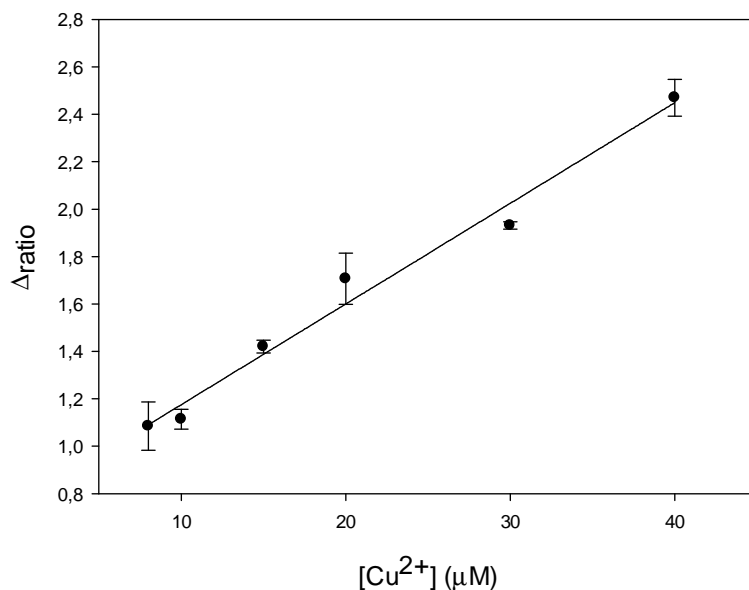


**Figure 4.4.** Calibration curve versus  $\text{Cu}^{2+}$  concentration. Uncertainty values corresponding to replicated experiments ( $n = 5$ ).

As the copper concentration rises, the interfacial electron transfer resistance between the electrode surface and solution also increases up to 40  $\mu\text{M}$  of  $\text{Cu}^{2+}$ . As can be seen, a linear trend is obtained with a linear range from 10  $\mu\text{M}$  to 40  $\mu\text{M}$  for  $\text{Cu}^{2+}$ . From the least squares fitting, sensitivity appeared to be of  $4 \cdot 10^{-2} \mu\text{M}^{-1}$  and the

detection limit of 6.5  $\mu\text{M}$ . The repeatability of the method showed a relative standard deviation (% RSD) between 2 and 6%, obtained from series of 5 replicates carried out for each standard in the linear range.

#### 4.3.4 Selectivity of *DNAzyme* based sensor

Next, the selectivity of the assay for the detection of  $\text{Cu}^{2+}$  over other divalent metal ions, frequently found together with copper, such as nickel, cadmium and lead was investigated. All concentrations tested were 30  $\mu\text{M}$ . As can be seen from the Figure 4.5 only in the presence of copper, the primary species, biosensor gives significant response, so, the interference with other metal ions can be considered negligible.

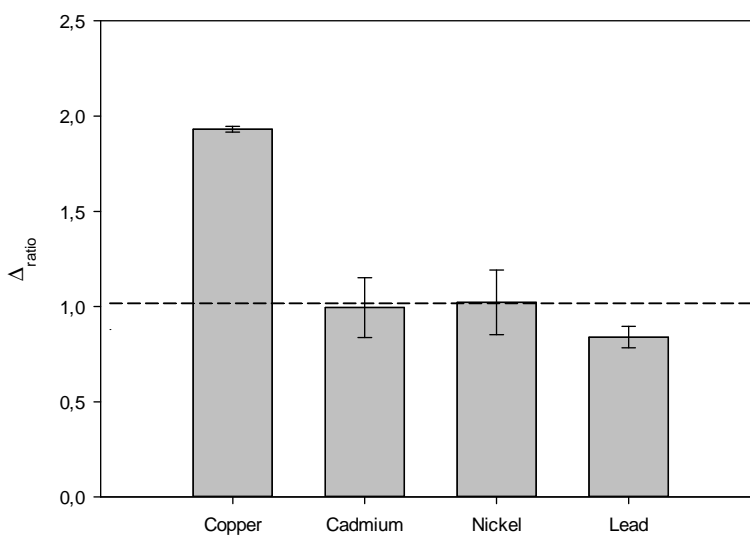


**Figure 4.5.** Impedimetric response obtained with different metals assayed at the same concentration (30  $\mu\text{M}$ ). Uncertainty values corresponding to replicated experiments ( $n = 5$ ).



## 4.4 Conclusions

In conclusion, we have described a simple biosensor for the determination of copper (II) based on its *DNAzyme* immobilized by strong non-covalent avidin-biotin interaction on the electrode surface. Upon reconstitution with  $\text{Cu}^{2+}$  this *DNAzyme* catalyzes oxidation of AA with oxygen, leading to blocking of the electrode surface by the reaction products. The immobilization step and the catalytic event inhibiting the electron-transfer kinetics of the redox probe at the electrode interface, can be monitored by labelless electrochemical impedance spectroscopy. The *DNAzyme* biosensor shows a linear response range of 10  $\mu\text{M}$  to 40  $\mu\text{M}$   $\text{Cu}^{2+}$  and a detection limit of 6.5  $\mu\text{M}$ . Interference to some related metals can be considered negligible. Advantages of the reported label-free method for  $\text{Cu}^{2+}$  detection over other conventional techniques are their simplicity and high selectivity.

---

## ***Chapter 5. Unconventional application of conventional enzymatic substrate: First fluorogenic immunoassay based on enzymatic formation of QDs***

### **5.1 Introduction**

Traditional ELISA is based on specific interaction between an antigen and antibody, and it is a very powerful technique for the detection of clinically important analytes in a variety of biological matrixes [148-150]. To produce a measurable signal in response to a binding event, antibody (or antigen) is tethered to some kind of detectable label. Enzymes are widely used as labels in immunoassays and are especially useful in highly diluted samples, as a single enzyme molecule can catalytically transform many molecules of substrate into a product ( $10^1 - 10^4$  molecules  $\text{min}^{-1}$ ). This amplification effect provides the basis for very sensitive detection of analytes through affinity interactions. ALP is widely used as a labeling enzyme due to its high turnover number, high stability, low cost and broad substrate specificity [151]. It catalyzes the hydrolysis of orthophosphoric monoesters, to yield phosphate and corresponding alcohols. Usually, ALP activity is determined by measuring the amount of generated alcohol. However, depending on the substrate many methods for detection of ALP activity in immunoassays have been reported. Among the various detection methods, colorimetric immunoassays are simple and highly efficient but suffer from poor sensitivity [152, 153]. Most routine detection

methods are based on the formation of luminescent or fluorescent products, which are determined by luminometry or fluorimetry, respectively [154-156]. In addition, electrochemical assays, based on the transformation of electro-inactive substrate into an electro-active product, have also been described [157-162]. Electrochemical immunoassays improve the limit of detection, but they require multiple steps of deposition and stripping making the whole analysis complicated. Thus, an important step in further development of ALP-based immunoassay is to increase sensitivity to ALP activity detection, decrease cost and simplify the whole procedure.

The design of fluorescent sensors for ALP activity detection has attracted great attention because of the higher sensitivity of fluorescent spectroscopy over traditionally used UV-Vis spectroscopic methods. However, the majority of fluorescent probes is based on organic dyes and requires complicated organic synthesis and surface modification to be used in labeling [163-166]. They also tend to be expensive and unstable. Fluorescent semiconductor NPs, otherwise known as QDs, possess several advantages over conventional fluorophores such as wide range of optical properties [167], higher brightness, better resistance to photobleaching and longer lifetime [168]. These intrinsic benefits over molecular fluorophores make QDs attractive optical labels for numerous biological assays [169].

Upon photoexcitation electron/hole couples are generated inside QDs. When the hole and the electron are recombined, the emission light is generated. The wavelength and intensity of the light emitted by QDs is dependent on their size and nature [170]. Semiconductor QDs can be used as elements of signal transduction of enzymatic reactions. Currently, researchers exploit QDs as FRET donors. Biomolecular linkers, such as proteins, peptides and oligonucleotides are frequently used to immobilize QDs and create FRET-based sensors for detection enzyme activity [171, 172]. Above mentioned QDs-based methods for detection of ALP activity rely on the use of presynthesized QDs as labels or donors of FRET pairs.

QDs have also been successfully used as substitutes for traditional organic dyes in immunoassays [173, 174]. These methods are based on detection of binding between analyte (antigen) and QD-labeled immunomolecule (antibody). Recently, FRET-based QD immunoassays for highly sensitive and accurate detection of biological targets have been published [175]. Some of these assays rely on the competition between a free analyte with a quencher-labeled analyte that is bound to a QD-conjugated IgG antibody [176].

However, the above mentioned methods suffer from high background signals due to insufficient quenching of a donor couple or non-specific adsorption of modified QDs on surfaces. Growth of inorganic NPs triggered by biocatalytic processes expands new horizons for the design of sensitive bioassays. These methods are based on the reduction of metal ions by a product of enzymatic reaction, followed the deposition of generated metal atoms on the surface of seeding NPs [177-180]. Another more traditional approach was the application of metal NPs decorated with biorecognition elements to biosensing [181].

Recent efforts by our group have been directed toward combining the power of enzymatic amplification with advantages of QDs to develop highly sensitive assays for enzymatic activities and their inhibition [182, 183]. For instance, we demonstrated that ALP from *Escherichia coli* can hydrolyze artificial substrate thiophosphate to  $H_2S$ , which interacts with  $Cd^{2+}$  to yield CdS QDs [184]. Unfortunately, the inhibition of a bovine ALP by artificial substrate thiophosphate limits the application of this method in ALP-based ELISAs. In this article, we offer an alternative approach for bovine ALP activity detection based on *in situ* growth of fluorescent CdS QDs. pNPP, used as a substrate, undergoes enzymatic cleavage by ALP, giving p-nitrophenol (pNP) and phosphate ions as the products of the reaction. Upon the addition of  $Cd^{2+}$  and  $S^{2-}$  ions to the reaction mixture, phosphate stabilized fluorescent nanocrystals of CdS are formed. Our method was applied for heterogeneous immunoassays employing bovine ALP as a labeling enzyme. The

proposed assay performed in 96 microtiter well plate is perfectly suitable for clinical, pharmaceutical and environmental application.

## 5.2 Experimental part

### 5.2.1 Materials and methods

ALP (from bovine intestinal mucosa), cadmium nitrate ( $\text{Cd}(\text{NO}_3)_2$ ), sodium sulfide ( $\text{Na}_2\text{S}$ ), anti-rabbit IgG(whole molecule)-ALP, anti-bovine serum albumin (developed in rabbit), albumin from bovine serum (BSA), trizma base, diethanolamine (DEA), magnesium chloride, 4-nitrophenyl phosphate disodium salt, phosphate buffered saline system, casein blocking buffer were obtained from Sigma-Aldrich (Spain). Enzymatic activity assays based on formation of fluorescent QDs were performed in black flat-well (330  $\mu\text{L}$ ) NUNC 96-wells microtiter plates. The standard assay for quantification of ALP was performed in transparent flat-well (330  $\mu\text{L}$ ) NUNC 96 wells microtiter plates. The absorbance and fluorescence spectra were recorded with Varioscan Flash spectral scanning multimode reader (Thermo Scientific). All water used was Milli-Q ultrapure grade (EMD Millipore).

### 5.2.2 Detection of ALP by standard method

Different concentrations of ALP (from 0 to 800  $\text{mU mL}^{-1}$ ) was added to the solution containing 0.5 mM pNPP, 0.5 mM  $\text{MgCl}_2$  in 10 % DEA buffer (pH 9.8). The resulting solution was incubated at 37 °C for 30 min. Then the reaction was terminated by addition of 2 M  $\text{Na}_2\text{CO}_3$ , and brought to the RT for 20 min. The absorbance at  $\lambda=405$  nm was measured.

### 5.2.3 Detection of ALP activity by QD based method

Different concentrations of ALP (from 0 to 800 mU mL<sup>-1</sup>) was added to the solution containing 0.5 mM pNPP, 0.5 mM MgCl<sub>2</sub> in 50 mM TrisHCl buffer (pH 9.8). The resulting solution was incubated at 37 °C for 90 min. Then 5 µL of 6 mM Na<sub>2</sub>S and 10 µL of 12.5 mM Cd(NO<sub>3</sub>)<sub>2</sub> were added to each well. After 5 min of incubation the fluorescence emission spectra were recorded at λ<sub>ex</sub>=290 nm.

### 5.2.4 Detection of Anti-BSA antibody by standard immunoassay

A 96-well NUNC microtiter plate was coated with BSA (2 µg mL<sup>-1</sup>) in PBS for overnight at 4 °C. Unspecific binding was blocked by 2 h of incubation with casein blocking buffer. The plate was washed three times with PBS/0.05 % Tween 20 (PBST). Different concentrations of anti-BSA antibody in PBS were incubated for 2h at RT and the plate was then washed for three times with PBST. The anti rabbit-ALP conjugate (2 µg mL<sup>-1</sup>) in PBS was incubated on the plate for 1h at RT. The plate was then washed three times with PBST and one time with 10 % DEA buffer (pH 9.8). Then 85 µL of ALP substrate (0.5 mM pNPP in 10 % DEA buffer and 0.5 mM MgCl<sub>2</sub>, pH 9.8) was added to each well, incubated for 30 min at 37 °C. The reaction was stopped by addition of 15 µL of 2 M Na<sub>2</sub>CO<sub>3</sub>. The plate was brought to RT and absorbance at λ=405 nm was measured.

### 5.2.5 Detection of Anti-BSA Antibody by QD based method

A 96-well NUNC microtiter plate was coated with BSA (2 µg mL<sup>-1</sup>) in PBS for overnight at 4 °C. Unspecific binding was blocked by 2 h incubation with casein blocking buffer. The plate was washed three times with PBST. Different

concentrations of anti-BSA antibody in PBS were incubated for 2h at RT and the plate was then washed for three times with PBST. The anti rabbit-ALP conjugate ( $2 \mu\text{g mL}^{-1}$ ) in PBS was incubated on the plate for 1h at RT. The plate was then washed three times with PBST and one time with 10 % DEA buffer (pH 9.8). Then 85  $\mu\text{L}$  of ALP substrate (0.5 mM pNPP in 50 mM TrisHCl buffer and 0.5 mM  $\text{MgCl}_2$ , pH 9.8) was added to each well, incubated for 90 min at 37  $^\circ\text{C}$ . After samples were drawn from the wells and placed to black 96-well NUNC microtiter plate. Then 5  $\mu\text{L}$  of 6 mM  $\text{Na}_2\text{S}$  and 10  $\mu\text{L}$  of 12.5 mM  $\text{Cd}(\text{NO}_3)_2$  were added and the fluorescence emission spectra of the resulting suspension were recorded after 5 min at  $\lambda_{\text{ex}}=290$  nm.



### 5.3 Results and discussion

The ALP activity is routinely estimated by colorimetric measurement of pNP liberated by enzymatic hydrolysis of pNPP substrate. This reaction, however, in alkaline conditions yields one more product, orthophosphate ion, which can also be used to quantify phosphatase activity. Recently, we found out that under certain experimental conditions thiophosphate ( $\text{PO}_3\text{S}^{3-}$ ) ions can stabilize CdS NPs produced from  $\text{Na}_2\text{S}$  and  $\text{Cd}(\text{NO}_3)_2$  *in situ* [182]. Inspired by this fact, we hypothesized that orthophosphate ions ( $\text{PO}_4^{3-}$ ) also would be able to stabilize CdS QDs produced *in situ*. The experimental results confirmed our hypothesis that orthophosphate ions induce the formation of fluorescent CdS NPs. When exciting the reaction mixture at 290 nm the characteristic fluorescence emission spectrum for CdS QDs is observed, with the peak between 400 and 700 nm and a maximum emission at about 520 nm (Figure 5.1, Curve a,). In the absence of orthophosphate ion no detectable growth in fluorescence is observed (Figure 5.1, Curve b).

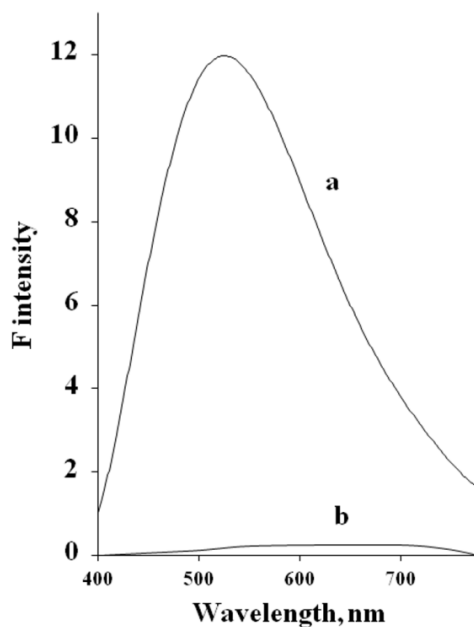


**Figure 5.1.** Emission spectra of the CdS QDs formed in the presence of  $\text{Na}_2\text{S}$  (0.3 mM),  $\text{Na}_3\text{PO}_4$  (0.3 mM),  $\text{Cd}(\text{NO}_3)_2$  (1.25 mM) (a) and in the absence of  $\text{Na}_3\text{PO}_4$  (b)

Having confirmed the crucial role of phosphate in the formation of CdS NPs, we studied the effect of bovine ALP on the generation of CdS NPs by the mechanism depicted in Figure 5.2, according to which ALP hydrolyzes pNPP to  $\text{PO}_4^{3-}$  stabilizing the growth of CdS QDs from cadmium nitrate and sodium sulfide.

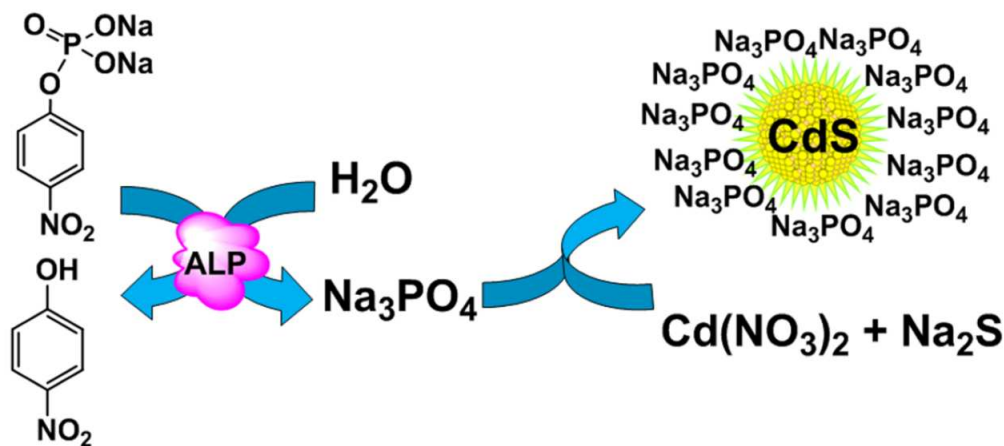


**Figure 5.2.** Detection of ALP activity by enzymatic growth of CdS QDs.

To investigate the influence of different enzyme concentrations on the fluorescence signal, various amounts of bovine ALP were added to the system and emission spectra were recorded. Figure 5.3 (A) shows emission spectra of different concentrations of ALP (from 0 to 800 mU mL<sup>-1</sup>) in a 50 mM Tris-HCl buffer (pH 9.8).

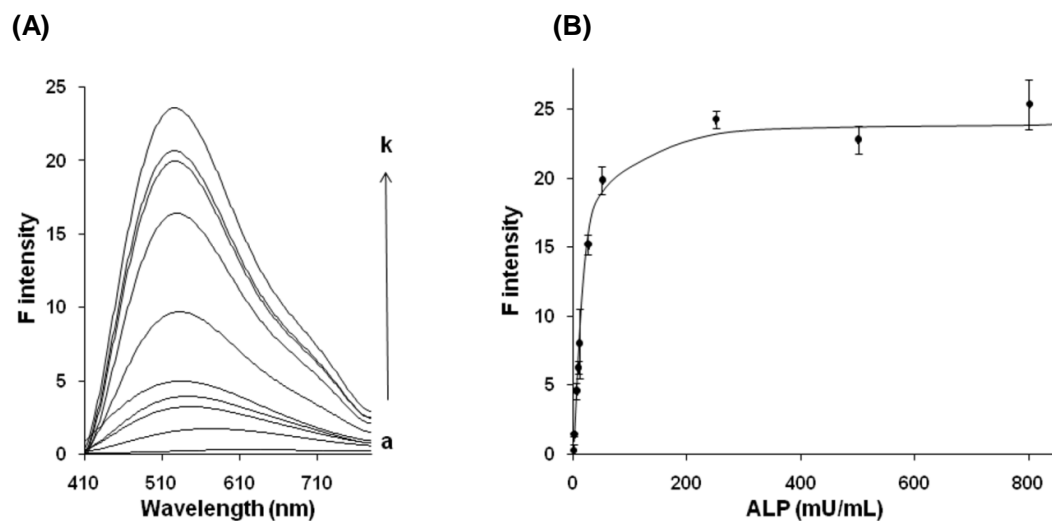


**Figure 5.3.** (A) Emission spectra of CdS QDs in the system containing  $\text{Cd}(\text{NO}_3)_2$  (1.25 mM),  $\text{Na}_2\text{S}$  (0.9 mM), pNPP (0.5 mM),  $\text{MgCl}_2$  (0.5 mM) and various concentrations of ALP: (a) 0  $\text{mU mL}^{-1}$ ; (b) 0.5  $\text{mU mL}^{-1}$ ; (c) 5  $\text{mU mL}^{-1}$ ; (d) 8  $\text{mU mL}^{-1}$  (e) 10  $\text{mU mL}^{-1}$  (f) 25  $\text{mU mL}^{-1}$ ; (g) 50  $\text{mU mL}^{-1}$ ; (h) 200  $\text{mU mL}^{-1}$ ; (i) 400  $\text{mU mL}^{-1}$ ; (j) 800  $\text{mU mL}^{-1}$ . (B) Calibration curve of ALP at  $\lambda=520$  nm (RSD=3.9 %,  $n=3$ ).

When the concentration of ALP increased, orthophosphate concentration also increased, leading to a higher fluorescent signal. Figure 5.3 (B) shows the calibration plot of fluorescence intensity (F) versus ALP concentration, at an emission wavelength of 520 nm, showed a linear response up to 50  $\text{mU mL}^{-1}$  and limit of detection of 0.5  $\text{mU mL}^{-1}$ .

The control experiments were carried out to exclude the effect of intrinsic fluorescence of ALP on the readout signal. The reaction was performed in the medium containing ALP at maximum concentration (800  $\text{mU mL}^{-1}$ ),  $\text{Cd}(\text{NO}_3)_2$  and  $\text{Na}_2\text{S}$ , in the absence of enzymatic substrate. No significant fluorescence peak was observed under these conditions (Figure 5.4, Curve b). In the presence of all the components of enzymatic reaction clear fluorescence signal was detected (Figure 5.4, Curve a).

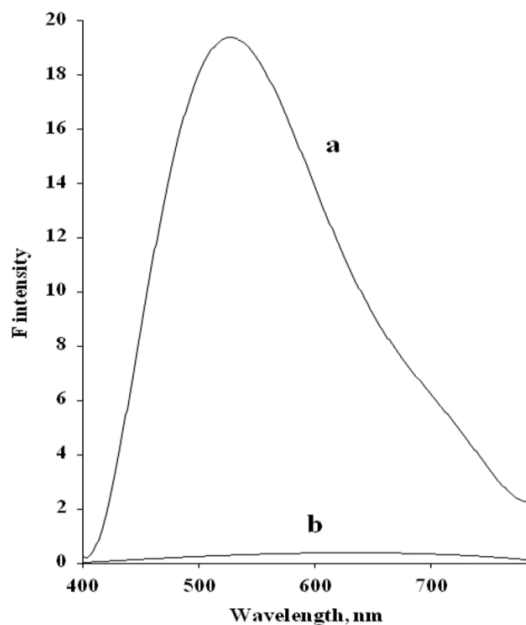


**Figure 5.4.** Emission spectra of the CdS QDs formed in the presence of Na<sub>2</sub>S (0.3 mM), Cd(NO<sub>3</sub>)<sub>2</sub>, ALP 800 mU/mL, pNPP 0.5 mM (a) and in the absence of pNPP (b). (B) TEM image of the CdS QDs formed in the presence of Na<sub>2</sub>S (0.6 mM), ALP (250 mU mL<sup>-1</sup>) and Cd(NO<sub>3</sub>)<sub>2</sub> (12.5 mM), pNPP 0.5 mM.

The enzymatic generation of CdS NPs was confirmed by transmission electron microscopy (TEM), and diameter of formed spherical CdS QDs appeared to be between 2 and 3 nm (Figure A-7, Appendix). TEM image (Figure A-7) clearly shows the presence of fluorescent nanostructures between 2-3 nm in the assay mixture. The only way to yield fluorescence in our system is the formation of CdS QDs. The control experiments conducted in the absence of cadmium cations or sulphide anions do not demonstrate any significant fluorescent signal (data not shown). Furthermore, we also compared our method with the standard chromogenic pNPP assay. Figure 5.5 shows the calibration plots of normalized fluorescence/absorbance at an emission/absorption wavelength of 520 nm/405 nm versus ALP activity.

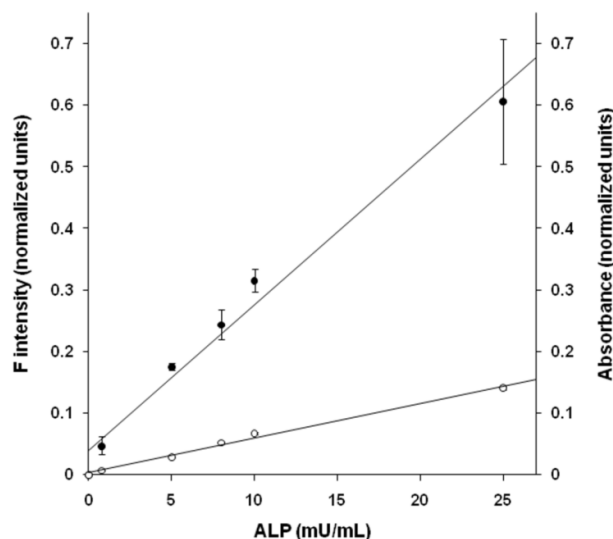


**Figure 5.5.** Calibration curve of ALP measured by the QD-based method (●) and the standard pNPP-based method (○).

As could be noted, the lowest ALP activity detected by the fluorogenic and standard chromogenic method was found to be  $0.5 \text{ mU mL}^{-1}$  and  $5 \text{ mU mL}^{-1}$ , respectively ( $S/N=3$ ). Thus, the limit of detection of ALP activity was significantly improved by the fluorogenic method described within this work. We studied the effect of varying concentrations of pNPP in homogeneous system on the fluorescence intensity arising from the generated QDs and found the formal apparent  $K_m$ , defined as the concentration of substrate at which 50% of the maximum fluorescence intensity is reached, equal to  $0.1 \text{ mM}$ . Therefore, we used saturating  $0.5 \text{ mM}$  concentration of pNPP in ELISA to reach the highest enzymatic reaction rate.

To validate the applicability of our fluorogenic method in ELISA assays, we took advantage of the model assay for detection of anti-BSA antibodies, which could serve as a model of clinical heterogeneous immunoassays for detection of different antibodies in human serum. Figure 5.6 outlines the model assay for analyzing anti-BSA antibody by CdS QDs-based method.

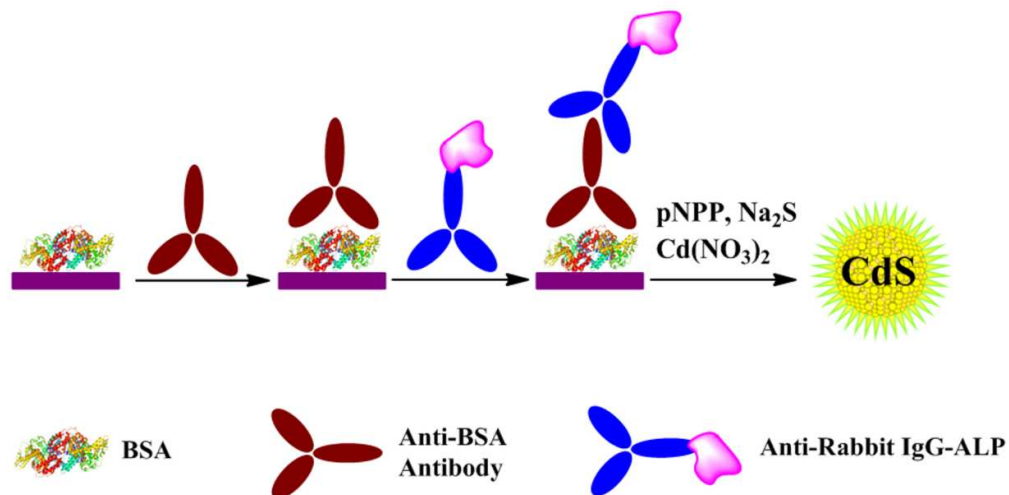


**Figure 5.6.** Detection of Anti-BSA antibody based on enzymatic growth of CdS QDs.

The assay consists of coating polystyrene microtiter plates with BSA and successive incubation with the solutions of anti-BSA antibody from rabbit and ALP-conjugated anti-rabbit IgG. The activity of ALP was measured using the reaction media described above. Figure 5.7 (A) represents fluorescence emission spectra of CdS QDs corresponding to different concentrations of anti-BSA antibody (from 0 to 500 ng mL<sup>-1</sup>) in buffer solution. As one can observe, the increase in the amount of absorbed antibody leads to rising in the fluorescence intensity. Figure 5.7 (B) shows the calibration plot of fluorescence intensity (F) at a fixed emission wavelength of 520 nm versus anti-BSA antibody concentration.

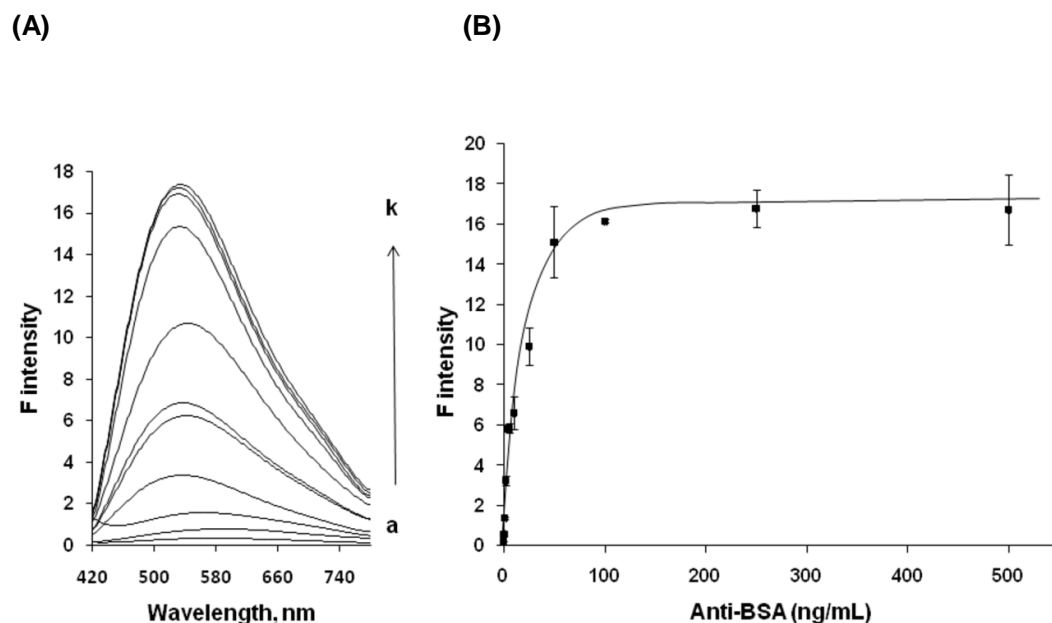


**Figure 5.7.** (A) Emission spectra of CdS QDs in the system containing  $\text{Cd}(\text{NO}_3)_2$  (1.25 mM),  $\text{Na}_2\text{S}$  (0.9 mM), pNPP (0.5 mM),  $\text{MgCl}_2$  (0.5 mM) and various concentrations of anti-BSA antibody: (a) 0  $\text{mU mL}^{-1}$ ; (b) 0.4  $\text{ng mL}^{-1}$ ; (c) 1  $\text{ng mL}^{-1}$ ; (d) 2.5  $\text{ng mL}^{-1}$ ; (e) 5  $\text{ng mL}^{-1}$ ; (f) 8  $\text{ng mL}^{-1}$ ; (g) 25  $\text{ng mL}^{-1}$ ; (h) 50  $\text{ng mL}^{-1}$ ; (i) 100  $\text{ng mL}^{-1}$ ; (j) 250  $\text{ng mL}^{-1}$ ; (k) 500  $\text{ng mL}^{-1}$ . (B) Calibration curve of anti-BSA antibody at  $\lambda=520$  nm (RSD=9.9%,  $n=3$ ).

The response to varying anti-BSA antibody concentrations was linear up to 10  $\text{ng mL}^{-1}$ . The lowest concentration of anti-BSA antibody could be detected by this system was found to be 0.4  $\text{ng mL}^{-1}$  (S/N=3).

Afterwards, we compared the performance of our method with that of the standard immunoassay based on the enzymatic hydrolysis of chromogenic substrate pNPP, followed by UV-Vis spectroscopy (Figure 5.8).



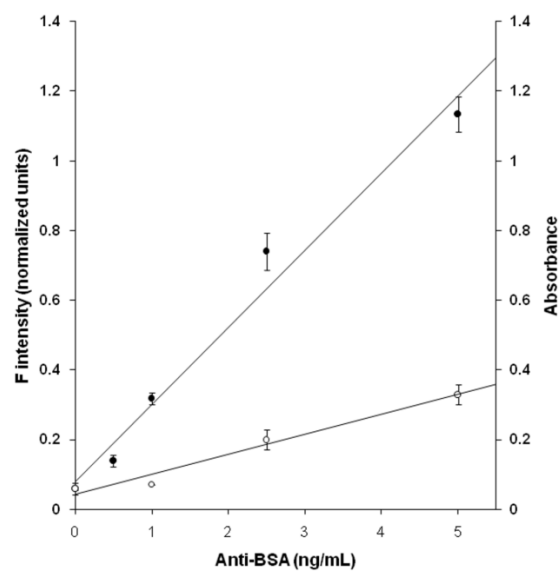


**Figure 5.8.** Calibration curve of anti-BSA antibody measured by the QD-based method (●) and the standard pNPP-based method (○).

The sensitivity to anti-BSA antibody by the QDs-based method was found to be 6.5 times higher than that demonstrated by conventional procedure based on colorimetric measurement of resulting pNP.

## 5.4 Conclusions

A novel fluorogenic ALP assay, easily applied for the detection of analytes through the traditional ELISA assays is reported. This method is based on the unconventional generation of fluorescent CdS QDs using the conventional chromogenic substrate pNPP of ALP. The proposed assay is cost-effective, convenient and does not require any complicated synthetic procedures for the synthesis of fluorogenic enzymatic substrates. At the same time, this simple fluorogenic method exhibits a higher sensitivity compared with that of the traditional chromogenic assay for ALP. We believe that the proposed analytical technique using pNPP substrate may hold potential applications in the clinical diagnosis.

---

## ***Chapter 6. Development of SERS sensor for MnSOD-2 protein detection based on specific DNA probe and gold nanostructure substrate***

### **6.1 Introduction**

Manganese superoxide dismutase 2 (MnSOD-2) is one of the major antioxidant enzymes converting superoxide radicals ( $O_2^{\bullet-}$ ) to hydrogen peroxide ( $H_2O_2$ ) and molecular oxygen ( $O_2$ ) in the response to oxidative stress. Previous investigations showed that high concentration and activity of MnSOD-2 have been linked to several chronic liver diseases [185, 186]. It was also shown that overexpression of MnSOD-2 suppresses the tumorigenicity of human melanoma cells, breast cancer cells and glioma cells, suggesting that MnSOD-2 is a tumor suppressor gene in a wide variety of cancers [187-189]. The accurate determination of MnSOD-2 protein level in biological fluids can give better understanding of the complexity of oxidative stress related with various diseases.

Recently, different kinds of protein-binding oligonucleotides have been published. Due to their specificity to the analyte of interest such kind of molecules have become important tools for diagnostics and therapeutics [190-195]. Biosensors based on this type of oligonucleotides possess several advantages compared with

antibody and enzyme based biosensors. These molecules are chemically stable and can be easily synthesized in the laboratory. The application of oligonucleotides as sensing tool offers a great opportunity for the sensitive and selective protein detection. Vibrational spectroscopic techniques, such as Raman scattering, is a very powerful tool for monitoring DNA-protein interactions because it produces a precise spectral fingerprint, unique to each molecular structure. However, Raman scattering signal is extremely weak. For this reason, SERS has been widely utilized in bioanalysis as it significantly magnifies Raman scattering intensity. Colloidal NPs of different morphology, such as nanospheres, nanocubes, nanorods and nanotriangles due to their interesting optical properties are often used as SERS substrates [196-199]. The geometry parameters of the NPs as well as the separation distance between them play an essential role for SERS-based sensors design [200, 201]. To produce significant electromagnetic field enhancement NPs should aggregate creating so-called "hot spots" [202]. However, only small part of NPs inside this assembly is "optically hot" and improve efficiently SERS signal. To overcome this disadvantage together with low reproducibility of such substrates proper design and assembly of a nanostructure should be performed. Nanolithography is known to provide nanostructures with defined size, shape and spacing parameters and, thus, allowing to control Raman enhancement. Recently, fabricated metal nanowire structures possessing fascinating optical properties have been exploited as SERS substrates [203]. In such kind of structures owing to the optical antenna effect additional electromagnetic field enhancement can be observed. Raman enhancement showed to be dependent on laser excitation and nanowire length. Thus by changing the latter parameter optical properties of the system can be easily tuned to achieve the best sensitivity. Additional enhancement of SERS signal can be obtained by coupling of the nanoantennas tip-to-tip end across the small gap (nm range). Such dimers create a "hot spot" leading electromagnetic field enhancement by several orders of magnitude in comparison with uncoupled structures [204].

---

In this work we report a novel label-free SERS biosensor for MnSOD-2 protein detection based on specific DNA probe and well organized nanolithographed structures. The sensor achieves high sensitivity of 100 nM by monitoring the SERS signal change upon binding even between MnSOD-2 and DNA immobilized on the nanostructures. The proposed sensing platform may be applied for multiplexed protein detection using different DNA probes.

## 6.2 Experimental part

### 6.2.1 Materials and methods

Human superoxide dismutase 2 was ordered in Abfrontier (South Korea), potassium chloride, trizma base, 6-mercapto-1-hexanol, magnesium chloride hexahydrate, ammonium hydroxide solution 28%-30% and ethanol were purchased from Sigma-Aldrich (Spain). Standard DNA phosphoramidites, 5'-thiol-modifier C6-CE phosphoramidite and other reagents required for solid phase oligonucleotide synthesis were purchased from Link Technologies (UK). Oligonucleotide purification cartridges (OPG), 2.0 M triethylamine acetate buffer, trifluoroacetic acid, acetonitrile were ordered in Applied Biosystems (Spain). Milli-Q water (18.2 M $\Omega$ ) was used to prepare all solutions.

### 6.2.2 Preparation and characterization of oligonucleotides

**Synthesis of oligonucleotides.** Following DNA sequence was synthesized: *thiolated MnSOD-2 probe* (5'- HS- (-O-CH<sub>2</sub>-CH<sub>2</sub>- O)<sub>6</sub> TT TTT TTT TTT TTC TTC TCT AGC TGA ATA ACC GGA AGT AAC TCA TCG TTT CGA TGA GTT ACT TCC GGT TAT TCA GCT AGA GAA G-3'), where (-O-CH<sub>2</sub>-CH<sub>2</sub>- O)<sub>6</sub> corresponds to spacer-CE phosphoramidite 18. Synthetic DNA oligonucleotide was prepared by automated solid-phase chemical synthesis on 3400 DNA synthesizer (Applied Biosystems). The powdered prepackaged phosphoramidites were dissolved in anhydrous ACN at 0.1 M concentration and attached manually to DNA synthesizer

ports. The oligonucleotide sequence was created using Web browser connected to 3400 DNA Synthesizer. The synthesis run was set up by creating a custom cycle script. The synthesis was realized in 1  $\mu$ M scale. The DNA was synthesized on the solid-phase column with the first appropriate phosphoramidite attached. After the synthesis was finished the column was removed from the 3400 DNA Synthesizer and the oligonucleotide was collected to a tightly sealed oligonucleotide collection vial. Base deprotection step was performed by ammonolysis reaction. 1.5 ml of concentrated ammonium hydroxide was added to the collection vial with oligonucleotide. After it was placed in the heating block (Eppendorf) and heated for 8-15 hours at +55 °C while shaking. After the oligonucleotide solution in ammonium hydroxide was put in a refrigerator for 10 minutes and the latter was removed by vacuum. Final purification of oligonucleotide was performed on the OPC cartridge.

***Purification of oligonucleotides.*** Cleaved and deprotected on the previous stage oligonucleotide was purified using OPC column. The 5-ml Luer slip-tip syringe was connected to the end of the OPC cartridge, a male-to-male Luer tip was connected to other end. The OPC cartridge was flushed with 5 mL of HPLC-grade ACN followed by 5 mL of 2.0 M TEAA. Crude deprotected oligonucleotide was diluted by deionized water to achieve final volume of 1.5 ml. The above solution was loaded to the syringe and gently pushed through the column, collecting the eluted fractions. The eluate was reloaded and pushed through the cartridges again. The column was flushed with 5 ml of 1.5 M ammonium hydroxide and then twice with 5 ml of deionized water. The OPC cartridge-bound oligonucleotide was detritylated with 3% of TFA solution. 1mL of TFA was gently pushed through the column and incubated for 5 minutes. After incubation step, remaining TFA solution was flushed through the cartridge, followed by washing with 5 ml of deionized water (twice). Purified, detritylated oligonucleotide was slowly eluted by 1 mL of 20 % ACN/H<sub>2</sub>O solution. The concentration of pure oligonucleotide was determined by measuring absorbance at  $\lambda=260$  nm on ND 1000 Spectrophotometer. The oligonucleotide

solution was lyophilized and 4  $\mu\text{M}$  aliquots were prepared in Milli-Q sterilized water and stored at  $-80\text{ }^{\circ}\text{C}$ .

### 6.2.3 Functionalization protocol

***Nanoantenna substrate treatment.*** Nanoantenna substrate was cleaned in absolute ethanol (overnight stirring) and dried under a stream of nitrogen. Afterwards, the sample was treated by ultraviolet radiation during 30 minutes.

***DNA probe immobilization.*** A 20  $\mu\text{l}$  drop of thiolated DNA probe was placed on the nanostructure and incubated during one hour at RT. Next, nanoantenna substrate was washed twice for five minutes in water (while gently shaking) to remove unbound DNA and dried under the stream of nitrogen.

***Surface blocking.*** Nanoantenna substrate with immobilized DNA probe was immersed to 6-MHO solution (2 mM in EtOH), incubated during one hour at RT while gentle shaking. Then the sample was washed twice for five minutes in EtOH to remove unbound 6-MHO and dried under the stream of nitrogen.

***Protein detection:*** After previous immobilization steps, various concentrations of MnSOD-2 in working buffer (50 mM Tris-HCl, 100 mM NaCl, 5 mM  $\text{MgCl}_2$ , pH 8.2) were tested starting from the most diluted probe (10 nM, 100 nM 1  $\mu\text{M}$ ). The drop of protein in working buffer (WB) was placed on the nanostructure and incubated during one hour. Then unreacted protein was washed out by WB, rinsed quickly in water to remove excess of the buffer salts and dried under a stream of nitrogen.



### 6.2.4 LSPR and SERS detection

Extinction and SERS spectra were recorded on a Horiba Jobin-Yvon HR800 spectrometer coupled to an Olympus Bx51 optical microscope. The extinction spectra were recorded in transmission configuration with a 20x objective (numerical aperture, NA=0.4). As a reference signal we used a light signal transmitted through the CaF<sub>2</sub> substrate. The sample was illuminated in normal incidence with collimated white light. The SERS spectra were measured using a 100x magnification objective (NA=0.9) in backscattering configuration, with a spectral resolution 2.5 cm<sup>-1</sup>. All SERS spectra were acquired using a He-Ne lamp ( $\lambda=633$  and  $\lambda=785$  nm) with a power of 15 and 30 mW, respectively). The position of the band maxima was reproducible within  $\pm 1$  cm<sup>-1</sup>.

## 6.3 Results and discussion

### 6.3.1 Sensor work

A schematic representation of the labelless SERS sensor for MnSOD-2 detection is shown on the Figure 6.1. The sensing mechanism is based on the single-step binding event between analyte and *probe DNA*, immobilized on the surface of nanostructure. The extinction and SERS spectra after each step described in experimental part were acquired upon laser excitation.

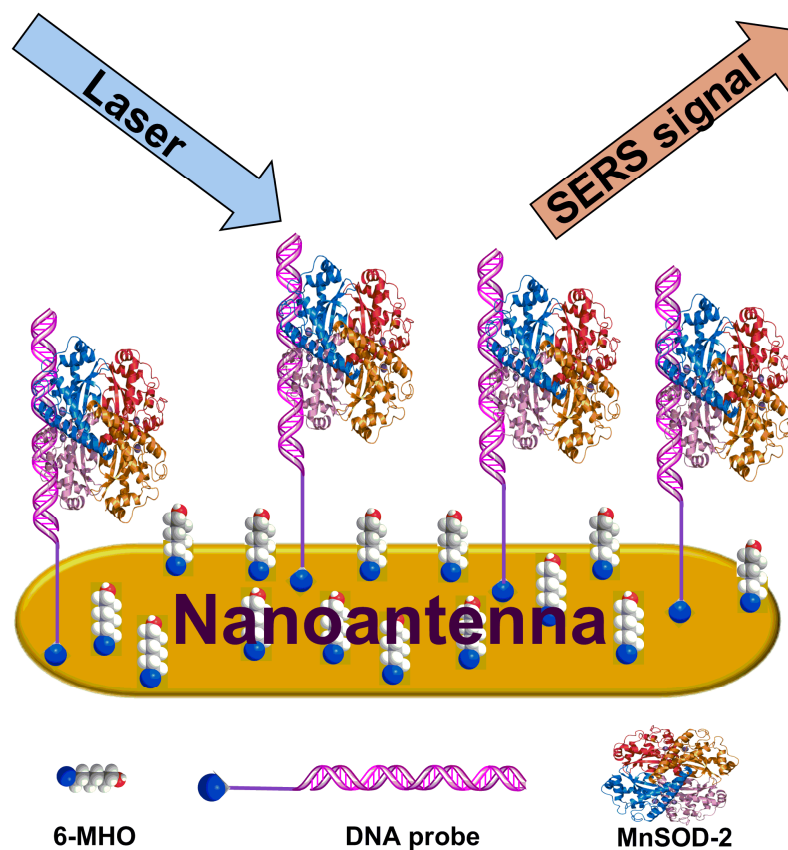
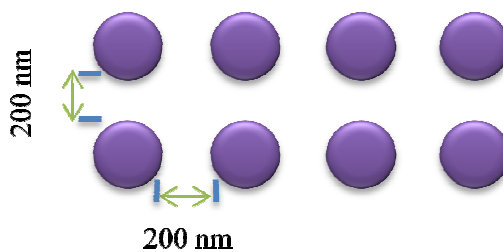


**Figure 6.1.** Schematics of illustration of labelless SERS sensor for MnSOD-2 detection.

To find the best conditions for SERS signal enhancement and, therefore protein detection two types of gold nanostructures (non coupled nanocylinder and coupled nanoantenna arrays), fabricated on glass substrate by electron beam lithography (EBL) and lift-off technique [205, 206], were used in the experiment. The diameter of nanocylinders shown on Figure 6.2 (A) in plain varied from 90 to 200 nm, inter-cylinder distance in both directions was 200 nm, the height out of plain was 50 nm.

The length of nanoantenna (Figure 6.2 (B)) was 100 nm with the 60 nm wide and 50 nm high; the gap between coupled antennas was 200 nm in both directions with 20 nm gap inside dimer.

(A)



(B)

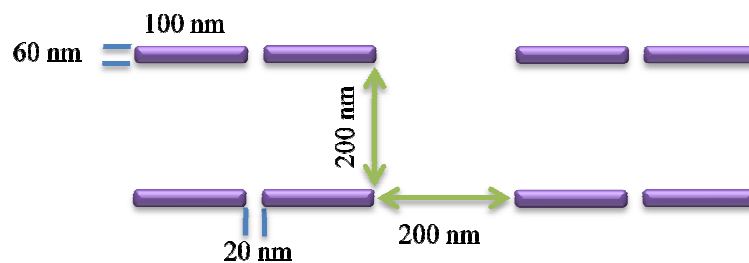


**Figure 6.2.** Schematic representation of nanocylinders (A) and nanoantenna (B) based SERS substrate.

The scanning electron microscope images of gold nanocylinders and gold nanoantenna SERS substrates obtained by EBL are shown on Figure 6.3 (A, B).

(A)

(B)

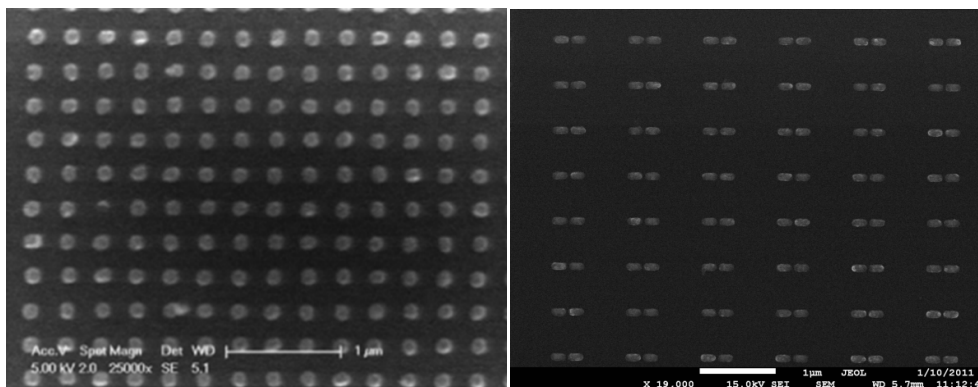


**Figure 6.3.** Scanning electron microscopy images of the nanocylinder (A) and nanoantenna (B) array obtained by EBL (made in UTT, Paris).

For functionalization of the nanostructures specially designed *DNA probe* (developed in Laboratory of Dr. V. Pavlov, data not published) linking to MnSOD-2 protein was used. The dsDNA was labeled on the 5'- end with the thiol group to obtain strong covalent binding with the gold surface. To reach high surface coverage the immobilization of DNA was provided in the solution with high ionic strength (1M KCl) to screen DNA strands repulsion. To protect antennas from unspecific absorption of the proteins the surface was blocked with 6-MHO (2 mM). Afterwards, reaction between immobilized DNA probe and different concentrations of MnSOD-2 was preformed.

### 6.3.2 Extinction measurements: nanocylinders

To investigate the interaction of *DNA probe* with MnSOD-2 visible extinction spectra were measured after each deposition step in order to determine the effect of the protein on the LSPR shift. Figure 6.4 represents UV-Vis absorption spectra of clean gold nanocylinders depending on their diameter. The position of LSPR extinction maximum ( $\lambda_{\max}$ ) of gold nanocylinders was used to determine LSPR shift.

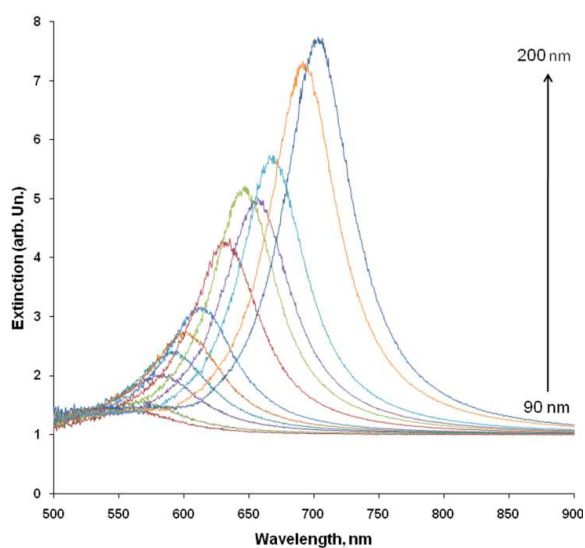


**Figure 6.4.** Extinction spectra of clean gold nanocylinders.

Figure 6.5 represents  $\lambda_{\max}$  of clean nanocylinders (reference) and after deposition of *DNA probe*, 6-MHO and 10 nM MnSOD-2 protein versus cylinders diameter.

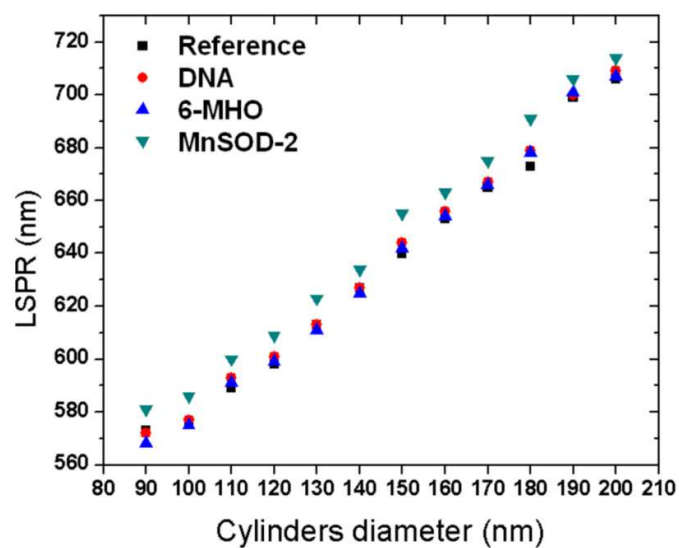


**Figure 6.5.** Position of the LSPR Vs nanocylinder diameter after each deposition step

Since the LSPR of the NPs is highly dependent on the local environment,  $\lambda_{\max}$  will shift when molecules will bind to the surface of the NPs. The LSPR shift,  $\Delta\lambda_{\max}$ , induced by the adsorbates is given by the following equation:

$$\Delta\lambda_{\max} = \lambda_{\max}(\text{after}) - \lambda_{\max}(\text{before})$$

The shift in the LSPR extinction maximum ( $\Delta\lambda_{\max}$ ) of the nanocylinders was calculated and summarized in Table 6.1.

Cylinders diameter (nm)	LSPR shift (nm)		
90	-1	-4	13
100	2	-2	11
110	4	-2	9
120	3	-2	10
130	0	-2	12
140	0	-2	9
150	4	-2	13
160	3	-2	9
170	2	-1	9
180	6	-1	13
190	1	1	5
200	3	-2	7

**Table 6.1.** LSPR shift on nanocylinders (diameter from 90 to 200 nm).

According to this data the LSPR shift for DNA varied from -1 to 6 nm, with 2.25 nm in average, showing that we can detect DNA probe deposition based on LSPR position. The shift value for 6-MHO was negative and varied from -4 to -1, with 1.75 nm in average showing slightly blue shift which is considered normal as little 6-MHO molecules replace bulk DNA probe organizing a monolayer and preventing nonspecific DNA-gold interaction [207]. The biggest LSPR shift was observed for MnSOD-2 and varied from 7 to 13 nm, with 10 nm in average. This is in accordance with the previously published work on LSPR-based protein sensors reporting that binding of the proteins in nanoscale induces large shift in the LSPR. Thus, the data obtained on the LSPR shift for MnSOD-2 suggest that we can detect the presence of the protein.



### 6.3.3 SERS measurements: nanocylinders

SERS spectra were recorded for each of the above described experimental steps. All the spectra were collected under identical conditions at excitation wavelengths of 785 nm (Figure 6.6 (A)) and 660 nm (Figure 6.6 (B)) with laser power of 1.3 mW and an acquisition time of 10 s (no baseline correction).

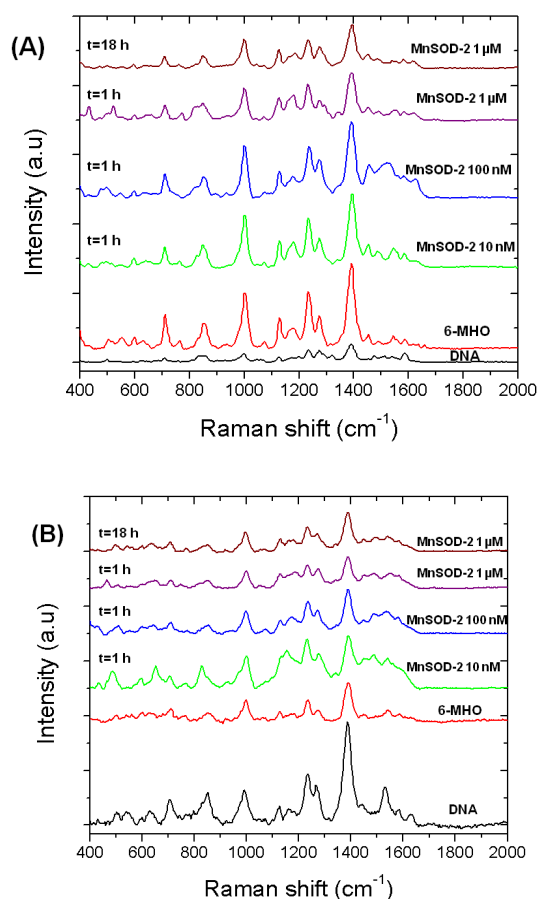


**Figure 6.6.** SERS spectra at excitation wavelength of 785 nm (A) and 660 nm (B) acquired on nanocylinders after each deposition step: DNA probe functionalization (black curve), 6-MHO blocking (red curve), different concentrations and incubation time with MnSOD-2 10

nM, 1h (green curve), 100 nM, 1h (blue curve), 1  $\mu$ M 1h (purple curve) and 1  $\mu$ M 18h (brown curve).

The SERS spectra confirm the success of the coverage of the nanocylinders surface with the *DNA probe*. The black curve (*DNA probe*) on both figures is obtained as the average of 10 spectra acquired in different positions and clearly reveals the typical nucleic acids vibrational bands of the DNA reported in literature. The Figure 6.6 shows the spectra acquired on the nanocylinders after the protection of the gold surface with 6-MHO. There is no evident shift of the vibrational DNA bands, and only an increase in the background intensity is observed as the DNA molecules are partially replaced from the gold surface by 6-MHO, what was mentioned before for the LSPR analysis data. The antennas functionalized with the DNA probe and blocked with 6-MHO were immersed for 1 hour in the WB containing MnSOD-2 at initial concentration of 10 nM, then washed and dried following the protocol. For the different concentrations used (from 10 nM to 1  $\mu$ M), we observed the spectra shown in Figure 6.7, obtained as average of 10 measurements in different positions of the sample. For the lowest concentration the spectra acquired after the incubation of the protein showed the characteristic band at 1500  $\text{cm}^{-1}$ , which can be attributed to the amide I band of proteins. This band increases and become wider compare with the spectra acquired only with *DNA probe* + 6-MHO. Moreover, the shape of the DNA peaks change and we observe a new peak at 650  $\text{cm}^{-1}$ . However, further increase of the concentration of MnSOD-2 leads to decrease of 1500  $\text{cm}^{-1}$  band.

### 6.3.4 SERS measurements: nanoantennas

SERS spectra were recorded for each of the previous described experimental step. All the spectra were collected in the identical conditions at excitation wavelength of 785 nm (Figure 6.7) with laser power of 1.3 mW and an acquisition time of 60 s (no baseline correction).

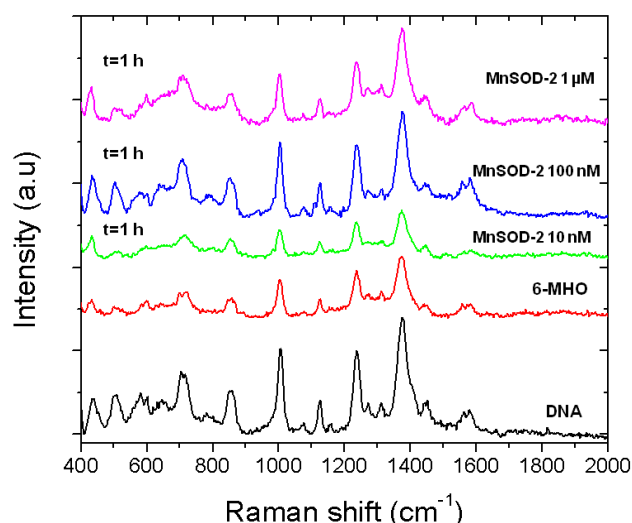


**Figure 6.7.** SERS spectra at excitation wavelength of 785 nm acquired on nanoantennas after each deposition step: *DNA probe* functionalization (black curve), 6-MHO blocking (red curve), different concentrations of MnSOD-2 10 nM, 1h (green curve), 100 nM, 1h (blue curve) and 1  $\mu$ M 1h (purple curve).

The SERS spectra confirm the success of the coverage of the nanoantenna surface with the *DNA probe* as for the nanocylinders and exploits the typical nucleic acids vibrational bands of the DNA. Moreover, the Figure 6.7 shows the spectra acquired by the nanoantenna after the immobilization of the gold surface with the 6-MHO. There is no evident shift of the vibrational DNA bands, and only an increasing

of the background intensity is observed. After deposition of 10 nm MnSOD-2 we did not see any changes in the spectra. However after deposition of 100 nM protein on the antenna  $1500\text{ cm}^{-1}$  band which is characteristic of the amide I band of proteins, increased and became wider with rising the concentration of MnSOD-2. Moreover, the shape of the DNA peaks changed and a new peak at  $650\text{ cm}^{-1}$  appeared.

On the spectra (Figure 6.8 (black line)) the presence of the MnSOD-2 linked to the *DNA probe* is confirmed by the appearance of different bands in the range  $600\text{--}1600\text{ cm}^{-1}$  that can be associated with the MnSOD-2 vibrational modes based on the assignments carried out from the Raman measurements in solution.

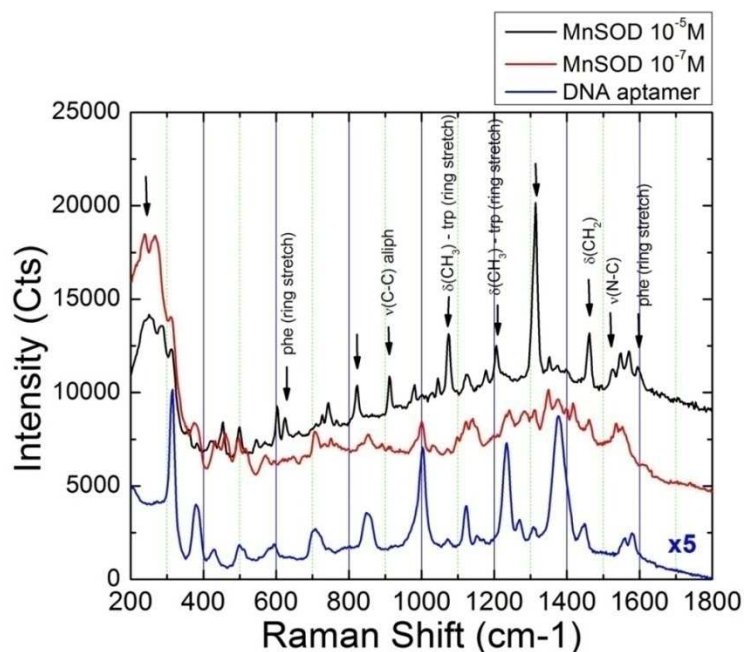


**Figure 6.8.** SERS spectra of MnSOD-2 protein after the incubation of the antennas sample in a proteins solution at concentration of  $10\text{ }\mu\text{M}$  (black curve) and  $100\text{ nM}$  (red curve). These spectra are compared with the one acquired after the *DNA probe* immobilization. The arrows highlight the difference between the spectra before (blue line) and after the capture of the MnSOD-2 protein by the *DNA probe*. (The appeared bands are assigned to the respective vibrations of MnSOD-2, following to that what found in the Raman measurements in solution at concentration higher than  $10\text{ mM}$  (limit of detection for our Raman setup))

In particular two pairs of modes associated to the aromatic side chain of the phenylalanine and the tryptophan amino acids, are visible at 623 and 1594  $\text{cm}^{-1}$ , and 1073 and 1203  $\text{cm}^{-1}$ , respectively. The peak at 911  $\text{cm}^{-1}$  is assigned to the aliphatic C-C stretching vibration, while the modes at 1462 and 1525  $\text{cm}^{-1}$  are related to the C-H<sub>2</sub> non-aromatic bending and the C-N stretching respectively.

The obtained results prove that the functionalized antennas are able to detect the MnSOD-2 protein at low concentration. The active sites for the detection are localized only in specific region of the antennas array and are not distributed homogeneously across all nanostructured gold surface of the sample. Despite this fact even for high concentrations we were able to detect the protein on the entire surface.

To evaluate the reliability of the developed method experiments with human serum on nanocylinder array were performed (Figure 6.9). The procedure of MnSOD-2 detection in human serum was performed in the same conditions as for pure MnSOD-2 protein.

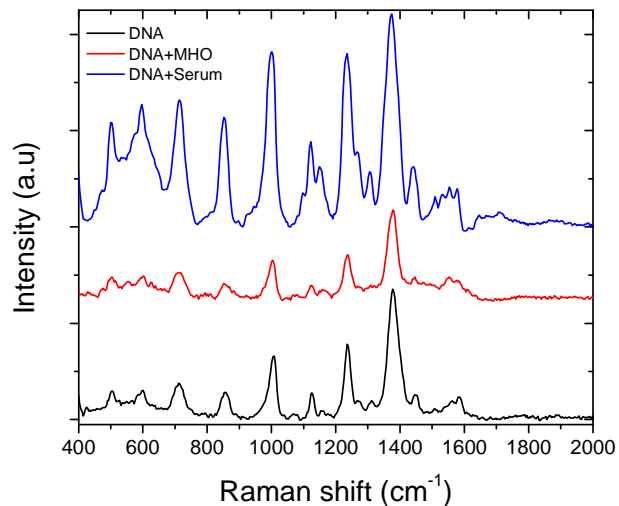


**Figure 6.9.** Nanocylinder functionalization with the *DNA probe* (black curve), blocking with 6-MHO (red curve) and incubation with human serum (blue line).

The experiments were performed using non coupled cylinders. The concentration of MnSOD-2 in human serum measured by standard ELISA was 10  $\mu\text{M}$ . The results were obtained with the laser excitation wavelength of 660 nm. The recorded Raman spectra clearly showed the presence of MnSOD-2 protein in human serum.

## 6.4 Conclusions

The present study demonstrated that the use of nanolithographed SERS substrates can be used for sensitive detection of MnSOD-2 based on the binding event between specially designed *DNA probe* and the protein. In this assay, we were able to detect 100 nM concentration of the MnSOD-2 what is comparable with very sensitive analytical methods such as ELISA. The enhancement of the vibrational bands of MnSOD-2 relying on advantageous properties of the gold nanostructures allowed us to increase significantly the response of the system compare with traditional Raman spectroscopy. The investigation of biological media showed positive results. First experiments with human serum led to great success in MnSOD-2 protein detection at very low concentrations. This work is very promising in light of potential applications in biosensors for detection of disease biomarkers.

## ***General conclusions***

In this PhD study novel methods for the signal amplification in bioanalytical assays based on the combination of biochemical reaction with the surface chemistry of nanomaterials were developed.

The major findings of this research are summarized below:

A DNAzyme based optical biosensor for the rapid, sensitive and selective detection of AA where 13 nm Au NPs were used as carriers for fluorogenic substrate molecule was developed. To achieve maximum surface coverage the reaction between NPs and thiolated oligonucleotide was performed in the buffer with high salt concentration. It was found that the enormous signal enhancement in this assay was due to catalytic redox properties of gold nanoclusters. The later allowed us to diminish significantly the volume of the analyzed samples.

A self-cleavage DNAzyme based impedimetric biosensor for copper (II) ions detection was designed. To provide efficient binding between GEC electrode and oligonucleotide avidin-biotin chemistry was used. To achieve the maximum surface coverage of the electrode the DNA concentration was optimized. The response of the system rising from the tiny disturbance at the surface of the electrode in the presence of  $\text{Cu}^{2+}$  was investigated. The combination of the DNAzyme together with EIS allowed us to create a very promising platform for the sensitive and selective  $\text{Cu}^{2+}$  detection.

A first fluorogenic immunoassay based on *in situ* generation of semiconductor QDs in the presence of the products of enzymatic reaction was



developed. A conventional system including pNPP as a substrate and ALP-conjugated antibodies was used to perform the method. The fluorescence response of the reaction rising from the quantum dot formation was investigated in the presence of different concentrations on the analyte (antibody). The limit of detection in standard assay was improved by application of QDs and allow us to apply this model system in bioanalysis.

A labelless SERS biosensor based on nanoantenna device in combination with specific DNA probe for the detection of MnSOD-2 was developed. Two types of nanostructures (cylinders and wires) were used as SERS substrate. Resonant excitation of the nanoantenna provides large enhancement of the vibrational signal of the target molecule and consequently high sensitivity of the assay. The response of the sensor in the presence of various concentrations of MnSOD-2 was investigated and showed to have high sensitivity.

# Appendix

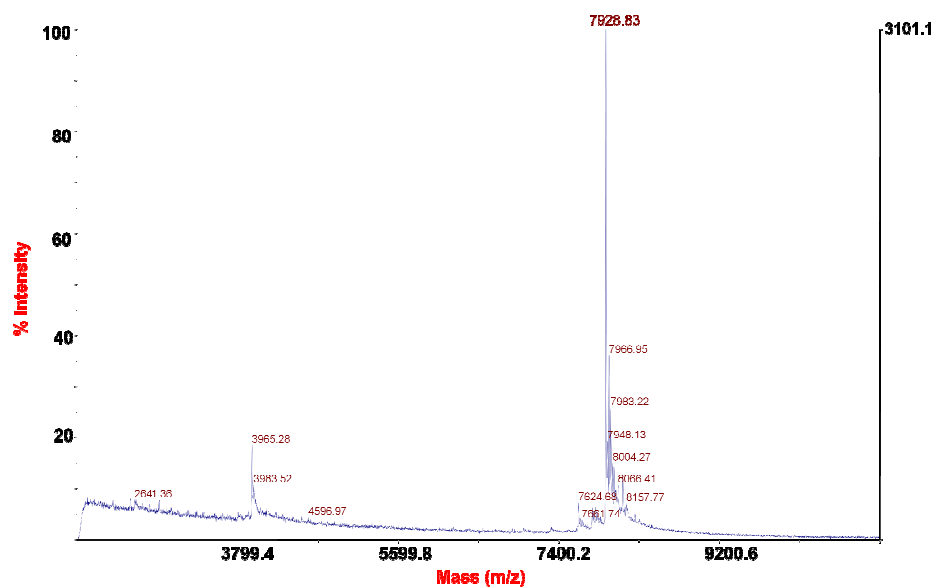


**Figure A- 1.** MALDI-TOF spectra of *catalyst DNA*: experimental, 7928.83; calculated 7928.01

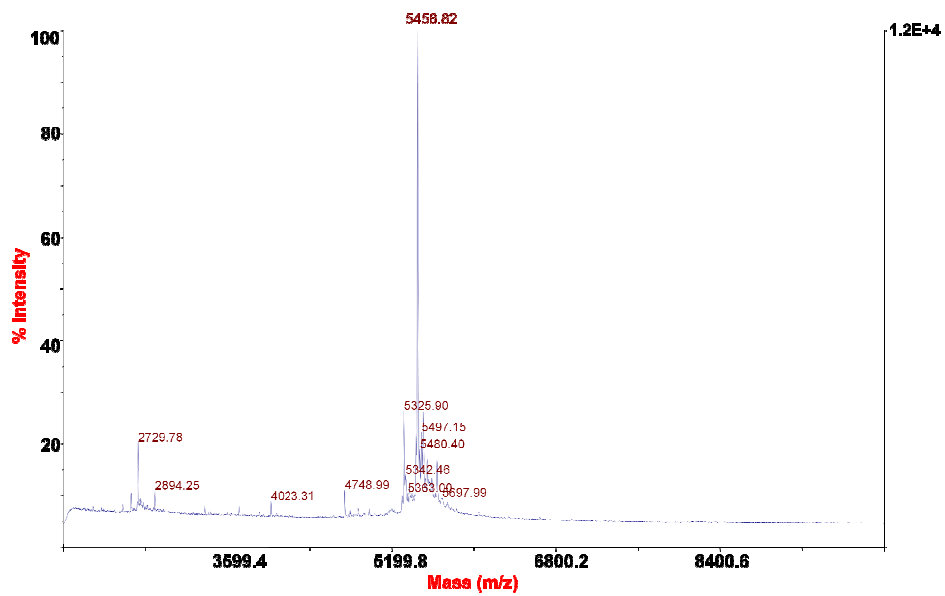
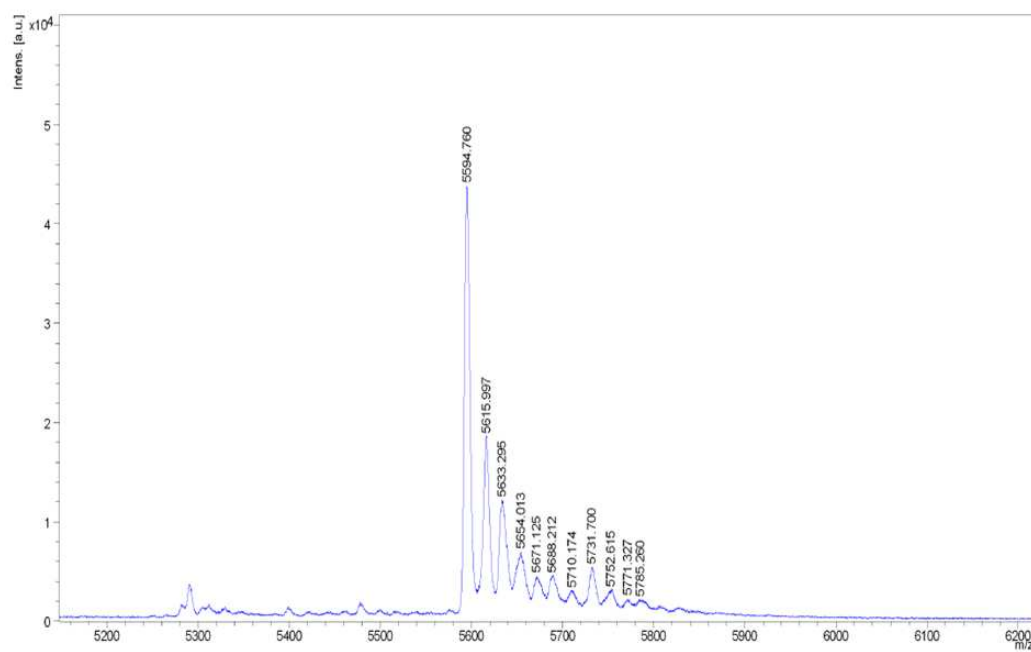
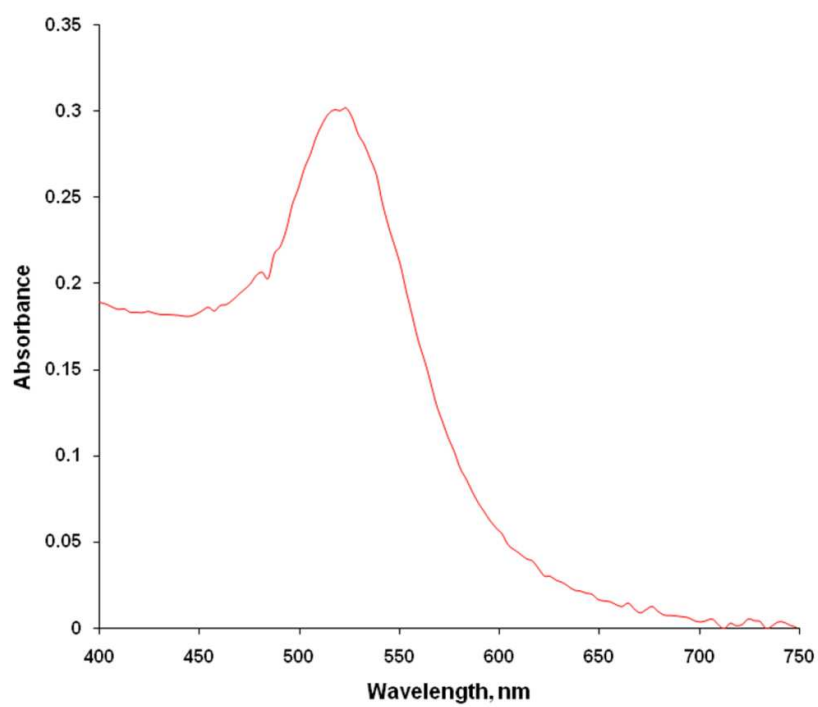


Figure A- 2. MALDI-TOF spectra of substrate DNA: experimental, 5458.82; calculated, 5458.02

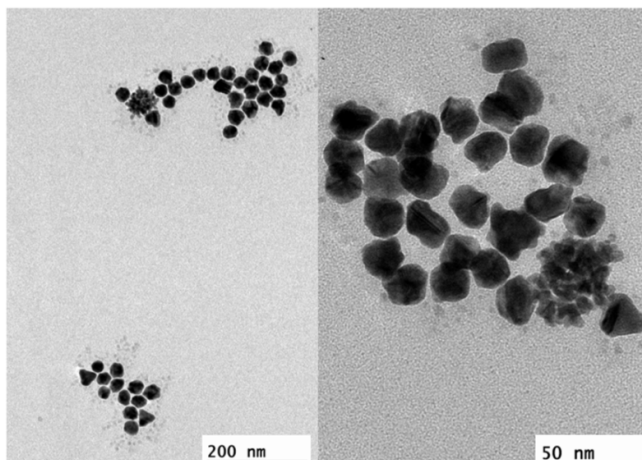


**Figure A- 3.** MALDI-TOF spectra of reduced by DTT *thiolated substrate DNA*: experimental, 5594.76; calculated, 5593.07.



**Figure A- 4.** UV spectra of solution of citrate capped AuNPs.

(A)



(B)

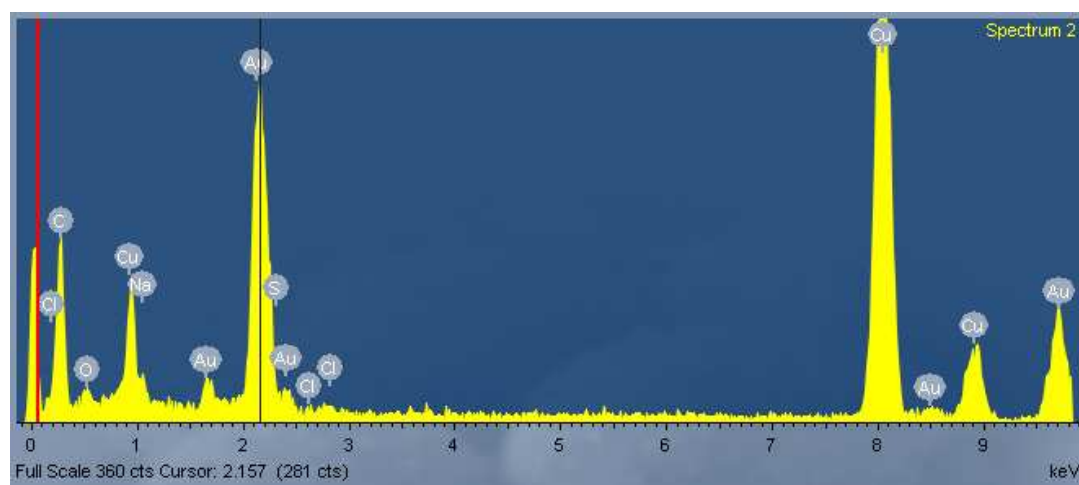


**Figure A- 5.** TEM micrographs (A) and EDS spectra (B) of 13 nM Au NPs received by citrate method. The TEM image were taken on JEM-2100F UHR TEM.

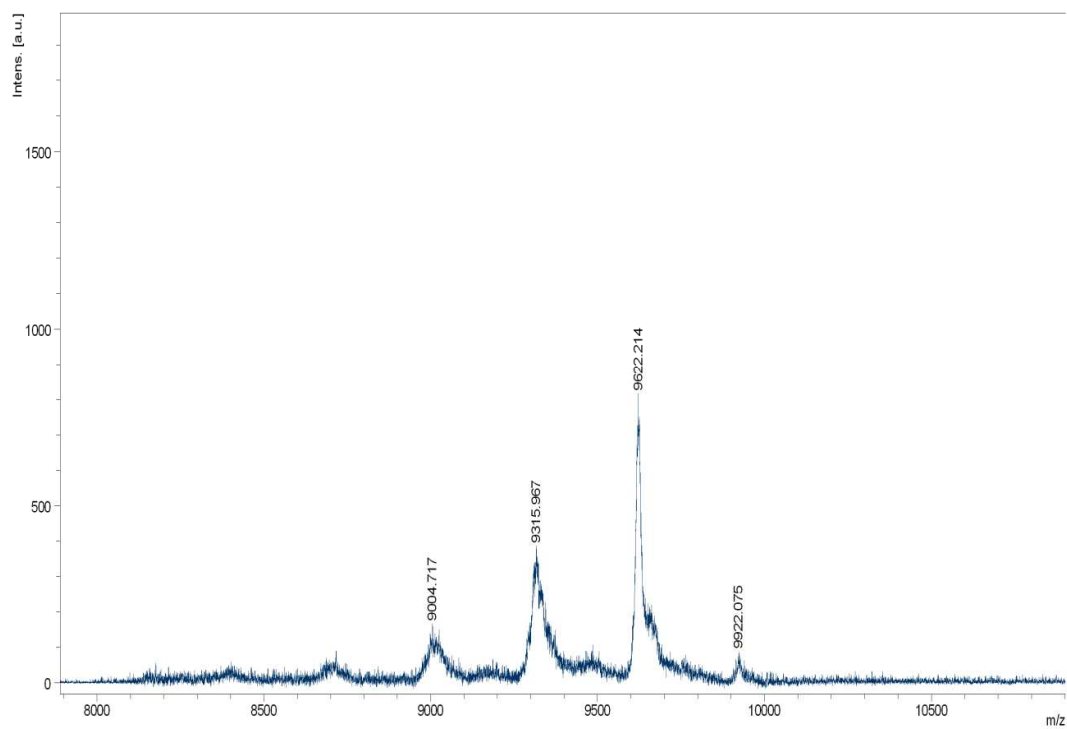
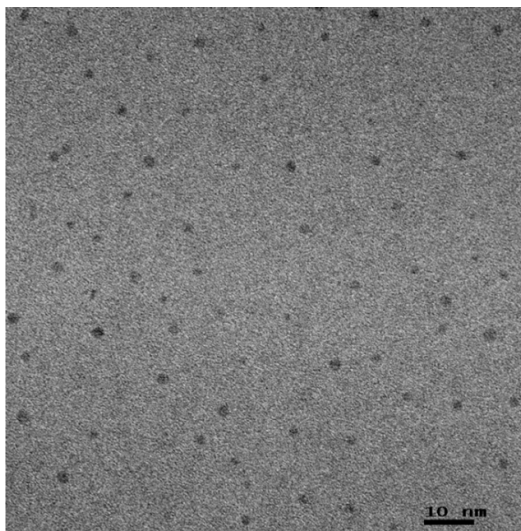


**Figure A- 6.** MALDI-TOF spectra of DNAzyme: experimental, 9622.23; calculated 9628.57.

(A)



(B)

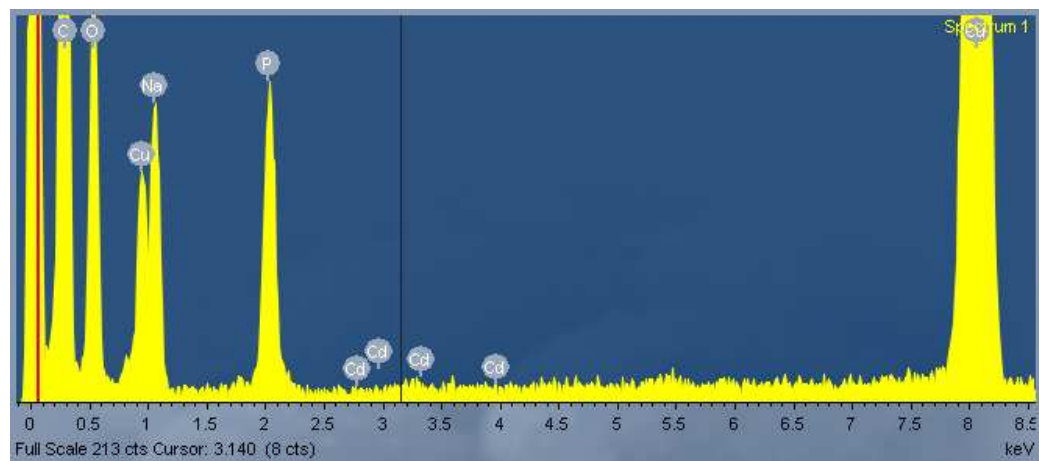


**Figure A- 7** TEM image (A) and EDS spectra (B) of the CdS QDs formed in the presence of Na<sub>2</sub>S (0.6 mM), ALP (250 mU mL<sup>-1</sup>) and Cd(NO<sub>3</sub>)<sub>2</sub> (12.5 mM), pNPP 0.5 mM. The TEM image were taken on JEM-2100F UHR TEM.



	<b>F-F<sub>0</sub> (units/s)</b>
Fructose	0.00034±0.00011
Glucose	0.0021±0.0016
Citric acid	0.00089±0.00009
Urea	0.00071±0.00013

**Table A- 1.** Interference assay for DNAzyme based sensor.

	<b>F-F<sub>0</sub> (units/s)</b>
Fructose	- 0.0000067±0.0000031
Glucose	0.000055±0.000009
Citric acid	- 0.000011±0.000005
Urea	0.000071±0.000004

**Table A- 2** Interference assay for gold NPs based sensor.

## ***References***

1. Cook, D.B., et al., Lectin ELISA for the c-erb-B2 Tumor Marker Protein p185 in Patients with Breast Cancer and Controls. *Clin. Chem.*, 1999. 45(2): p. 292-295.
2. Acevedo, B., et al., Development and validation of a quantitative ELISA for the measurement of PSA concentration. *Clin. Chim. Acta*, 2002. 317(1-2): p. 55-63.
3. Guergova-Kuras, M., et al., Discovery of Lung Cancer Biomarkers by Profiling the Plasma Proteome with Monoclonal Antibody Libraries. *Mol. Cell. Proteomics*, 2011. 10(12): p. 1-14.
4. Döpel, S.-H., et al., Application of a human monoclonal antibody in a rapid competitive anti-HIV ELISA. *J. Immunol. Methods*, 1989. 116(2): p. 229-233.
5. Rehle, T.M., et al., Evaluation of a quantitative double ELISA strategy for confirmation and differentiation of HIV infection. *J. Virol. Methods*, 1997. 66(2): p. 203-209.
6. Ma, X., et al., Development of monoclonal antibodies and a competitive ELISA detection method for glycinin, an allergen in soybean. *Food Chem.*, 2010. 121(2): p. 546-551.
7. Layton, G.T. and D.R. Stanworth, The Quantitation of IgG4 Antibodies to Three Common Food Allergens by ELISA with Monoclonal Anti-IgG4. *J. Immunol. Methods*, 1984. 73(2): p. 347-356.

8. Chassaigne, H., et al., Investigation on sequential extraction of peanut allergens for subsequent analysis by ELISA and 2D gel electrophoresis. *Food Chem.*, 2007. 105(4): p. 1671-1681.
9. An, S.F., A. Ciardi, and F. Scaravilli, PCR detection of HIV proviral DNA (gag) in the brains of patients with AIDS: comparison between results using fresh frozen and paraffin wax embedded specimens. *J. Clin. Pathol.*, 1994. 47: p. 990-994.
10. QU, W., et al., PCR Detection of Human Papillomavirus: Comparison between MY09/MY11 and GP51/GP61 Primer Systems. *J. Clin. Microbiol.*, 1997. 35(1304-1310).
11. Rosales-Reynoso, M.A., et al., PCR Approach for Detection of Fragile X Syndrome and Huntington Disease Based on Modified DNA: Limits and Utility. *Genet. Test.*, 2007. 11(2): p. 153-159.
12. Boehnke, M., et al., Fine-Structure Genetic Mapping of Human Chromosomes Using the Polymerase Chain Reaction on Single Sperm: Experimental Design Considerations. *Am. J. Hum. Gen.*, 1989. 45: p. 21-32.
13. Kingsmore, S.F. and D.D. Patel, Multiplexed protein profiling on antibody-based microarrays by rolling circle amplification. *Curr. Opin. Biotechnol.*, 2003. 14(1): p. 74-81.
14. Ma, C., et al., Homogeneous and label-free fluorescence detection of single-nucleotide polymorphism using target-primed branched rolling circle amplification. *Anal. Biochem.*, 2011. 26(7): p. 3309-3312.
15. Zhao, W., et al., Rolling Circle Amplification: Applications in Nanotechnology and Biodetection with Functional Nucleic Acids. *Angew. Chem Int. Ed.*, 2008. 47(34): p. 6330-6337.

16. Kolpashchikov, D.M., A Binary Deoxyribozyme for Nucleic Acid Analysis. *ChemBioChem*, 2007. 8(17): p. 2039-2042.
17. Sando, S., et al., Amplified Nucleic Acid Sensing Using Programmed Self-Cleaving DNAzyme. *J. Am. Chem. Soc.*, 2003. 125(51): p. 15720-15721.
18. Silverman, S.K., Catalytic DNA (deoxyribozymes) for synthetic applications—current abilities and future prospects *Chem. Commun.*, 2008: p. 3467-3485.
19. Chen, J., et al., Gold nanoparticles-based fluorescence resonance energy transfer for competitive immunoassay of biomolecules. *Analyst*, 2012. 137(24): p. 5885-5890.
20. Csáki, A., et al., The optical detection of individual DNA-conjugated gold nanoparticle labels after metal enhancement. *Nanotech.*, 2003. 14(12): p. 1262-1268.
21. Zhang, J., et al., Surface-Enhanced Fluorescence of Fluorescein-Labeled Oligonucleotides Capped on Silver Nanoparticles. *J. Phys. Chem. B.*, 2005. 109(16): p. 7643-7648.
22. Li, J.-M., et al., Multiplexed SERS detection of DNA targets in a sandwich-hybridization assay using SERS-encoded core-shell nanospheres. *J. Mater. Chem.*, 2012. 22: p. 12100-12106.
23. Harper, M.M., et al., Detection of SERS active labelled DNA based on surface affinity to silver nanoparticles. *Analyst*, 2012. 137: p. 2063-2068.
24. Nenga, J., et al., A versatile SERS-based immunoassay for immunoglobulin detection using antigen-coated gold nanoparticles and malachite green-conjugated protein A/G. *Biosens. Bioelectron.*, 2010. 26(3): p. 1009-1015.

25. Ambrosi, A., F. Airò, and A. Merkoçi, Enhanced Gold Nanoparticle Based ELISA for a Breast Cancer Biomarker. *Anal. Chem.*, 2010. 82(3): p. 1151–1156.
26. Chai, Y., et al., A novel electrochemiluminescence strategy for ultrasensitive DNA assay using luminol functionalized gold nanoparticles multi-labeling and amplification of gold nanoparticles and biotin–streptavidin system. *Chem. Commun.*, 2010. 46: p. 7560-7562.
27. Liu, Q., et al., CdSe quantum dots as labels for sensitive immunoassay of cancer biomarker proteins by electrogenerated chemiluminescence. *Analyst*, 2011. 136: p. 5197-5203.
28. Luo, Y., et al., Sensitive and rapid quantification of C-reactive protein using quantum dot-labeled microplate immunoassay. *J. Transl. Med.*, 2012. 10.
29. Gerion, D., et al., Sorting Fluorescent Nanocrystals with DNA. *J. Am. Chem. Soc.*, 2002. 124(24): p. 7070-7074.
30. Gerion, D., et al., Room-Temperature Single-Nucleotide Polymorphism and Multiallele DNA Detection Using Fluorescent Nanocrystals and Microarrays. *Anal. Chem.*, 2003. 75(18): p. 4766-4772.
31. Pathak, S., et al., Hydroxylated Quantum Dots as Luminescent Probes for in Situ Hybridization. *J. Am. Chem. Soc.*, 2001. 123(17): p. 4103-4104.
32. Hočevár, S., B., et al., Carbon Nanotube Modified Microelectrode for Enhanced Voltammetric Detection of Dopamine in the Presence of Ascorbate. *Electroanalysis*, 2005. 17: p. 417-422.
33. Cai, H., et al., Carbon nanotube-enhanced electrochemical DNA biosensor for DNA hybridization detection *Anal. Bioanal. Chem.*, 2003. 375(2): p. 287-293.

34. Shan, C., et al., Direct Electrochemistry of Glucose Oxidase and Biosensing for Glucose Based on Graphene. *Anal. Chem.*, 2009. 81(6): p. 2378–2382.
35. Kanga, X., et al., Glucose Oxidase–graphene–chitosan modified electrode for direct electrochemistry and glucose sensing. *Biosens. Bioelectron.*, 2009. 25: p. 901-905.
36. Lu, C.H., et al., A graphene platform for sensing biomolecules. *Angew. Chem Int. Ed.*, 2009. 48(26): p. 4785-4787.
37. Ingle, J.D.J. and S.R. Crouch, *Spectrochemical analysis*. Prentice Hall, New Jersey 1988.
38. Lakowicz, J.R., *Principles of Fluorescence Spectroscopy*. Springer; 3rd edition, 2006.
39. Wild, D.G., *The Immunoassay Handbook*. Elsevier Science; 3 edition, 2005.
40. Crowther, J.R., *The ELISA Guidebook*. Humana Press; 2nd edition, 2008.
41. Willets, K.A. and R.P. Van Duyne, Localized Surface Plasmon Resonance Spectroscopy and Sensing. *Annu. Rev. Phys. Chem.*, 2007. 58: p. 267-297.
42. Sokolov, K., G. Chumanov, and T.M. Cotton, Enhancement of Molecular Fluorescence near the Surface of Colloidal Metal Films. *Anal. Chem.*, 1998. 70(18): p. 3898–3905.
43. Karlsson, R. and A. Fält, Experimental design for kinetic analysis of protein-protein interactions with surface plasmon resonance biosensors. *J. Immunol. Methods*, 1997. 200(1-2): p. 121-133.
44. Gabudean, A.M., D. Biro, and S. Astilean, Localized surface plasmon resonance (LSPR) and surface-enhanced Raman scattering (SERS) studies of 4-

- aminothiophenol adsorption on gold nanorods. *J. Mol. Struct.*, 2011. 993(1-3): p. 420-424.
45. Blackie, E.J., E.C. Le Ru, and P.G. Etchegoin, Single-Molecule Surface-Enhanced Raman Spectroscopy of Nonresonant Molecules. *J. Am. Chem. Soc.*, 2009. 131(40): p. 14466–14472.
46. Nie, S. and S.R. Emory, Probing Single Molecules and Single Nanoparticles by Surface-Enhanced Raman Scattering. *Science*, 1997. 275(5303): p. 1102-1106
47. Rodríguez-Lorenzo, L., et al., Zeptomol Detection Through Controlled Ultrasensitive Surface-Enhanced Raman Scattering. *J. Am. Chem. Soc.*, 2009. 131(13): p. 4616-8.
48. Kneipp, K., et al., Ultrasensitive Chemical Analysis by Raman Spectroscopy. *Chem. Rev.*, 1999. 99(10): p. 2957–2976.
49. Moskovits, M., Surface-enhanced spectroscopy. *Rev. Mod. Phys.*, 1985. 57: p. 783-826.
50. Tian, Z.-Q. and B. Ren, Adsorption and reaction at electrochemical interfaces as probed by surface-enhanced Raman spectroscopy. *Annu. Rev. Phys. Chem.*, 2004. 55: p. 197-229.
51. Beaucage, S.L. and R.P. Iyer, Advances in the Synthesis of Oligonucleotides by the Phosphoramidite Approach. *Tetrahedron*, 1992. 48(12): p. 2223-2311.
52. Karas, M. and F. Hillenkamp, Laser Desorption Ionization of Proteins with Molecular Masses Exceeding 10 000 Daltons. *Anal. Chem.*, 1988. 60: p. 2301-2303.
53. Börnsen, K.O., et al., Influence of Solvents and Detergents on Matrix-assisted Laser Desorption/Ionization Mass Spectrometry Measurements of Proteins



and Oligonucleotides. *Rapid Communications in Mass Spectrometry*, 1997. 11(6): p. 603-609.

54. Nordhoff, E., et al., Matrix-assisted laser desorption/ionization mass spectrometry of nucleic acids with wavelengths in the ultraviolet and infrared. *Rapid Communications in Mass Spectrometry*, 1992. 6(12): p. 771-776.

55. Hillenkamp, F. and J. Peter-Katalinić, MALDI MS: A Practical Guide to Instrumentation, Methods and Applications. Wiley-VCH Verlag GmbH & Co. KGaA, 2007.

56. Randviir, E.P. and C.E. Banks, Electrochemical impedance spectroscopy: an overview of bioanalytical applications. *Anal. Methods*, 2013. 5: p. 1098-1115.

57. Willner, I., DNAzymes for sensing, nanobiotechnology and logic gate applications. *Chem. Soc. Rev.*, 2008. 37: p. 1153-1165.

58. Breaker, R.R. and G.F. Joyce, A DNA enzyme that cleaves RNA. *Chem. Biol.*, 1994. 1(4): p. 223-229.

59. Breaker, R.R. and G.F. Joyce, A DNA enzyme with Mg<sup>2+</sup>-dependent RNA phosphoesterase activity. *Chem. Biol.*, 1995. 2(10): p. 655-660.

60. Faulhammer, D. and M. Famulok, The Ca<sup>2+</sup> Ion as a Cofactor for a Novel RNA-Cleaving Deoxyribozyme. *Angew. Chem Int. Ed.*, 1996. 35(23-24): p. 2837-2841.

61. Geyer, C.R. and D. Sen, Lanthanide probes for a phosphodiester-cleaving, lead-dependent, DNAzyme. *J. Mol. Biol.*, 1998. 275(3): p. 483-489.

62. Liu, J. and Y. Lu, G-quadruplex-based DNAzyme for facile colorimetric detection of thrombin. *J. Am. Chem. Soc.*, 2003. 125(31): p. 6642-6643.

63. Xiao, Y., A.A. Rowe, and K.W. Plaxco, Electrochemical Detection of Parts-Per-Billion Lead via an Electrode-Bound DNAzyme Assembly. *J. Am. Chem. Soc.*, 2007. 129(2): p. 262-263.
64. Witting, P.K., et al., A DNA Oligonucleotide–Hemin Complex Cleaves t-Butyl Hydroperoxide through a Homolytic Mechanism. *Inorg. Chem.*, 2001. 40(19): p. 5017.
65. Travascio, P., Y. Li, and D. Sen, DNA-enhanced peroxidase activity of a DNA aptamer-hemin complex. *Chem. Biol.*, 1998. 5(9): p. 505-517.
66. Travascio, P., et al., The Peroxidase Activity of a Hemin-DNA Oligonucleotide Complex: Free Radical Damage to Specific Guanine Bases of the DNA. *J. Am. Chem. Soc.*, 2001. 123(7): p. 1337.
67. Xiao, Y., et al., Catalytic Beacons for the Detection of DNA and Telomerase Activity. *J. Am. Chem. Soc.*, 2004. 126(24): p. 7430-7431.
68. Xiao, Y., et al., Lighting Up Biochemiluminescence by the Surface Self-Assembly of DNA± Hemin Complexes. *ChemBioChem*, 2004. 5: p. 374-379.
69. Pavlov, V., et al., Amplified Chemiluminescence Surface Detection of DNA and Telomerase Activity Using Catalytic Nucleic Acid Labels. *Anal. Chem.*, 2004. 76(7): p. 2152–2156.
70. Niazov, T., et al., DNAzyme-Functionalized Au Nanoparticles for the Amplified Detection of DNA or Telomerase Activity. *Nano Lett.*, 2004. 4(9): p. 1683-1687.
71. Kukielka, E. and A.I. Cederbaum, Stimulation of NADH-dependent microsomal DNA strand cleavage by rifamycin SV. *Biochem. J.*, 1995. 307: p. 361-367.

72. Chiou, S.H., et al., Specific Cleavages of DNA by Ascorbate in the Presence of Copper Ion or Copper Chelates. *J. Biochem.*, 1985. 98(6): p. 1723-1726.
73. Halliwell, B. and M.C. Cutteidge, Role of free radicals and catalytic metal ions in human disease: An overview. *Methods Enzymol.*, 1990. 186: p. 1-85.
74. Davies, M.B., J. Austin, and S.A. Partridge, *Vitamin C: Its Chemistry and Biochemistry*. The Royal Society of Chemistry, Cambridge, 1991.
75. Ullah, M.F., et al., The antioxidant ascorbic acid mobilizes nuclear copper leading to a prooxidant breakage of cellular DNA: implications for chemotherapeutic action against cancer. *Cancer Chemother. Pharmacol.*, 2011. 67(1): p. 103-110.
76. Emmerie, A. and M. Van Eekelen, The chemical determination of vitamin C with removal of interfering reducing and coloured substances. *Biochem. J.* , 1934. 28: p. 1153-1154.
77. Horwitz, W., *Official Methods of the Association of Official Analytical Chemists*, 15th ed.; Association of Official Analytical Chemists, Arlington, VA, 1990: p. 1058-1059.
78. ZANNONI, V., et al., Rapid Micromethod for the Determination of Ascorbic Acid in Plasma and Tissues. *Biochem. Med.*, 1974. 11(1): p. 41-48.
79. Rahman Khan, M.M., et al., A Simple UV-spectrophotometric Method for the Determination of Vitamin C Content in Various Fruits and Vegetables at Sylhet Area in Bangladesh. *J. Biol. Sci.*, 2006. 6(2): p. 388-392.
80. Ruedas Rama, M.J., A. Ruiz Medina, and A. Molina Diaz, A Prussian blue-based flow-through renewable surface optosensor for analysis of ascorbic acid. *Microchem. J.*, 2004. 78(2): p. 157-162.

81. Kutnink, M.A., et al., An internal standard method for the unattended high-performance liquid chromatographic analysis of ascorbic acid in blood components. *Anal. Biochem.*, 1987. 166(2): p. 424-430.
82. Gazdik, Z., et al., Determination of Vitamin C (Ascorbic Acid) Using High Performance Liquid Chromatography Coupled with Electrochemical Detection. *Sensors*, 2008. 8(11): p. 7097-7112.
83. Herrero-Martinez, J.M., et al., Determination of Ascorbic Acid and Total Ascorbic Acid in Vascular and Nonvascular Plants by Capillary Zone Electrophoresis. *Anal. Biochem.*, 1998. 265(2).
84. Castelletti, L., et al., Development of an integrated capillary electrophoresis/sensor for L-ascorbic acid detection. *Electrophoresis*, 2002. 23(2): p. 209-214.
85. Sun, X., et al., Determination of ascorbic acid in individual rat hepatocyte cells based on capillary electrophoresis with electrochemiluminescence detection. *Electrophoresis*, 2008. 29(13): p. 2918-2924.
86. Janda, P., et al., Detection of Ascorbic Acid Using a Carbon Fiber Microelectrode Coated with Cobalt Tetramethylpyridopyrroazine. *Anal. Chem.*, 1996. 68(6): p. 960-965.
87. Kannan, P. and S. Abraham John, Determination of nanomolar uric and ascorbic acids using enlarged gold nanoparticles modified electrode. *Anal. Biochem.*, 2009. 386(1): p. 65-72.
88. Xu, Q., et al., PDMS-based gold electrode for sensing ascorbic acid. *Colloids Surf. B: Biointerfaces*, 2011. 88(1): p. 362-365.
89. Guo, H., et al., Potentiometric measurement of ascorbate by using a solvent polymeric membrane electrode. *Talanta*, 2008. 75(3): p. 851-855.

90. Ensafi, A.A., Determination of Ascorbic Acid by Electrocatalytic Voltammetry with Methylene Blue. *Anal. Lett.*, 2003. 36(3): p. 591-604.
91. Nezhad, M.R.H., M.A. Karimi, and F. Shahheydari, A Sensitive Colorimetric Detection of Ascorbic Acid in Pharmaceutical Products Based on Formation of Anisotropic Silver Nanoparticles. *Trans. F: Nanotechnol.*, 2010. 17(2): p. 148-153.
92. Bossi, A., et al., An Assay for Ascorbic Acid Based on Polyaniline-Coated Microplates. *Anal. Chem.*, 2000. 72(18): p. 4296-4300.
93. Falat, L. and H.-Y. Cheng, Electrocatalysis of ascorbate and NASH at a surface modified graphite-epoxy electrode. *J. Electroanal. Chem.* , 1983. 157(2): p. 393-397.
94. Dürüst, N., D. Sümengen, and Y. Dürüst, Ascorbic Acid and Element Contents of Foods of Trabzon (Turkey). *Agric. Food Chem.* , 1997. 45(6): p. 2085-2087.
95. Ishii, K., et al., Phthalocyanine-based fluorescence probes for detecting ascorbic acid: phthalocyaninatosilicon covalently linked to TEMPO radicals. *Chem. Commun.*, 2011. 47(17): p. 4932-4934.
96. Carmi, N., L.A. Shultz, and R.R. Breaker, In vitro selection of self-cleaving DNAs. *Chem. Biol.*, 1996. 3(12): p. 1039-1046.
97. Carmi, N., S.R. Balkhi, and R.R. Breaker, Cleaving DNA with DNA. *Proc. Natl. Acad. Sci. U.S.A.*, 1998. 95(5): p. 2233–2237.
98. Grabar, K.C., et al., Preparation and Characterization of Au Colloid Monolayers. *Anal. Chem.*, 1995. 67(4): p. 735-743.
99. Aruoma, O.I., et al., Copper-ion-dependent damage to the bases in DNA in the presence of hydrogen peroxide. *Biochem. J.* , 1991. 273: p. 601-604.

100. Shigenaga, M.K. and B.N. Ames, Assays For 8-Hydroxy-2'-Deoxyguanosine: A Biomarker Of In Vivo Oxidative Dna Damage. *Free Radic. Biol. Med.*, 1991. 10(3-4): p. 211-216.
101. Tajmir-Riahi, H.A., M. Langlais, and R. Savoie, A laser Raman spectroscopic study of the interaction of calf-thymus DNA with Cu(II) and Pb(II) ions: metal ion binding and DNA conformational changes. *Nucleic Acid Res.*, 1988. 16(2): p. 751-762.
102. Carmi, N. and R.R. Breaker, Characterization of a DNA-Cleaving deoxyribozyme. *Bioorg. Med. Chem.* , 2001. 9(10): p. 2589-2600.
103. Dubertret, B., M. Calame, and A.J. Libchaber, Single-mismatch detection using gold-quenched fluorescent oligonucleotides. *Nature Biotech.* , 2001. 19: p. 365-370.
104. Weiss, S., Fluorescence Spectroscopy of Single Biomolecules. *Science*, 1999. 283(5408): p. 1676-1683
105. Andrew, P. and W.L. Barnes, Förster Energy Transfer in an Optical Microcavity. *Science*, 2000. 290(5492): p. 785-788.
106. Leung, P.T., Decay of molecules at spherical surfaces: Nonlocal effects. *Phys. Rev. B* 1990. 42(12): p. 7622-7625.
107. Dulkeith, E., et al., Fluorescence Quenching of Dye Molecules near Gold Nanoparticles:Radiative and Nonradiative Effects. *Phys. Rev. Lett.*, 2002. 89(20): p. 203002-1 – 203002-4.
108. Turner, M., et al., Selective oxidation with dioxygen by gold nanoparticle catalysts derived from 55-atom clusters. *Nature*, 2008. 454: p. 981-983.

109. Zhang, L. and X. Jiang, Attachment of gold nanoparticles to glassy carbon electrode and its application for the voltammetric resolution of ascorbic acid and dopamine. *J. Electroanal. Chem.*, 2005. 583(2): p. 292-299.
110. Guerin, S., et al., A Combinatorial Approach to the Study of Particle Size Effects on Supported Electrocatalysts: Oxygen Reduction on Gold. *J. Comb. Chem.*, 2006. 8(5): p. 679–686.
111. Que, E.L., D.W. Domaille, and C.J. Chang, Metals in Neurobiology: Probing Their Chemistry and Biology with Molecular Imaging. *Chem. Rev.*, 2008. 108: p. 1517-1549.
112. Georgopoulos, P.G., et al., Environmental Copper: Its Dynamics And Human Exposure Issues. *J. Toxicol. Environ. Health, Part B*, 2001. 4(4): p. 341-394.
113. United States Environmental Protection Agency Consumer Fact Sheet on Copper, et al.
114. Chan, M.-S. and S.-D. Huang, Direct determination of cadmium and copper in seawater using a transversely heated graphite furnace atomic absorption spectrometer with Zeeman-effect background corrector. *Talanta*, 2000. 51: p. 373–380.
115. Gonzáles, A.P.S., et al., Peat as a natural solid-phase for copper preconcentration and determination in a multicommuted flow system coupled to flame atomic absorption spectrometry. *Anal. Chim. Acta*, 2009. 636(2): p. 198–204.
116. Beck, N.G., R.P. Franks, and K.W. Bruland, Analysis for Cd, Cu, Ni, Zn, and Mn in estuarine water by inductively coupled plasma mass spectrometry coupled with an automated flow injection system. *Anal. Chim. Acta*, 2002. 455: p. 11-22.

117. Wu, J. and E.A. Boyle, Low Blank Preconcentration Technique for the Determination of Lead, Copper, and Cadmium in Small-Volume Seawater Samples by Isotope Dilution ICPMS. *Anal. Chem.*, 1997. 69(13): p. 2464–2470.
118. Tanyanyiwa, J. and P. Hauser, High-voltage contactless conductivity detection of metal ions in capillary electrophoresis. *Electrophoresis*, 2002. 23(21): p. 3781–3786.
119. Ganjali, M.R., M. Emami, and M. Salavati-Niasari, Novel Copper(II)-Selective Sensor Based on a New Hexadentates Schiff's Base. *Bull. Korean Chem. Soc.*, 2002. 23(10): p. 1394-1398.
120. Petkovic, B.B., et al., A Copper(II) Ion-Selective Potentiometric Sensor Based on N,N',N'',N'''-Tetrakis(2-pyridylmethyl) -1,4,8,11-tetraazacyclotetradecane in PVC Matrix. *Electroanalysis*, 2010. 22(16): p. 1894 – 1900.
121. Singh, A.K., S. Mehtab, and A.K. Jain, Selective electrochemical sensor for copper (II) ion based on chelating ionophores. *Anal. Chim. Acta*, 2006. 575: p. 25-31.
122. Mahajan, R.K. and P. Sood, Novel Copper(II)-Selective Electrode Based on 2,2': 5',2''-Terthiophene in PVC Matrix. *Int. J. Electrochem. Sci.*, 2007. 2: p. 832-847.
123. Etienne, M., J. Bessiere, and A. Walcarius, Voltammetric detection of copper (II) at a carbon paste electrode containing an organically modified silica. *Sens. Actuators, B*, 2001. 76: p. 531-538.
124. Mohadesi, A. and M.A. Taher, Voltammetric determination of Cu(II) in natural waters and human hair at a meso-2,3-dimercaptosuccinic acid self-assembled gold electrode. *Talanta*, 2007. 72(1): p. 95–100.



125. High, B., D. Bruce, and M.M. Richter, Determining copper ions in water using electrochemiluminescence. *Anal. Chim. Acta*, 2001. 449(1-2): p. 17-22.
126. Qiu, S., et al., Development of ultra-high sensitive and selective electrochemiluminescent sensor for copper(II) ions: a novel strategy for modification of gold electrode using click chemistry. *Analyst*, 2011. 136: p. 1580-1585.
127. He, C.-L., et al., A Fluorescent Chemosensor for Copper(II) Based on a Carboxylic Acid-functionalized Tris(2,2'-bipyridine)-ruthenium(II) Complex. *Analyt. Sci.*, 2006. 22: p. 1547-1551.
128. Lv, X.-L., Y. Wei, and S.-Z. Luo, A "Turn-On" Fluorescent Chemosensor Based on Peptidase for Detecting Copper(II). *Analyt. Sci.*, 2012. 28(8): p. 749-752.
129. Jung, H.S., et al., Coumarin-Derived Cu<sup>2+</sup>-Selective Fluorescence Sensor: Synthesis, Mechanisms, and Applications in Living Cells. *J. Am. Chem. Soc.*, 2009. 131(5): p. 2008-2012.
130. Xiang, Y., et al., New Fluorescent Rhodamine Hydrazone Chemosensor for Cu(II) with High Selectivity and Sensitivity. *Org. Lett.*, 2006. 8(13): p. 2863-2866.
131. Silverman, S.K., Deoxyribozymes: DNA catalysts for bioorganic chemistry. *Org. Biomol. Chem.*, 2004. 2: p. 2701-2706.
132. Santoro, S.W., et al., RNA Cleavage by a DNA Enzyme with Extended Chemical Functionality. *J. Am. Chem. Soc.*, 2000. 122(11): p. 2433-2439.
133. Mei, S.H.J., et al., An Efficient RNA-Cleaving DNA Enzyme that Synchronizes Catalysis with Fluorescence Signaling. *J. Am. Chem. Soc.*, 2003. 125(2): p. 412-420.
134. Li, J., et al., In vitro selection and characterization of a highly efficient Zn(II)-dependent RNA-cleaving deoxyribozyme. *Nucleic Acids Res*, 2000. 28(2): p. 481-8.

135. Wang, F., J. Elbaz, and I. Willner, Enzyme-Free Amplified Detection of DNA by an Autonomous Ligation DNAzyme Machinery. *J. Am. Chem. Soc.*, 2012. 134: p. 5504-5507.
136. Lan, T., K. Furuyab, and Y. Lu, A highly selective lead sensor based on a classic lead DNAzyme. *Chem. Commun.*, 2010. 46: p. 3896-3898.
137. Liu, J., et al., A catalytic beacon sensor for uranium with parts-pertrillion sensitivity and millionfold selectivity. *PNAS*, 2007. 104(7): p. 2056-2061.
138. Wang, Z., J.H. Lee, and Y. Lu, Highly sensitive "turn-on" fluorescent sensor for Hg<sup>2+</sup> in aqueous solution based on structure-switching DNA. *Chem. Commun.*, 2008. 6005-6007.
139. Liu, J. and Y. Lu, A DNAzyme Catalytic Beacon Sensor for Paramagnetic Cu<sup>2+</sup> Ions in Aqueous Solution with High Sensitivity and Selectivity. *J. Am. Chem. Soc.*, 2007. 129: p. 9838-9839.
140. Liu, M., et al., A "turn-on" fluorescent copper biosensor based on DNA cleavage-dependent graphene-quenched DNAzyme. *Biosens. Bioelectron.*, 2011. 26(10): p. 4111-4116.
141. Fang, Z., et al., Lateral flow nucleic acid biosensor for Cu<sup>2+</sup> detection in aqueous solution with high sensitivity and selectivity. *Chem. Commun.*, 2010. 46: p. 9043-9045.
142. Zacco, E., M.I. Pividori, and S. Alegret, Electrochemical biosensing based on universal affinity biocomposite platforms. *Biosens. Bioelectron.*, 2006. 21(7): p. 1291-1301.
143. Katz, E. and I. Willner, Probing Biomolecular Interactions at Conductive and Semiconductive Surfaces by Impedance Spectroscopy: Routes to Impedimetric

- Immunosensors, DNA-Sensors, and Enzyme Biosensors. *Electroanalysis*, 2003. 15(11): p. 913-947.
144. Merkoçi, A., et al., New materials for electrochemical sensing VI: Carbon nanotubes. *TrAC - Trend. Anal. Chem.*, 2005. 24(4): p. 341-349.
145. Pumera, M., et al., Direct voltammetric determination of gold nanoparticles using graphite-epoxy composite electrode. *Electrochim. Acta*, 2005. 50(18): p. 3702-3707.
146. Bonanni, A., et al., Impedimetric genosensors for the detection of DNA hybridization. *Anal. Bioanal. Chem.*, 2006. 385(7): p. 1195-1201.
147. Bonanni, A., M.I. Pividori, and M.d. Valle, Application of the avidin–biotin interaction to immobilize DNA in the development of electrochemical impedance genosensors. *Anal. Bioanal. Chem.*, 2007. 389(3): p. 851-861.
148. Chen, D., et al., ELISA Methodology for Detection of Modified Osteoprotegerin in Clinical Studies. *Clin. Chem.*, 2001. 47(4): p. 747-749.
149. Stejskal, D., et al., Proguanylin: development, analytical characterization, and clinical testing of a new ELISA. *Gen. Physiol. Biophys.*, 2007. 26(1): p. 62-5.
150. Miyai, K., K. Ishibashi, and M. Kawashima, Enzyme immunoassay of thyroxine in serum and dried blood samples on filter paper. *Endocrinol Jpn.*, 1980. 27(3): p. 375-80.
151. Ruan, C. and Y. Li, Detection of zeptomolar concentrations of alkaline phosphatase based on a tyrosinase and horse-radish peroxidase bienzyme biosensor. *Talanta*, 2001. 54(6): p. 1095–1103.
152. Lowry, O.H., *Methods Enzymol.*, 1957. 4: p. 366-381.

153. Baykov, A.A., O.A. Evtushenko, and S.M. Avaeva, A Malachite Green Procedure for Orthophosphate Determination and Its Use in Alkaline Phosphatase-Based Enzyme Immunoassay. *Anal. Biochem.*, 1988. 171(2): p. 266-270.
154. Fenoll, J., G. Jourquinb, and J.-M. Kauffmann, Fluorimetric determination of alkaline phosphatase in solid and fluid dairy products. *Talanta*, 2002. 56(6): p. 1021-1026.
155. Wolfbeis, O.S. and E. Koller, Photometric and fluorimetric assay of alkaline phosphatase with new coumarin-derived substrates. *Microchim. Acta*, 1985. 85(5-6): p. 389-395.
156. Kokado, A., H. Arakawa, and M. Maeda, Chemiluminescent assay of alkaline phosphatase using dihydroxyacetone phosphate as substrate detected with lucigenin. *Luminescence*, 2002. 17(1): p. 5-10.
157. Treloar, P.H., et al., Electrochemical immunoassay: Simple kinetic detection of alkaline phosphatase enzyme labels in limited and excess reagent systems. *Electroanalysis*, 1994. 6(7): p. 561-566.
158. Tang, H.T., et al., p-Aminophenyl Phosphate: An Improved Substrate For Electrochemical Enzyme Immunoassay. *Anal. Chim. Acta*, 1988. 214: p. 187-195.
159. Halsall, H.B. and W.R. Heineman, Electrochemical immunoassay: an ultrasensitive method. *J. Int. Fed. Clin. Chem.*, 1990. 2(4): p. 179-87.
160. Tang, H.T., H.B. Halsall, and W.R. Heinemann, Electrochemical Enzyme Immunoassay for Phenytoin by Flow-Injection Analysis Incorporating a Redox Coupling Agent. *Clin. Chem.*, 1991. 37(2): p. 245-248.
161. Frew, J.E., et al., Measurement of alkaline phosphatase activity by electrochemical detection of phosphate esters. *J. Electroanal. Chem.*, 1989. 266(2): p. 309-316.

162. Krezer, M.P., C.K. O'Sullivan, and G.G. Guilbault, Alkaline phosphatase as a label for immunoassay using amperometric detection with a variety of substrates and an optimal buffer system. *Anal. Chim. Acta*, 1999. 393(1-3): p. 95-102.
163. Chen, J., et al., Real-Time Fluorescence Turn-On Detection of Alkaline Phosphatase Activity with a Novel Perylene Probe. *Chem. Asian. J.*, 2013. 8(1): p. 276-281.
164. O'Shea, D.J., et al., Homogeneous time-resolved fluorescence assays for the detection of activity and inhibition of phosphatase enzymes employing phosphorescently labeled peptide substrates. *Anal. Chim. Acta*, 2007. 583(2): p. 349-356.
165. Liu, Y. and K.S. Schanze, Conjugated Polyelectrolyte-Based Real-Time Fluorescence Assay for Alkaline Phosphatase with Pyrophosphate as Substrate. *Anal. Chem.*, 2008. 80(22): p. 8605-8612.
166. Gong, H., et al., Alkaline phosphatase assay using a near-infrared fluorescent substrate merocyanine 700 phosphate. *Talanta*, 2011. 84(3): p. 941-946.
167. Alivisatos, A.P., W. Gu, and C. Larabell, Quantum Dots As Cellular Probes. *Annu. Rev. Biomed.*, 2005. 7: p. 55-76.
168. Lin, C.-A.J., et al., Bioanalytics and biolabeling with semiconductor nanoparticles (quantum dots) *J. Mater. Chem.*, 2007. 17: p. 1343-1346.
169. Algar, W.R., et al., Semiconductor Quantum Dots in Bioanalysis: Crossing the Valley of Death. *Anal. Chem.*, 2011. 83(23): p. 8826-8837.
170. Schmid, G., et al., Nanoparticles: From Theory to Application. Günter, S., Ed.; Wiley-VCH: Weinheim, Germany, 2004: p. 4-49.

171. Algar, W.R., et al., Proteolytic Activity at Quantum Dot-Conjugates: Kinetic Analysis Reveals Enhanced Enzyme Activity and Localized Interfacial "Hopping". *Nano Lett.*, 2012. 12(7): p. 3793-3802.
172. Freeman, R., et al., Probing Protein Kinase (CK2) and Alkaline Phosphatase with CdSe/ZnS Quantum Dots. *Nano Lett.*, 2010. 10(6): p. 2192-2196.
173. Chan, W.C.W. and S. Nie, Quantum Dot Bioconjugates for Ultrasensitive Nonisotopic Detection. *Science*, 1998. 281(5385): p. 2016-2018
174. Sun, B., et al., Microminiaturized immunoassays using quantum dots as fluorescent label by laser confocal scanning fluorescence detection. *J. Immunol. Methods*, 2001. 249: p. 285-289.
175. Ramadurai, D., et al., Fluorescent resonance energy transfer based detection of biological contaminants through hybrid quantum dot-quencher interactions. *IET Nanobiotechnol.*, 2008. 2(2): p. 47.
176. Kattke, M.D., et al., FRET-Based Quantum Dot Immunoassay for Rapid and Sensitive Detection of *Aspergillus amstelodami*. *Sensors*, 2011. 11(6): p. 6396-6410.
177. Willner, I., R. Baron, and B. Willner, Growing Metal Nanoparticles by Enzymes. *Adv. Mater.*, 2006. 18(9): p. 1109-1120.
178. Katz, E. and I. Willner, Integrated Nanoparticle-Biomolecule Hybrid Systems: Synthesis, Properties, and Applications. *Angew. Chem Int. Ed.*, 2004. 43(45): p. 6042-6108.
179. Pavlov, V., Y. Xiao, and I. Willner, Inhibition of the Acetylcholine Esterase-Stimulated Growth of Au Nanoparticles: Nanotechnology-Based Sensing of Nerve Gases. *Nano Lett.*, 2005. 5(4): p. 649-653.

180. Xiao, Y., et al., Shape and Color of Au Nanoparticles Follow Biocatalytic Processes. *Langmuir*, 2005. 21(13): p. 5659-5662.
181. Willner, I., B. Willner, and E. Katz, Biomolecule–nanoparticle hybrid systems for bioelectronic applications. *Bioelectrochem.*, 2007. 70(1): p. 2-11.
182. Garai-Ibabe, G., M. Möller, and V. Pavlov, Ultrasensitive Assay for Detection of Serum Paraoxonase by Modulating the Growth of Fluorescent Semiconductor Nanoparticles. *Anal. Chem.*, 2012. 84(18): p. 8033-8037.
183. Saa, L., J.M. Mato, and V. Pavlov, Assays for Methionine  $\gamma$ -Lyase and S-Adenosyl-L-homocysteine Hydrolase Based on Enzymatic Formation of CdS Quantum Dots in Situ. *Anal. Chem.*, 2012. 84(21): p. 8961-8965.
184. Saa, L., et al., Analytical Applications of Enzymatic Growth of Quantum Dots. *Chem. Eur. J.*, 2010. 16(21): p. 6187-6192.
185. McGlynn, K.A., R.E. Tarone, and H.B. El-Serag, A comparison of trends in the incidence of hepatocellular carcinoma and intrahepatic cholangiocarcinoma in the United States. *Cancer Epidemiol. Biomarkers Prev.*, 2006. 15(6): p. 1198-1203.
186. Tamai, T., et al., Serum manganese superoxide dismutase and thioredoxin are potential prognostic markers for hepatitis C virus-related hepatocellular carcinoma. *World J. Gastroenterol.*, 2011. 17(44).
187. Church, S.L., et al., Increased manganese superoxide dismutase expression suppresses the malignant phenotype of human melanoma cells. *Proc. Natl. Acad. Sci. U S A*, 1993. 90(7): p. 3113-3117.
188. Li, J.J., et al., Phenotypic changes induced in human breast cancer cells by overexpression of manganese-containing superoxide dismutase. *Oncogene*, 1995. 10(10): p. 1989-2000.

189. Zhong, W., et al., Suppression of the malignant phenotype of human glioma cells by overexpression of manganese superoxide dismutase. *Oncogene*, 1997. 14(4): p. 481-490.
190. Fang, Z., et al., A lateral flow biosensor for rapid detection of DNA-binding protein c-jun. *Biosens. Bioelectron.*, 2011. 27(1): p. 192-196.
191. Miao, Y., et al., Inhibition of high-mobility-group A2 protein binding to DNA by netropsin: a biosensor-surface plasmon resonance assay. *Anal. Biochem.*, 2008. 374(1): p. 7-15.
192. Wu, L., et al., Effects of small molecular inhibitors on the binding between HIV-1 reverse transcriptase and DNA as revealed by SPR biosensor. *Sens. Actuators, B*, 2007. 122(1): p. 243-252.
193. Hong, S.R., H.D. Jeong, and S. Hong, QCM DNA biosensor for the diagnosis of a fish pathogenic virus VHSV. *Talanta*, 2010. 82(3): p. 899-903.
194. Garai-Ibabe, G., et al., Label free and amplified detection of cancer marker EBNA-1 by DNA probe based biosensors. *Biosens. Bioelectron.*, 2011. 30(1): p. 272-275.
195. Keefe, A.D., S. Pai, and A. Ellington, Aptamers as therapeutics. *Nat. Rev. Drug. Discov.*, 2010. 9(7): p. 537-550.
196. Pavan Kumar, G.V., Plasmonic nano-architectures for surface-enhanced Raman scattering. *J. Nanophoton.*, 2012. 6(1): p. ID 064503.
197. Costa, J.C., et al., High performance gold nanorods and silver nanocubes in surface-enhanced Raman spectroscopy of pesticides. *Phys. Chem. Chem. Phys.*, 2009. 11: p. 7491-7498.



198. Yang, Y., et al., Solvothermal synthesis of multiple shapes of silver nanoparticles and their SERS properties. *J. Phys. Chem. C*, 2007. 111(26): p. 9095-9104.
199. Vigderman, L. and E.R. Zubarev, Starfruit-shaped gold nanorods and nanowires: synthesis and SERS characterization. *Langmuir*, 2012. 28(24): p. 9034-9040.
200. Stiles, P.L., et al., Surface-enhanced Raman spectroscopy. *Annu. Rev. Anal. Chem.*, 2008. 1(1): p. 601-626.
201. Haes, A.J., et al., Plasmonic materials for surface-enhanced sensing and spectroscopy. *MRS Bulletin*, 2005. 30(5): p. 368-375.
202. Prodan, E., et al., A hybridization model for the Plasmon response of complex nanostructures. *Science*, 2003. 302(5644): p. 419-422.
203. Billot, L., et al., Surface enhanced Raman scattering on gold nanowire arrays: Evidence of strong multipolar surface plasmon resonance enhancement. *Chem. Phys. Lett.*, 2006. 422(4-6): p. 303-307.
204. Fisher, H. and O.J.F. Martin, Engineering the optical response of plasmonic nanoantennas. *Opt. Express*, 2008. 16(112): p. 9144-9154.
205. Grand, J., et al., Role of localized surface plasmons in surface-enhanced Raman scattering of shape-controlled metallic particles in regular arrays. *Phys. Rev. B*, 2005. 72(3): p. 033407.
206. Grand, J., et al., Optimization of SERS-active substrates for near-field Raman spectroscopy. *Synth. Met.*, 2003. 139(3): p. 621-624.
207. Steel, A.B., T.M. Herne, and M.J. Tarlov Electrochemical Quantitation of DNA Immobilized on Gold. *Anal. Chem.*, 2000. 70(22): p. 4670-4677.

# Curriculum Vitae

## PERSONAL INFORMATION

**Name:** Natalia Malashikhina  
**Adress:** Volodarskogo str. 38-51, 188230, Luga, Russia  
**Telephone:** +7 965 048 81 56; +34 634 71 38 30  
**Fax:** + 34 943 00 53 15  
**E-mail:** natalia.malashikhina@gmail.com  
**Date of birth:** 14-06-1986  
**Nationality:** Russian

## EDUCATION

10/2009- 10/2013	PhD student in the group of Dr. V. Pavlov Development of new methods for signal amplification in bioanalytical assays <b>CIC biomaGUNE, San Sebastian, Spain</b>
09/2010- 06/2011	Master Thesis in Molecular Biology and Biomedicine, Supervisor: Dr. V. Pavlov <b>The University of the Basque Country (UPV/EHU), Leioa, Spain</b>

09/2003- 06/2008	Specialist Diploma in Organic Chemistry, Supervisor Prof. Dr. V. Nikolaev <b>Saint-Petersburg State University (SPBU), Saint-Petersburg, Russia</b>
---------------------	---

### RESEARCH EXPERIENCE

10/2008- 07/2009	<b>University of Fribourg, Department of Chemistry, Switzerland,</b> 9 month scholarship in division of Physical Chemistry Matrix isolation and computational studies of photochemical Wolff rearrangement Mentor: Prof. Dr. T. Bally
06/2007- 08/2007	<b>University of Georgia, Department of Chemistry, USA,</b> Summer Student, "Photoremovable protecting groups for different functionalities", Mentor: Prof. Dr. V. Popik
01/2007- 02/2007	<b>University of Leipzig, Institut of Organic Chemistry, Germany,</b> Euler research project, "Synthesis of diazocarbonyl compounds and estimation of their biological activity", Mentor: Prof. Dr. V. Nikolaev, Prof. Dr. A. Giannis

### RESEARCH PRESENTATIONS

09/2013      Development of ultrasensitive bioanalytical assays based on metal and semiconductor nanoparticles. TNT2013, Sevilla, Spain, Oral  
N. Malashikhina, G. Garai Ibabe, V. Pavlov

05/2012 A new catalytic DNAzyme based biosensors for ascorbic acid and copper (II) ions detection, Biosensors2012, Cancun, Mexico, Oral  
N. Malashikhina, C. Ocaña, M. Del Valle, V. Pavlov

05/2012 Impedimetric biosensor for Cu<sup>2+</sup> detection based on DNAzyme  
Biosensors2012, Cancun, Mexico, Poster  
C. Ocaña, N. Malashikhina, V. Pavlov, M. del Valle, Poster, Cancún, México

10/2012 Label-free impedimetric detection of copper based on DNAzyme  
Ibersensor2012, Isla verde, Puerto Rico, Poster  
C. Ocaña, N. Malashikhina, V. Pavlov, M. del Valle, Poster, Cancún, México

11/2011 A DNAzyme based sensor for the detection of ascorbic acid",  
*NanoSensorPhotonics*, Dead Sea, Israel, Poster  
N. Malashikhina, V. Pavlov

06/2008 Synthesis of  $\alpha,\alpha$ -diarylsubstituted diazoketones of tetrahydrofurane series using the Favorsky acetylene, *International Conference on Organic Chemistry*, St.Petersburg, Russia, Poster  
N. A. Malashikhina, O. S. Galkina, S. A. Malashikhin

05/2007 Synthesis of diazocarbonyl compounds and estimation of their biological activity, *Student conference*, St. Petersburg, Russia, Poster  
N. A. Malashikhina, V. A. Nikolaev

### SCIENTIFIC PUBLICATIONS

Malashikhina N., Grai-Ibabe G, Pavlov V., ***Unconventional Application Of Conventional Enzymatic Substrate: First Fluorogenic Immunoassay Based On Enzymatic Formation Of Qds*** Anal. Chem. **2013**, 85, 6866-6870

Ocaña C., Malashikhina N., del Valle M., Pavlov V., ***Label-Free Selective Impedimetric Detection Of Cu<sup>2+</sup> Ions Using Catalytic DNA*** *Analyst*, **2013**, 138, 1995-1999

Malashikhina N. and Pavlov V.; ***DNA-Decorated Nanoparticles As Nanosensors For Rapid Detection Of Ascorbic Acid***. *Biosens. Bioelectron.*, **2012**, 33, 241- 246

Alexey P. Kostikov, Natalia Malashikhina, Vladimir V. Popik, ***Caging Of Carbonyl Compounds As Photolabile (2,5-Dihydroxyphenyl)Ethylene Glycol Acetals*** *J. Org. Chem.*, **2009**, 74 (4), 1802–1804

### **AWARDS AND HONOURS**

Euler scholarship, Germany, 2007

Graduate Student Award for the 59th Meeting of Nobel Laureats in Lindau, Germany, 2009

### **MEMBERSHIPS**

Since 2011- Spanish society of Analytical Chemistry (SEQA)

### **LANGUAGE SKILLS**

*Russian*-mother tongue

*English*-fluent

*Spanish*-fluent

*German*-good